KU LEUVEN

FACULTY OF ENGINEERING TECHNOLOGY

GROUP T LEUVEN CAMPUS

Modeling and Impact Analysis of Heat Extraction from Surface Water

Sebastian BAES

Jan DENAYER

Supervisor: Prof. Dr. Ir. Maarten Vanierschot

Co-supervisors: Stijn De Jonge, Thomas Holemans

Master Thesis submitted to obtain the degree of Master of Science in Engineering Technology: Electromechanics - Intelligent Mobility

Academic Year 2019 - 2020

Acknowledgements

We would like to express our most sincere gratitude to the following individuals:
First and foremost, to **Stijn De Jonge** and **Thomas Holemans**, on behalf of CORE, for giving us the opportunity to work and broaden our understanding on this interesting topic. In addition, we would like to thank both of them for their time to discuss our progress and guide us every two weeks throughout this academic year. A great debt of gratitude to **Maarten Vanierschot**, our supervisor, for the aid on implementing different fundamental concepts in this paper. He was eager to listen to the problems we encountered and, through his insights, he was able to help us in developing the mathematical basis of this research. To **Giel Vandersteen**, our daily supervisor, for the substantial feedback on our written work. Lastly, we would like to express our gratitude to **Wouter Meynendonckx** for his generous assistance as he provided useful heat demand data.

Abstract

Het ontwikkelen van duurzame en rationele concepten voor energiegebruik is een cruciale trend in het huidige tijdperk gekenmerkt door een aanzienlijke menselijke impact. CORE is een coöperatie van ingenieursstudenten en professionele partners wiens werk bijdraagt tot deze essentiële ontwikkeling. De hantering van innovatieve technieken om warmte te onttrekken uit water is één van de centrale thema's binnen CORE. Momenteel wordt intensief onderzoek uitgevoerd naar het onttrekken van warmte uit oppervlaktewater in rivieren via warmtepompen. Deze thesis onderzoekt het potentieel van de aanwezige warmte in de Dijle in en rondom Leuven. Daarnaast wordt ook de temperatuursdaling en diens invloed na het onttrekken van de gevraagde warmte uit de waterloop geanalyseerd. Een restrictie op de totale temperatuursdaling is vastgelegd op maximaal $3°C$ in dit onderzoek, gebaseerd op richtlijnen van de Vlaamse Milieu Maatschappij (VMM). Om een antwoord te bieden op de gestelde onderzoeksvragen worden twee modellen ontwikkeld in MATLAB. Beide modellen simuleren een watertemperatuur door de verschillende warmte-uitwisselingsprocessen van een rivier te modelleren. De modellen worden met elkaar vergeleken en hun accuraatheid wordt getoetst aan de hand van verschillende testen gebaseerd op rivierdata. Na het onderschrijven van deze accuraatheid worden de modellen gebruikt voor de analyse van het warmtepotentieel in de Dijle. De bekomen resultaten uit dit onderzoek stellen dat de aanwezige warmte in de Dijle gebruikt kan worden voor het verwarmen van residentiële gebouwen in Leuven. Dit is toepasbaar in een warmtenet van 1000 meter rond de Dijle zonder dat de riviertemperatuur een ontoelaatbare daling kent.

Extended Abstract

The development of new concepts and products that aim for an efficient use of energy is essential during the current era of significant human impact. Establishing such sustainable concepts is the main vision of CORE, a cooperation between students and professional associates in Leuven. Developing innovative techniques for heat extraction from waterbodies is one of the central topics at CORE. Currently, the principle of heat extraction from river surface water by heat pumps is being investigated, with the aim of supplying heat to residential buildings in Leuven through this method.

This master's thesis researches the heat potential of the river Dyle in and near the city of Leuven. In addition, the resulting temperature drop in the river and its influence is analyzed. Two MATLAB models are created to answer these research questions. Both models simulate the temperature of a river by modeling the mass flow and the different heat exchange processes that define the heat budget of a river. The models differ in their approach to model the mass flow and the temperature relation between subsequent locations in the river. However, the models show nearly identical behaviour when a comparison is made, which signifies that the two modeling methodologies are correct. The accuracy of both models is further assessed by conducting tests across different fields and seasons based on online data sets. Based on these tests, it is concluded that both models show accurate behaviour which enables them to assess the heat potential of a river correctly. From the obtained results on heat potential, it is shown that the ambient heat stored in the river Dyle can be used to fully replace heating through gas in all residential buildings in the city of Leuven during each month of the year. This signifies that, after heat extraction, the river temperature does not experience a drop of more than $3°C$ along the entire river, which is defined as a critical value in this research based on regulations from the Vlaamse Milieu Maatschappij (VMM). The temperature drop due to heat extraction is calculated for the month of February and July within this research, with the maximum drop reaching $1.66°C$ in February. Since the critical temperature drop of $3°C$ is not attained through heat extraction in Leuven, additional heat can be extracted by cities further downstream. Accordingly, the heat demand and potential for Mechelen is analyzed within this research and results indicate the applicability of heat extraction from surface water for this city as well.

This research can be used as a tool for assessing the influence of heat extraction at any location in any river. Through this capability, the research should aid the implementation of systems for heat extraction from surface water in any city.

Keywords: Heat extraction, Surface water, River temperature, CORE, KU Leuven, MATLAB model

Table of Contents

List of Figures

List of Tables

List of Symbols

A	:	albedo factor	[/]
A_c	:	cross sectional area of river	$[m^2]$
$A_{streambed}$	:	streambed surface	$[m^2]$
$A_{surface}$	:	area of the river surface	$[m^2]$
A_{var}	:	amplitude of variation for T_{air} and T_{ground}	$[^\circ C]$
a	:	empirical constant	$[m/(s \cdot kPa)]$
b	:	empirical constant	$[1/kPa]$
C_b	:	Bowen coefficient	$[hPa/K]$
C_L	:	cloud cover	[/]
c_p	:	specific heat of main river	$[J/(kg \cdot K)]$
$c_{p_{inflow}}$	:	specific heat of inflow	$[J/(kg \cdot K)]$
D_h	:	hydraulic diameter of river	$[m]$
D_L	:	dispersion coefficient	$[m^2/s]$
D_{river}	:	river depth	$[m]$
dt	:	time step	$[s]$
dx	:	longitudinal distance step (length of element or control volume)	$[m]$
E	:	rate of evaporation	$[m/s]$
f	:	friction factor	[/]
$f(v_{wind})$	:	wind speed function	$[W/(m^2 \cdot hPa)]$
g	:	gravitational acceleration	$[m/s^2]$
$h_{int.conv.}$	:	internal forced convection coefficient	$[W/(m^2 \cdot K)]$
$k_{int.conv.}$	:	thermal conductivity of river	$[W/(m \cdot K)]$
k_{soil}	:	thermal conductivity of ground	$[W/(m \cdot K)]$
L_e	:	latent heat of vaporization	$[J/kg]$
L_{soil}	:	distance from streambed where ground temperature is uniform	$[m]$
$\dot{m}$	:	mass flow rate of the stream	$[kg/s]$
$\dot{m}_{inflow}$	:	mass flow of inflow	$[kg/s]$
N	:	number of elements or control volumes in the studied river	[/]
$Nu_{int.conv.}$	:	Nusselt number (for internal forced convection)	[/]
$Pr_{int.conv.}$	:	Prandtl number (for internal forced convection)	[/]
p_a	:	actual vapor pressure	$[kPa]$
p_{air}	:	air pressure	$[hPa]$
p_o	:	reference air pressure	$[hPa]$
p_s	:	saturation vapor pressure	$[kPa]$
p_s^w	:	saturation vapor pressure of the evaporating surface	$[kPa]$

Q	:	total rate of heat transfer into or out of the river	$[W]$
$Q_{estimate}$	:	estimated rate of heat transfer between water column and ground	$[W]$
$Q_{heat.extr.}$	:	rate of heat transfer due to heat extraction from surface water	$[W]$
Q_{inflow}	:	rate of heat transfer due to inflow	$[W]$
q	:	total heat flux transferred to or from the river	$[W/m^2]$
$q_{ext.conv.}$	:	external forced convection heat flux	$[W/m^2]$
q_{in}	:	incoming solar radiative fluxes	$[W/m^2]$
$q_{int.conv.}$	:	internal forced convection heat flux	$[W/m^2]$
$q_{latentheat}$	:	latent heat flux	$[W/m^2]$
$q_{lw,atmospheric}$	:	atmospheric longwave radiation	$[W/m^2]$
$q_{lw,backradiation}$	:	longwave back radiation from the stream surface	$[W/m^2]$
$q_{lw,landcover}$	:	longwave radiation from landcover	$[W/m^2]$
$q_{lw,net}$	:	net longwave radiation	$[W/m^2]$
$q_{shortwave}$	:	shortwave radiation	$[W/m^2]$
$Re_{int.conv.}$	:	Reynolds number (for internal forced convection)	[/]
R_{ground}	:	thermal conduction resistance	$[K/W]$
R_{water}	:	thermal convection resistance	$[K/W]$
S	:	channel slope	[/]
SF	:	shading factor	[/]
$s_{1,t}$	:	first approximation of the slope	$[^\circ C/s]$
$s_{2,t}$	:	second approximation of the slope	$[^\circ C/s]$
T_a	:	air temperature	$[K]$
$T_{estimate}$	:	estimated water temperature after occurrence of inflow	$[K]$
T_{ground}	:	ground temperature (dry soil)	$[K]$
T_{inflow}	:	initial temperature of inflow	$[K]$
$T_{streambed}$	:	streambed temperature	$[K]$
T_w	:	water temperature	$[K]$
$T_{w,e}$	:	end temperature of a river part	$[K]$
$T_{w,i}$	:	inlet temperature of a river part	$[K]$
$T_{w,mixed}$	:	bulk water temperature after mixing	$[K]$
t	:	time	$[s]$
$time_{sim}$	:	total time of the river simulation	$[s]$
vts	:	view to sky coefficent	[/]
v_{shear}	:	shear velocity	$[m/s]$
v_{stream}	:	velocity of the stream	$[m/s]$
v_{wind}	:	wind velocity	$[m/s]$
W_{river}	:	river width	$[m]$
$X_{daytime}$	:	counter running from 1 to $\Delta t_{element}/hours_{daylight}$	[/]
$X_{nighttime}$	:	counter running from 1 to $\Delta t_{element}/(24 - hours_{daylight})$	[/]
x	:	longitudinal distance	$[m]$
Y	:	Y-value on variation graphs, corresponding to temperature	$[^\circ C]$
Y_{avg}	:	24-hour average Y-value, relating to input for T_{air} and T_{ground}	$[^\circ C]$
$\Delta t_{element}$	:	time step within every element	$[s]$
ε_{atm}	:	emissivity of the atmosphere	[/]
ε_w	:	emissivity of the stream	[/]
$\rho_{int.conv.}$	:	mass density (for internal forced convection)	$[kg/m^3]$
ρ_w	:	density of water	$[kg/m^3]$
σ	:	Stefan-Boltzmann constant	$[W/(m^2 \cdot K^4)]$
τ	:	shear stress	$[kg/(m \cdot s^2)]$
$\mu_{int.conv.}$	:	dynamic viscosity (for internal forced convection)	$[kg/(m \cdot s)]$

Chapter 1

Introduction

1.1 Problem Statement

The era we are currently living in is marked as a period of significant human impact on our climate and ecosystems. During this so called Anthropocene, efficient use of energy can significantly reduce our impact on the environment [1]. While energy efficiency improvements have been documented for various applications, developments in efficient energy use for the heating of buildings are limited [2]. Current practices frequently exploit the finite supply of fossil fuels and burning them increases the amount of greenhouse gasses in the atmosphere. A new and more rational approach to heat buildings consists of using the ambient energy stored in rivers. This is done by a heat pump that extracts heat from surface water of the waterbody, a method currently researched in Leuven using the river Dyle. A restriction of $3°C$, based on regulations from the Vlaamse Milieu Maatschappij (VMM), applies on the amount of heat that can be extracted in order to avoid altering the thermal regime of the river. Therefore, a river model is needed to predict this impact. In literature, methods to model a river have been discussed. Many of these models are site-specific and therefore difficult to adapt when a different river is concerned. This poses limitations on their applicability on the Dyle. Moreover, an adaptable and flexible model enables the user to accurately investigate different sites of interest. Furthermore, most existing models have no implementation for extracting heat and thereby do not assess the influence of heat extraction. Accordingly, river temperature regeneration after heat extraction has not yet been assessed which makes it currently impossible to estimate the potential of heat extraction in cities located further downstream.

1.2 Research Questions

The goal of this research is to study the existing heat potential of the river Dyle in Leuven. In addition, induced temperature drops are investigated and their influence on the downstream properties of the river is analyzed. This is performed based on an impact analysis that studies physical and ecological consequences as well as the remaining downstream applicability after heat extraction from the Dyle at the location of interest. A mathematical river model is needed to simulate the behavior of a river within a designated area and draw conclusions on the available heat potential. This river simulation will be based on meteorological parameters and flow conditions, whereby the effect of altering specific input parameters on the heat potential is evaluated. The designed model is expected to be adaptable, making it applicable to various rivers and regions of interest. Furthermore, the model is required to accurately simulate the river, which has to be evaluated by tests using online data sets as well as physical testing.

1.3 Paper Outline

Chapter 1 introduces the nature of the work, defines the goal of the research and gives an overview on the content of the paper's chapters. In chapter 2, fundamental concepts are explained that enable the understanding of the subsequent chapters. These concepts include heat extraction from surface water and the concept of a river model. The latter section will elucidate on the heat exchange processes that induce a river temperature and the mathematical basis for solving a temperature change due to these heat fluxes. Chapter 3 discusses the river models that have been created and consists of a validation of both models through a grid study and tests based on online river data. Furthermore, chapter 3 also proposes a methodology for conducting a physical test. In chapter 4, the results on the heat potential of the Dyle are described. First, the study site is detailed. Afterwards, the heat demand for the described study site is assessed, followed by the analysis of the available heat potential in the river. Subsequently, a sensitivity and impact analysis will be conducted. Chapter 5 and chapter 6 summarize the conclusions and propose further research respectively.

1.4 Adaption of Goals of This Master's Thesis Due to Corona Protective Measures

In accordance to the Corona protective measures, a physical test of the created models could not be conducted. The goal of this test was to assess the accuracy of the models in further detail than is accomplished by tests conducted using online data sets. As a consequence, this research only proposes a method for conducting a physical test in section 3.4.3 without results on the actual implementation of this testing method.

Chapter 2

Theoretical Framework

2.1 Heat Extraction from Surface Water

Rivers can be used as a heat source or a heat sink for the heating or cooling of buildings respectively. These types of thermal use are renewable, reliable, and can considerably lower the amount of fossil fuels burned for heating or cooling with current practices [3]. A surface water heat pump system is the most common method applied for heating and cooling of buildings when a nearby lake or river can be used as a heat source or sink. Within this method, two types of systems can be adopted: an open loop or a closed loop system. These systems are depicted in figure 2.1 and figure 2.2 respectively.

In an open loop system, river water is directly pumped to the heat pump unit of a building. In the case of heating, the heat pump will extract heat from the network in which the river water flows (heat source) to another network that can provide heat inside the building (heat sink). After the extraction of heat, the cooled water from the river water network (see figure 2.1) will be discharged into the river [4].

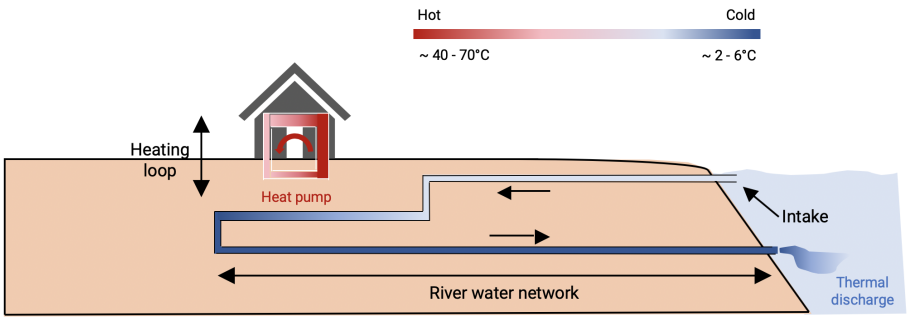

Figure 2.1: Schematic for heat extraction from surface water using an open loop system

A closed loop system consists of an enclosed network which circulates heat transfer fluid (mixture of antifreeze and water) to transfer heat to/from surface water for cooling/heating. Heat exchange happens twice in this system compared to a single heat exchange in the open loop system. First, heat is exchanged between the river water and the heat transfer fluid that flows through coiled pipes (see figure 2.2). Afterwards, heat is exchanged between the network of the heat transfer fluid and the interior network of the building by the heat pump [4].

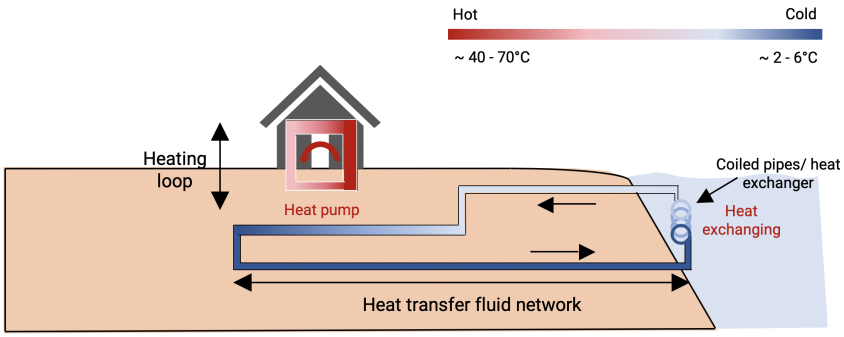

Figure 2.2: Schematic for heat extraction from surface water using a closed loop system

Open loop systems are more efficient than closed loop systems due to the great conductivity of water compared to the antifreeze that circulates in the closed loop system. Moreover, heat is extracted twice in a closed loop system resulting in more losses than in an open loop system. On the other hand, poor quality of river water can be an issue for an open loop system. Therefore, a filter should be installed to prevent heat pump damage in an open loop system [5].

The required heat of a specific study site can be found from the accumulated energy needed for the heating of buildings in a designated area. Once this required energy is obtained, it can be investigated whether the studied river is able to supply this amount of energy without the river temperature dropping below a critical predefined temperature of $3^{\circ}C$ (see section 4.4).

2.2 Concept of River Temperature Models

River temperature models calculate a temperature change in a volume of water by simulating the mass transfer within a river and the heat that enters and leaves the waterbody. In section 2.2.1, two different methods that calculate stream temperature changes are analyzed. Consequently, this results in two different models which are both discussed in chapter 3. Section 2.2.2 details the processes that define the heat that enters and leaves the waterbody.

2.2.1 Mathematical basis of stream temperature models

In order to model the temperature change of a river, an understanding of the different variables on which the river temperature depends is required. These specific variables are heat transfer and mass transfer. Heat transfer relates to several heat exchange processes that alter the amount of heat in a defined volume of water [6]. These processes are detailed in section 2.2.2. Heat exchange is closely related to the time of the day, the season, and the river surroundings and characteristics. Mass transfer concerns the transport of flow volume in the river which is a result of both advection and dispersion [6].

As previously stated, two different mathematical approaches will be used to calculate a change in temperature. The first method uses a Lagrangian approach, which indicates that a fluid volume is followed throughout the river to solve for its temperature variation. The second method is based on an Eulerian approach implying that the temperature over the entire river is analyzed at every point in time using a fixed reference frame.

Two assumptions will be made to apply both methods. The first assumption is the fundamental approximation of a one-dimensional flow. That is, properties of the fluid (velocity, pressure, density, viscosity, and temperature) are assumed to be constant in every direction but the flow direction. As a result, at any cross section normal to the flow, uniform values are used for all properties [7]. A second approximation holds that both methods assume a steady-flow, which indicates that flows, velocities, and river dimensions do not change over time [6].

Temperature equation for a moving control volume

The first method for solving a temperature change is based on a Lagrangian approach and uses heat transfer concepts described by Çengel and Ghajar in 'Heat and Mass Transfer: Fundamentals and Applications' [7].

Numerous systems that involve mass flow in and out of a system can be modeled as control volumes. These control volumes are often analyzed under steady-flow conditions. During a steady-flow process, the amount of energy entering a control volume must equal the amount of energy leaving the volume. Thus, the total energy (heat, work, mass flow) remains constant [7]. In the case of river models, the control volume reduces to the part of the river that is analyzed for its change in temperature (see figure 2.3).

The amount of mass that flows through the cross section defined by the control volume is called the mass flow rate. The mass flow rate is dependent on the cross section, the velocity of the flow, and the density of the fluid (water in the case of a river). Since a one-dimensional approach is used, properties (velocity, pressure, density, viscosity, and temperature) are uniform at any cross section normal to the flow and the mass flow rate of the stream is calculated by equation (2.1) [7].

$$\dot{m} = \rho_w \cdot v_{stream} \cdot A_c \tag{2.1}$$

where

$\dot{m}$	:	mass flow rate of the stream	$[kg/s]$
ρ_w	:	density of water	$[kg/m^3]$
v_{stream}	:	velocity of the stream	$[m/s]$
A_c	:	cross sectional area of river	$[m^2]$

The density of water is dependent on the temperature of the river water.

When a river is analyzed as a steady-flow system, the mass flow rate at which water enters the part of the river that is been analyzed must equal the mass flow rate at which water leaves [7]. This means the mass flow rate will be constant throughout the entire river.

The energy balance for a river under the steady-flow condition can be expressed with equation (2.2). In this equation, it is also assumed that kinetic and potential energies are negligible and there is no work interaction to the river. Consequently, the overall energy transfer reduces to the heat transfer that enters or leaves the river. The different heat fluxes that determine the total transferred heat are detailed in 2.2.2. The part on the right side of the equal sign in equation (2.2) is the mass transfer component. More specifically, it is called advection. Advection can be defined as the transport of water and heat by river flow. Advection is a process driven by gravity and accordingly only occurs in the downstream direction,

which is defined as the positive longitudinal direction of the river [6].

$$Q = \dot{m} \cdot c_p \cdot (T_w, e - T_w, i) \tag{2.2}$$

where

Q	:	total rate of heat transfer into or out of the river	$[W]$
c_p	:	specific heat of main river	$[J/(kg \cdot K)]$
T_w, e	:	end temperature of a river part	$[K]$
T_w, i	:	inlet temperature of a river part	$[K]$

Similar to the density of water, the specific heat will depend on the temperature of the water.

In a given situation where the inlet temperature of a certain part of the river is known (point 1 in figure 2.3) as well as the heat transferred to or from the analyzed part (Q), the end temperature of that river section can be found (point 2 in figure 2.3). Note that in order to practice a Lagrangian approach, a smaller control volume is used which will follow the river and equation 2.2 solves for the next outlet temperature every time the control volume is shifted further downstream. Doing so, an end temperature at point 2 in figure 2.3 will again result after multiple iterations. This Lagrangian solving method for a moving control volume is further and more thoroughly explained in the model implementation of the so called 'Fluid Trajectory Model' (see section 3.1).

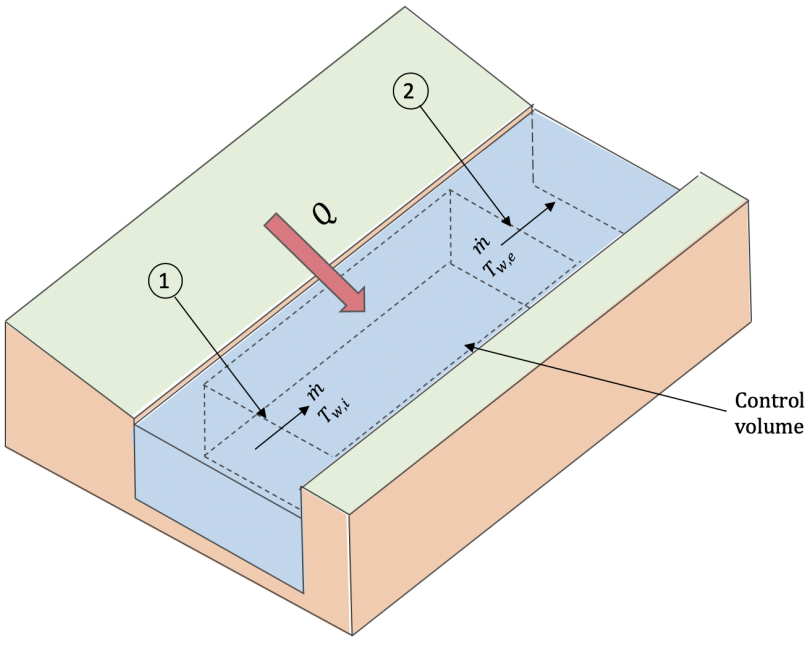

Figure 2.3: Schematic of a river for steady-flow conditions

Temperature equation for stationary control volumes

The second calculation method described in this paper is most often applied in literature. This method uses a one-dimensional heat advection-dispersion equation [8], defined with formula (2.3). This equation enables the implementation of an Eulerian method to solve for changing temperatures at every location in the river over time. Note that each location corresponds to a stationary control volume.

$$\frac{\partial T_w}{\partial t} = \overbrace{\underbrace{-v_{stream} \cdot \frac{\partial T_w}{\partial x}}_{\text{Advection}} + \underbrace{D_L \cdot \frac{\partial^2 T_w}{\partial x^2}}_{\text{Dispersion}}}^{\text{Mass transfer}} + \overbrace{\frac{q}{c_p \cdot \rho_w \cdot D_{river}}}^{\text{Heat transfer}} \tag{2.3}$$

where

T_w	:	water temperature	$[K]$
t	:	time	$[s]$
x	:	longitudinal distance	$[m]$
D_L	:	dispersion coefficient	$[m^2/s]$
q	:	total heat flux transferred to or from the river	$[W/m^2]$
D_{river}	:	river depth	$[m]$

The second order differential equation consists of rate change in temperature, advection, dispersion, and heat transfer. While advection and heat transfer are both implemented in equation (2.2), dispersion and the temperature dependency in time are additional expressions compared to the temperature equation for a moving control volume. It can be shown that equation (2.3) reduces to equation (2.2) when dispersion and the transient temperature factor are neglected. If both the left part of equation (2.3) and the dispersion term are equalled to zero and afterwards the advection and heat transfer term are rearranged, equation (2.2) results. However, remark that this temperature dependency in time is inherently present in the Lagrangian solving method used together with equation (2.2), which is further detailed in section 3.1.

Similar to advection, dispersion accounts for the transportation of water and energy throughout the river. However, while advection only involves downstream transfer, dispersion occurs in both the downstream and upstream direction of the river. Dispersion refers to the effect of turbulent mixing and molecular diffusion [6] (see figure 2.4).

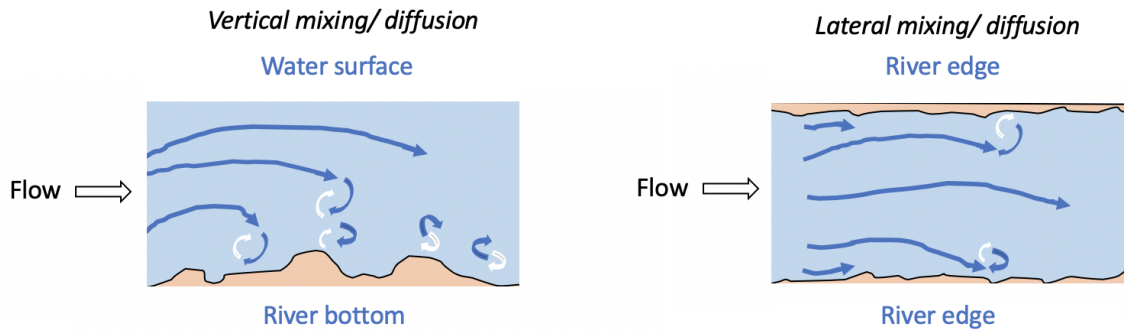

Figure 2.4: Turbulent flow represented in the vertical and longitudinal direction of the flow

The dispersion coefficient is a variable that calculates the turbulent diffusion using equation (2.4) [9].

$$D_L = 0.011 \cdot \frac{v_{stream}^2 \cdot W_{river}^2}{v_{shear} \cdot D_{river}} \tag{2.4}$$

where

W_{river}	:	river width	$[m]$
v_{shear}	:	shear velocity	$[m/s]$

Shear velocities at the river boundaries originate due to frictional forces exerted upon the flowing water. Shear velocities can be described as a function of shear stress using equation (2.5) [10].

$$v_{shear} = \sqrt{\frac{\tau}{\rho_w}} \tag{2.5}$$

where

τ	:	shear stress	$[kg/(m \cdot s^2)]$

Shear stresses are a function of the slope of the river and the river depth, they are calculated with equation (2.6) [10].

$$\tau = \rho_w \cdot g \cdot D_{river} \cdot S \tag{2.6}$$

where

g	:	gravitational acceleration	$[m/s^2]$
S	:	channel slope	[/]

The gravitational acceleration equals $9.81\ m/s^2$. The channel slope depends on the site/river which is studied and is therefore not a constant, it is calculated by dividing the change in elevation of the river with its length.

The temperature equation for stationary control volumes (equation (2.3)) solves for river temperatures with respect to location and time. That is, at every location, temperatures are calculated with respect to time and thus, at a certain moment in time, temperatures at every location can be found. This combination allows to solve for an outlet temperature of a certain river section when the inlet temperature and the transferred heat are known for that specific section. The method to calculate this outlet temperature uses a finite element approach with stationary control volumes (Euler) that is described in the explanation of the Finite Element Model (section 3.2).

2.2.2 Heat exchange processes defining stream temperature

Overview of the heat fluxes determining the temperature of a river

As described in section 2.2.1, heat exchange processes control the river water temperature. In total, seven types of heat fluxes/transfers are considered to contribute to the heat budget of a river as represented in figure 2.5. Shortwave radiation, longwave radiation, latent heat flux, external forced convection, and internal forced convection define the meteorological driven heat fluxes. In addition, inflows and heat extractions are considered [11].

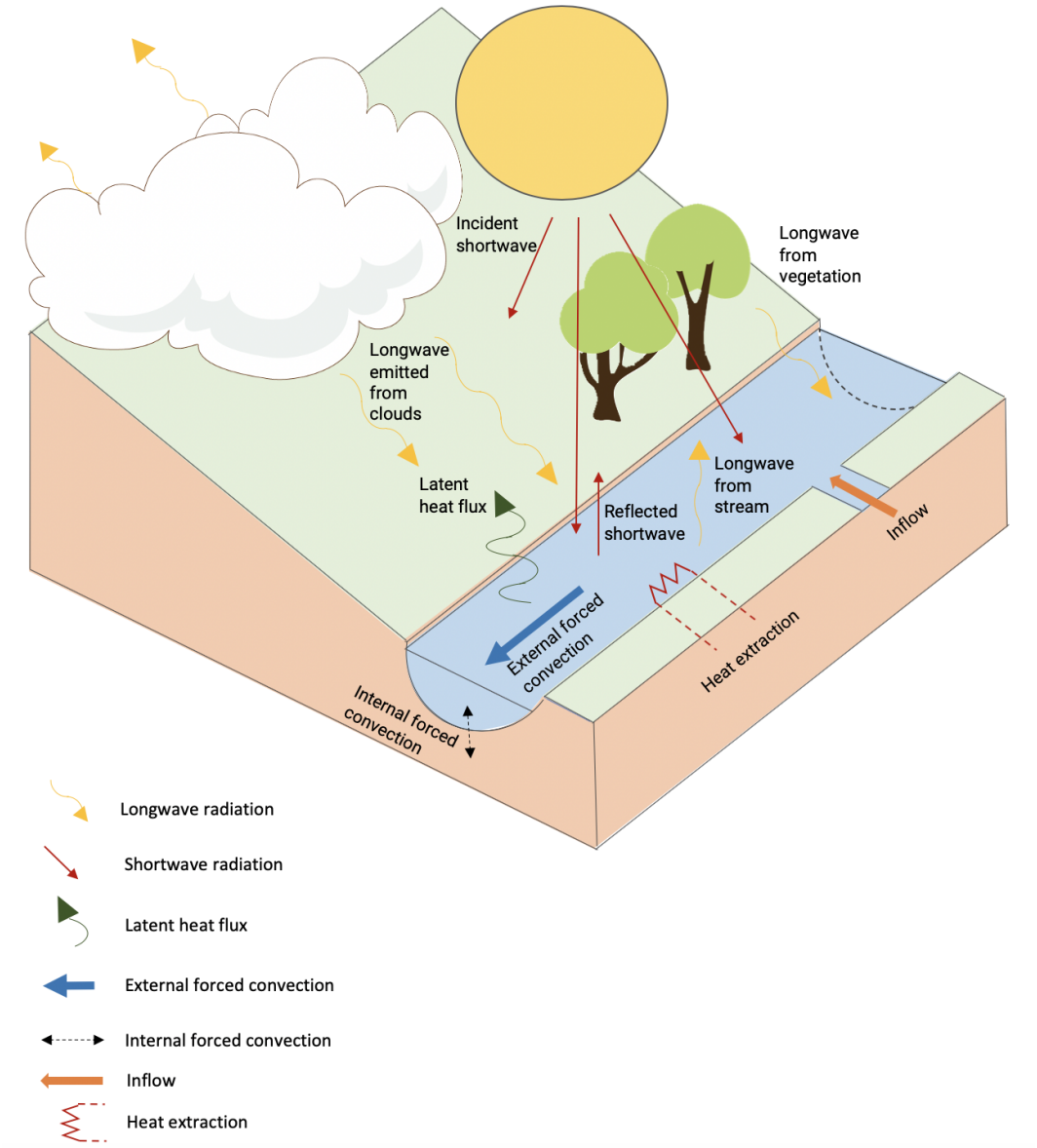

Figure 2.5: Schematic of heat fluxes controlling river temperature

Shortwave solar radiation

Two radiative fluxes contribute to the heat budget of a river environment: shortwave and longwave radiation. The former one is, generally speaking, the largest heat source for a river [12]. Shortwave radiation is sensitive to various elements such as:

- Position of the sun; radiation values are time- (day/night) and date- (seasonally) dependent. Higher values occur during summer and spring, and when the solar zenith angle is minimal (solar noon).
- Absorption and scattering; sunlight can be reflected by clouds and absorbed by atmospheric particles, gases, and dust.
- Shading; dependent on the vegetation conditions along the river.
- Reflection; a fraction of the solar radiation will be reflected by the water surface.

Taking these parameters into account, the net shortwave heat flux can be defined by equation (2.7).

$$q_{shortwave} = (1 - SF) \cdot q_{in} \cdot (1 - A) \tag{2.7}$$

where

$q_{shortwave}$	:	shortwave radiation	$[W/m^2]$
q_{in}	:	incoming solar radiative fluxes	$[W/m^2]$
SF	:	shading factor	[/]
A	:	albedo factor	[/]

The incoming solar radiative fluxes (influenced by scattering and absorption) are corrected by the shading factor and the albedo factor. The former one takes into account the amount of radiative flux lost due to vegetation conditions. The higher the value for SF, the more fluxes are lost. Shading is dependent of season, with a higher value for spring and summer (thicker foliage) compared to fall and winter (trees have dropped their leaves). The albedo factor accounts for the part of the solar flux that is being reflected by the river and is site-specific. A higher value for A signifies more reflection. Albedo, depending mainly on the color of a surface, ranges from 1% to 10% for water. In river models, the value for albedo is assumed to be constant along the stream [13].

Longwave radiation

Longwave radiation will contribute to the heat budget of a river through the following three parameters:

- Radiation coming from the atmosphere.
- Radiation from the river itself.
- Radiation emitted by the landcover alongside the river.

The radiative electromagnetic wavelengths emitted by those elements are longer than the wavelengths of solar insolation (shortwave radiation), hence longwave radiation. The total longwave radiation flux is simply the instantaneous summation of the three different parameters listed above.

Atmospheric longwave radiation is calculated by equation (2.8).

$$q_{lw,atmospheric} = \varepsilon_w \cdot \varepsilon_{atm} \cdot vts \cdot \sigma \cdot T_a^4 \tag{2.8}$$

where

$q_{lw,atmospheric}$	:	atmospheric longwave radiation	$[W/m^2]$
ε_w	:	emissivity of the stream	[/]
ε_{atm}	:	emissivity of the atmosphere	[/]
vts	:	view to sky coefficient	[/]
σ	:	Stefan-Boltzmann constant	$[W/(m^2 \cdot K^4)]$
T_a	:	air temperature	$[K]$

The emissivity of water (ε_w), and thus the stream, has a constant value of 0.97. The view to sky coefficient ranges from 0 to 1, indicating no view to sky to a clear view respectively [11]. The coefficient is calculated by the ratio of the diffuse sky radiation received by a surface to the radiation which would be received by the same surface if it were completely exposed to the sky [14]. The emissivity of the atmosphere is dependent on multiple factors and therefore not constant. However, it can be approximated using formula (2.9) [15].

$$\varepsilon_{atm} = 1.72 \cdot \left(\frac{p_a}{T_a}\right)^{\frac{1}{7}} \cdot \left(1 + 0.22 \cdot C_L^2\right) \tag{2.9}$$

where

p_a	:	actual vapor pressure	$[kPa]$
C_L	:	cloud cover	[/]

The dimensionless cloud cover parameter accounts for the percentage of overcast (0 for no clouds and 1 for complete overcast). The actual vapor pressure can be calculated from the saturation vapor pressure using the relative humidity of the air, as in equation (2.10) [16].

$$p_a = \left(\frac{H}{100\%}\right) \cdot p_s \tag{2.10}$$

where

p_s	:	saturation vapor pressure	$[kPa]$
H	:	relative humidity	$[\%]$

Saturation vapor pressure is expressed with equation (2.11) [16].

$$p_s = 0.611 \cdot exp\left(\frac{17.27 \cdot (T_a - 273)}{237.3 + T_a - 273}\right) \tag{2.11}$$

The second parameter which defines the net long wave radiation is the back radiation from the stream surface and is calculated using formula (2.12) [6]. Since this heat flux comprises heat fluxes leaving the river, resulting in heat loss, the back radiation will be a negative component. As can be seen from formula (2.12), back radiation is dependent on the water temperature (T_w) in Kelvin.

$$q_{lw,backradiation} = -\varepsilon_w \cdot \sigma \cdot T_w^4 \tag{2.12}$$

where

$q_{lw,backradiation}$: longwave back radiation from the stream surface $[W/m^2]$

Lastly, the net longwave radiation is influenced by the radiation from the riparian vegetation, which is largely controlled by physical characteristics (e.g. vegetation density and height) [6]. The radiation emitted by the landcover is defined by equation (2.13).

$$q_{lw,landcover} = \varepsilon_w \cdot (1 - vts) \cdot 0.96 \cdot \sigma \cdot T_a^4 \tag{2.13}$$

where

$q_{lw,landcover}$: longwave radiation from landcover $[W/m^2]$

From equation (2.8), (2.12) and (2.13) the net longwave radiation can be defined with equation (2.14). The formula comprises two positive fluxes and one negative flux.

$$q_{lw,net} = q_{lw,atmospheric} + q_{lw,backradiation} + q_{lw,landcover} \tag{2.14}$$

where

$q_{lw,net}$: net longwave radiation $[W/m^2]$

Latent heat flux

Latent heat flux is either the energy lost from the river when water evaporates, or the energy gained when there is condense to the waterbody [16]. Latent heat flux is calculated by equation (2.15) and the resulting value will be positive when condensation occurs and negative in case of evaporation.

$$q_{latentheat} = -\rho_w \cdot L_e \cdot E \tag{2.15}$$

where

$q_{latentheat}$	:	latent heat flux	$[W/m^2]$
L_e	:	latent heat of vaporization	$[J/kg]$
E	:	rate of evaporation	$[m/s]$

The density of water and the latent heat of vaporization are both a function of the water temperature. The latter one can be estimated by equation (2.16) [17].

$$L_e = 10^6 \cdot (2.501 - 0.002361 \cdot T_w) \tag{2.16}$$

The complexity of equation (2.15) lays in the calculation of the rate of evaporation. In literature, two methods are used to express E. Either the Penmann combination for open water is used or mass transfer methods are applied. In this paper, the mass transfer method is used following the approach of Dingman [16] resulting in equation (2.17).

$$E = (a + b \cdot v_{wind}) \cdot (p_s^w - p_a) \tag{2.17}$$

where

a	:	empirical constant	$[m/(s \cdot kPa)]$
b	:	empirical constant	$[1/kPa]$
v_{wind}	:	wind velocity	$[m/s]$
p_s^w	:	saturation vapor pressure of the evaporating surface	$[kPa]$

The constant values for a and b depend on site specific parameters (height at which actual vapor pressure and wind speed are measured) and therefore vary in literature. Boyd and Kasper [6] provide values from different studies. The constants determined by Dunne and Leopold for a and b are used in the models of this paper [18]. The values are as follows:

a : $1.505 \cdot 10^{-8}$
b : $1.6 \cdot 10^{-8}$

The saturation vapor pressure of the evaporating surface in equation (2.17) is calculated similar to equation (2.11). The air temperature is replaced with the temperature of water as can be seen in equation (2.18).

$$p_s^w = 0.611 \cdot exp\left(\frac{17.27 \cdot (T_w - 273)}{237.3 + T_w - 273}\right) \tag{2.18}$$

External convection

External convection defines the heat flux between the surface water of the river and the ambient air, when they are at different temperatures. More specifically, external forced convection is applied for this heat transfer process as both the river water and the ambient air will be in motion. Air will flow due to the phenomenon of wind, while water will move with the river stream.

In literature, different formulas are presented to compute this heat exchange process. A common expression for the external forced convection includes the Bowen ratio, which represents a constant of proportionality between the external convection heat flux and the latent heat flux at the air-water interface [6]. Based on this ratio, the formula for external convection heat flux (2.19) is derived [13].

$$q_{ext.conv.} = C_b \cdot \frac{p_{air}}{p_0} \cdot f(v_{wind}) \cdot (T_a - T_w) \tag{2.19}$$

where

$q_{ext.conv.}$	:	external forced convection heat flux	$[W/m^2]$
C_b	:	Bowen coefficient	$[hPa/K]$
p_{air}	:	air pressure	$[hPa]$
p_0	:	reference air pressure	$[hPa]$
$f(v_{wind})$	:	wind speed function	$[W/(m^2 \cdot hPa)]$

The Bowen coefficient, proportional to the Bowen ratio, has a value of approximately $0.62\ hPa/K$ [13]. The reference air pressure denotes atmospheric pressure and its value is defined at $1013\ hPa$. The wind speed function is an empirical proportionality factor in function of the wind speed. This parameter contains site-specific coefficients that can be estimated based on meteorological data. One of many relations available in literature has to be selected when calibration of the wind speed function is not possible in a practical application [13]. The general pattern for the wind speed function states that increasing wind speed enhances the rate of external forced convection heat transfer, whereby the value of proportionality depends on the chosen formula [13]. In this research, the wind function from Trabert (1896) using a square root relation is applied [19]. This wind speed function is given by equation (2.20).

$$f(v_{wind}) = 11.25 \cdot \sqrt{v_{wind}} \tag{2.20}$$

Internal convection

Internal convection describes the heat transfer between river water and its surrounding streambed. This is also a form of forced convection as the water is forced to flow over the streambed due to the discharge of the river. The streambed is defined as a moist transition layer between river water and dry soil. This dry soil corresponds to the ground layer where void spaces resulting from the soil's porosity level are no longer filled with river water. The streambed layer is constituted out of various types and sizes of alluvium, where alluvium itself consists of depositional materials and substrate that underlies the stream channel such as silt, sand, clay, and gravel [6]. Briefly, the streambed layer is a ground layer saturated with water and will therefore exhibit particular thermal properties.

The general formula to calculate internal forced convection is given by equation (2.21).

$$q_{int.conv.} = h_{int.conv.} \cdot \frac{T_{w,i} - T_{w,e}}{ln[(T_{streambed} - T_{w,e})/(T_{streambed} - T_{w,i})]} \tag{2.21}$$

where

$q_{int.conv.}$	:	internal forced convection heat flux	$[W/m^2]$
$h_{int.conv.}$	:	internal forced convection coefficient	$[W/(m^2 \cdot K)]$
$T_{streambed}$	:	streambed temperature	$[K]$

Note that this formula (2.21) is only valid when convection with a constant surface temperature is assumed. This corresponds to a constant streambed temperature ($T_{streambed}$) in the case of a river. Another important remark is the presence of both the initial ($T_{w,i}$) and final ($T_{w,e}$) water temperatures, corresponding to the temperatures upstream and downstream of a given river length that is studied respectively.

Figure 2.6 gives an accurately representation of the internal forced convection heat transfer process. Water is flowing through an open rectangular channel and exchanges heat with its surrounding streambed. Four crucial temperatures are drawn: the initial and final water temperatures, the streambed temperature, and the ground temperature (T_{ground}). At the start of a predefined river length, the initial water temperature is measured or estimated.

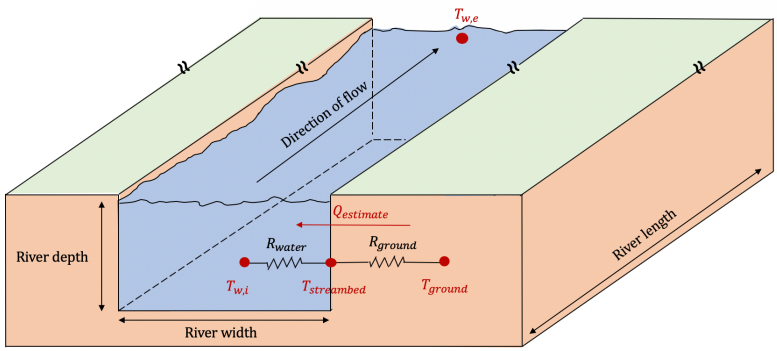

Figure 2.6: Thermal resistance network for internal forced convection: estimation of streambed temperature

As previously stated, the internal forced convection heat flux ($q_{int.conv.}$) is the heat transferred between the streambed and the river water. Therefore, the constant temperature of the streambed needs to be estimated in order to solve equation (2.21). Since the initial water temperature is known and online data can be used to predict the actual ground temperature (T_{ground}), a thermal resistance scheme is composed (see figure 2.6) to accurately estimate the value of the streambed temperature.

Using the thermal resistance scheme in figure 2.6, the streambed temperature can be calculated using equation (2.22).

$$T_{streambed} = Q_{estimate} \cdot R_{water} + T_{w,i} \tag{2.22}$$

where

$Q_{estimate}$	:	estimated rate of heat transfer between water column and ground (dry soil)	$[W]$
R_{water}	:	thermal convection resistance	$[K/W]$

The estimated rate of heat transfer between the river water and the ground (dry soil) is calculated by equation (2.23).

$$Q_{estimate} = \frac{T_{ground} - T_{w,i}}{R_{water} + R_{ground}} \tag{2.23}$$

where

T_{ground}	:	ground temperature (dry soil)	$[K]$
R_{ground}	:	thermal conduction resistance	$[K/W]$

Recall that this estimated rate of heat transfer is not equivalent to the internal forced convection heat flux ($q_{int.conv.}$) calculated by equation (2.21). The latter will be used to calculate the final rate of heat transfer between the water and the streambed, whilst the estimated heat transfer ($Q_{estimate}$) only serves to predict the streambed temperature also needed in equation (2.21). The reason for this distinction lays within the fact that equation (2.21) more accurately approaches the internal flow case [7].

The thermal conductive resistance is calculated by equation (2.24).

$$R_{ground} = \frac{L_{soil}}{k_{soil} \cdot A_{streambed}} \tag{2.24}$$

where

L_{soil}	:	distance from streambed where ground temperature is uniform	$[m]$
k_{soil}	:	thermal conductivity of ground	$[W/(m \cdot K)]$
$A_{streambed}$	:	streambed surface	$[m^2]$

The distance from the streambed (L_{soil}) at which the river has no influence on the ground temperature typically varies between $0.5\ m$ and $1\ m$ [20]. The thermal conductivity of the ground is estimated for dry soil. An average value of $0.8\ W/(m \cdot K)$ is used within this research. This is a relatively low value for the thermal conductivity as ground is a good thermal insulator [20]. It is therefore predicted that the streambed temperature will approach the water temperature for most flow cases.

The streambed surface represents the total surface surrounding the water column. Since the river is approximated as a rectangular open duct, this surface is given by the formula in equation (2.25).

$$A_{streambed} = 2 \cdot D_{river} \cdot L_{river} + W_{river} \cdot L_{river} \tag{2.25}$$

The thermal convective resistance (see equation (2.23)) is calculated by equation 2.26.

$$R_{water} = \frac{1}{h_{int.conv.} \cdot A_{streambed}} \tag{2.26}$$

Note that equation (2.26) contains the same convection coefficient ($h_{int.conv.}$) as the one used to calculate the actual internal forced convection heat flux (see equation (2.21)). This coefficient is calculated using equation (2.27).

$$h_{int.conv.} = \frac{Nu_{int.conv.} \cdot k_{int.conv.}}{D_h} \tag{2.27}$$

where

$Nu_{int.conv.}$	:	Nusselt number (for internal forced convection)	[/]
$k_{int.conv.}$	:	thermal conductivity of river	$[W/(m \cdot K)]$
D_h	:	hydraulic diameter of river	$[m]$

The thermal conductivity, which is used to estimate the internal convection coefficient, solely depends on the water temperature. In this research, the initial water temperature will be used. The thermal conductivity can be found in the tables for properties of saturated water at that specific temperature.

The hydraulic diameter depends on the river geometry (rectangular open duct) and is calculated by equation (2.28).

$$D_h = \frac{4 \cdot D_{river} \cdot W_{river}}{W_{river} + 2 \cdot D_{river}} \tag{2.28}$$

The Nusselt number from equation (2.27) is calculated based on the behavior of the stream. To identify whether the flow is laminar or turbulent, the Reynolds number for the case of internal forced convection has to be determined. Internal flows are said to be fully turbulent whenever their Reynolds number exceeds $10,000$ [7].

The Reynolds number for internal flow is determined with equation (2.29).

$$Re_{int.conv.} = \frac{\rho_{int.conv.} \cdot v_{water} \cdot D_h}{\mu_{int.conv.}} \tag{2.29}$$

where

$Re_{int.conv.}$	:	Reynolds number (for internal forced convection)	[/]
$\rho_{int.conv.}$	:	mass density (for internal forced convection)	$[kg/m^3]$
$\mu_{int.conv.}$	:	dynamic viscosity (for internal forced convection)	$[kg/(m \cdot s)]$

Both the mass density and the dynamic viscosity are determined from the table of properties for saturated water at the initial water temperature. Using equation (2.29), practically every river geometry and stream velocity will result in Reynolds numbers that exceed the turbulent threshold value. Therefore, the turbulent expression for the Nusselt number defined with equation (2.30) can be used.

$$Nu_{intc.conv.} = 0.125 \cdot f \cdot Re_{int.conv.} \cdot Pr_{int.conv.}^{1/3} \tag{2.30}$$

where

f	:	friction factor	[/]
$Pr_{int.conv.}$	:	Prandtl number (for internal forced convection)	[/]

The Prandtl number is found in the table for properties of saturated water at the initial water temperature. The friction factor is determined from equation (2.31). Note that this formula is only valid for $3,000 < Re_{int.conv.} < 5 \cdot 10^6$ [7].

$$f = (0.790 \cdot ln(Re_{int.conv.}) - 1.64)^{-2} \tag{2.31}$$

Referring to equation (2.21), only the final river temperature ($T_{w,e}$) is missing to calculate the internal convection heat flux between streambed and river water. This variable will remain unknown for now, as both

the final river temperature and the internal convection heat flux will be solved using an equation together with all other heat fluxes. In section 3.1, this process is discussed in further detail. Lastly, keeping the final river temperature unknown explains why previously all temperature-dependent properties were evaluated at the initial river temperature.

Inflow

Another heat exchange process that contributes to changes in river temperatures is the occurrence of inflows along the trajectory of the main stream. These inflows will alter the temperature of the main river whenever there is an initial temperature difference between both flows. Note that inflows always increase the total mass flow of the river further downstream. Referring to equation (2.2), inflows will therefore also influence the river temperature even if both the river and the inflow are initially at the same temperature. Inflows can represent side streams when a smaller river joins the main stream. However, in most cases, these inflows will result from e.g. sewage water, industrial waste water, cooling installations, rainfall, etc. Lastly, the assumption of steady-flow does not hold at the location of an inflow due to an increase in total mass flow.

The rate of heat transfer to or from the main river due to the presence of inflows can be translated into equation (2.32).

$$Q_{inflow} = \dot{m}_{inflow} \cdot c_{p_{inflow}} \cdot (T_{inflow} - T_{w,mixed}) \tag{2.32}$$

where

Q_{inflow}	:	rate of heat transfer due to inflow	$[W]$
$\dot{m}_{inflow}$	:	mass flow of inflow	$[kg/s]$
$c_{p_{inflow}}$	:	specific heat of inflow	$[J/(kg \cdot K)]$
T_{inflow}	:	initial temperature of inflow	$[K]$
$T_{w,mixed}$	:	bulk water temperature after mixing	$[K]$

Note that Q_{inflow} represents a rate of heat transfer. It is not applied to a certain surface area and is therefore not a heat flux. A positive result for Q_{inflow} resembles the addition of heat to the main river and an increase in overall river temperature. In this case, the temperature of the inflow (T_{inflow}) will drop to a lower equilibrium value equal to $T_{w,mixed}$. The opposite applies when the inflow is colder than the main stream.

Outflows are not considered as heat exchange processes since they do not directly influence the water temperature. In this research, outflows are defined as streams that separate themselves from the main river and which will not rejoin the studied river further downstream (e.g. split of a river). It is therefore a different phenomenon than heat extraction obtained by the open loop system from section 2.1, where cooled water from the open loop heat exchange does rejoin the main river. As opposed to inflows, outflows do not introduce a heat flux or temperature difference to the river. Similar to inflows, outflows alter the mass flow of the main river. Referring to equation (2.1), this will influence the stream velocity whenever the cross section of the stream does not change proportionally with its mass flow. A new stream velocity results in a different Reynolds number ($Re_{int.conv.}$) that can indirectly alter the river temperature downstream of the outflow. However, changes in stream velocity due to outflows are assumed to be minor within this research. Whenever e.g. a river splits and is separated into two smaller streams with decreased mass flow,

it is assumed that the cross section of each stream decreases accordingly causing only slight changes to the stream velocity. In conclusion, outflows do not directly introduce heat exchange with the main river and their contribution to the river temperature is therefore neglected.

Heat extraction

The final heat exchange process defines heat extraction from the surface water of the river. Heat extraction ($Q_{heat.extr.}$) represents a rate of heat transfer out of the river which has a constant cooling effect on the waterbody. Thus, it is not modelled as a heat flux and this rate of heat transfer will always have a negative value when it contributes in cooling the river. Note that a heat pump can be used for either cooling or heating of buildings. In the former case, the water temperature would increase as the rate of heat transfer from the heat pump to the river has a positive value. However, the application on the cooling of buildings is not studied within this research. As discussed in section 2.1, heat extraction from surface water is put into practice by a heat pump in either an open loop or a closed loop system. In the case of an open loop system, the rate of heat transfer from heat extraction is a result of the heat exchange from the river water directly with the heat pump (see figure 2.1). A closed loop system corresponds to the defined rate of heat transfer due to heat extraction taking place with a local heat exchanger inside the studied river (see figure 2.2). Recall that heat extraction does not alter the mass flow of the main river and solely affects its water temperature.

Chapter 3

Model Implementation

3.1 Fluid Trajectory Model

The first mathematical river model is called the Fluid Trajectory Model. This model is based on the temperature equation for a moving control volume (equation (2.2)) from section 2.2.1. Recall that this equation represents the energy balance for a steady-flow system [7]. The Lagrangian method for a moving control volume and steady-flow principle (constant values for mass flow, velocity, and cross section of the river) are optimally used to develop a straightforward solution strategy and solve for river temperatures over a studied length. This river model is created in MATLAB.

Recalling equation (2.2) and figure 2.3, the final river temperature ($T_{w,e}$) at point 2 of the studied river segment is determined by solving a mathematical heat transfer problem. Consider the initial river temperature ($T_{w,i}$) at point 1 to be known as a result of e.g. sensor measurements or online data sets. From equation (2.1), assuming steady-flow, the mass flow ($\dot{m}$) through the defined control volume is determined. That is, measurements or available data has to be used to find the velocity of the stream (v_{stream}) at point 1, together with the cross section of the river (A_c). The water density (ρ_w) depends on the current water temperature and can be found in the general table for properties of saturated water, using the initial temperature at point 1. For equation (2.2), the specific heat of water (c_p) is also found in a similar manner from the table of saturated water. Lastly, the total rate of heat transfer into or out of the river (Q) has to be determined in order to solve for the unknown final river temperature in equation (2.2). The solution strategy of the Fluid Trajectory Model is visualized in figure 3.1 and figure 3.4.

The calculation of the total rate of heat transfer between the defined control volume and its surroundings is the most extensive segment of this mathematical model. Every heat exchange process that is present will be implemented in the exact same way as described in section 2.2.2. The sum of these heat fluxes, in combination with the surface area that they act on, and the heat transfer of possible inflows and heat extractions results in the total rate of heat transfer into or out of the river represented by equation (3.1).

$$Q = (q_{shortwave} + q_{lw,net} + q_{latentheat} + q_{ext.conv.}) \cdot A_{surface} + q_{int.conv.} \cdot A_{streambed} + Q_{inflow} + Q_{heat.extr.} \quad (3.1)$$

where

$A_{surface}$	:	area of the river surface	$[m^2]$
$Q_{heat.extr.}$	:	rate of heat transfer due to heat extraction from surface water	$[W]$

Some important remarks regarding equation (3.1) need to be made. First, note that the heat exchange processes can be positive, negative or equal to zero. Shortwave solar radiation heat flux is an exception, as this is always positive or equal to zero. A positive solar radiation value is obtained anytime solar radiative fluxes reach the river surface and thus the river is heated. Absence of shortwave radiation and thus a value of zero occurs whenever the sun is under the horizon. Furthermore, heat extraction will always be negative as it constantly cools the river. The contribution of all heat exchange processes combined determines the sign of the total rate of heat transfer into or out of the river, where a positive sign corresponds to heating and a negative sign results in cooling of the river. A second remark on equation (3.1) concerns the contribution of inflows, which is only relevant whenever inflows actually occur. Similarly, heat extraction will only occur at locations where heat pumps are installed. Lastly, recall that the expression for the internal convection heat flux (see equation (2.21) already contains the final water temperature ($T_{w,e}$) at the end of the studied river section. This is the unknown variable which the Fluid Trajectory Model aims to solve. Therefore, the total rate of heat transfer (Q) does not represent a source term and equation (2.2) will be solved numerically within the model.

The area of the river surface corresponds to the top surface of the stream that is directly exposed to ambient air. For the studied river segment or predefined control volume, this surface area is calculated by equation (3.2).

$$A_{surface} = W_{river} \cdot L_{river} \tag{3.2}$$

Up till now, modeling the river temperature always corresponded to solving a single heat transfer problem as represented in figure 2.3. Here, a single constant value for every heat exchange process from 2.2.2 is calculated and therefore, a constant overall rate of heat transfer (Q) is obtained. Consequently, the final river temperature was calculated at the end of the studied river section. It is perceived that solely knowing the initial and final temperature of a predefined river length is not equivalent to accurately modeling the stream in order to draw detailed conclusions on potential heat extraction. For an accurate analysis, the temperature of a certain fluid or control volume moving throughout this river segment (Lagrangian approach of a moving control volume) has to be determined at multiple intermediate locations in between the previously calculated initial and final temperature at both ends. The influence of increasing the number of intermediate temperature locations is detailed in section 3.4.1.

The need for evaluating intermediate river temperatures defines the key concept of the Fluid Trajectory Model. Instead of solving one heat transfer problem where the control volume comprises the entire studied river section, the control volume is now drastically reduced in its longitudinal direction. Thus, the studied river is divided into multiple smaller control volumes or elements. The physical representation of this code implementation is shown in figure 3.1. The heat transfer problem from equation (2.2) is solved subsequently within each smaller element or control volume where the fluid volume is now shifted downstream to the next element with every iteration. Thus, a single control volume representing the fluid volume is shifted downstream between all predefined control volumes that make up the river. The resulting final temperature from each element will serve as the initial temperature for the next element, e.g. T_{w,e_1} equals T_{w,i_2} in figure 3.1. This process is continued until the entire length of the studied river is traveled. In other words, a certain fluid or control volume is followed along the studied river with the stream velocity and when it reaches the next element, the heat transfer problem from figure 2.3 is recalculated using a new initial temperature. This Lagrangian approach of a moving control volume also explains the name of the first mathematical river model, as it consists of a fluid volume which is followed along its trajectory in time and location. At every point in time, only a small fluid section of the studied river (equalling the size of

the control volume) is considered at a certain location along the studied river. The correlation between time and location of this particular fluid volume results from the stream velocity. Thus, every location of the followed fluid volume corresponds to a unique moment in time. Note that the steady-flow assumption remains valid for the entire simulation as the mass flow ($\dot{m}$) in figure 3.1 is assumed constant.

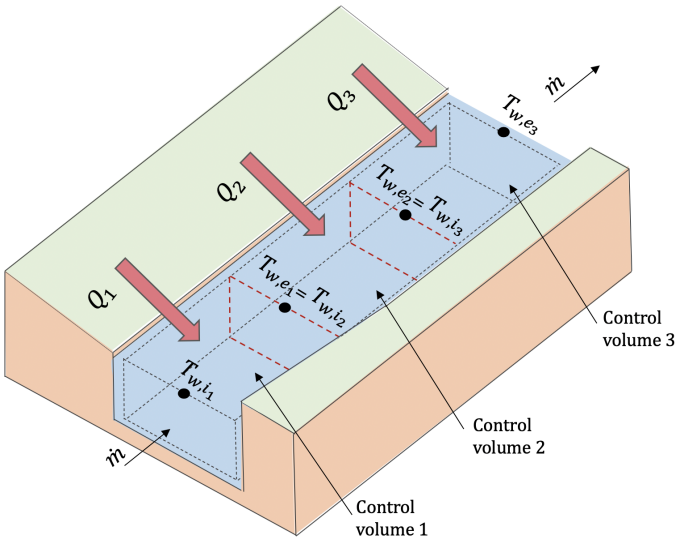

Figure 3.1: Physical representation of the code implementation for the Fluid Trajectory Model

There are a number of advantages to this fluid trajectory approach that enable the Fluid Trajectory Model to closely approximate reality and make it easy to implement. Most importantly, dividing the studied river into smaller elements allows variations in the total rate of heat transfer (Q) into or out of the river. Dependent on the stream velocity, the simulation of a fluid volume flowing downstream along its entire trajectory corresponds to a change in time. The Fluid Trajectory Model allows the user to take this time dependency into account as the contribution of every heat exchange process will be recalculated for every subsequent element. Referring to figure 3.1, every control volume or element has a unique total rate of heat transfer as e.g. Q_2 is not equal to Q_3. In other words, whenever the fluid volume is shifted one element further downstream to reiterate the temperature calculation, all time-dependent input parameters are recalculated based on the new absolute time value (time of day). This absolute time of the day is constantly updated as the mathematical model can determine the time it took the fluid to flow through the previous element based on its stream velocity. Therefore, this Lagrangian approach ensures that temperature dependency in time is indirectly included when solving the river temperatures with equation (2.2) in this model. The specific time-dependent input parameters are solar radiation, air temperature, and ground temperature.

Input parameters that depend on the water temperature are also systematically recalculated when the river simulation from the Fluid Trajectory is run. This is done by implementing the table for properties of saturated water in the MATLAB code, accompanied by an algorithm that selects all water properties occurring at a specific water temperature. Acknowledging that a new initial temperature is obtained for every element where the fluid volume passes, all values for the temperature-dependent parameters will be iterated in order to simulate each element with the most accurate input parameters. These parameters are represented in blue in figure 3.4, where they are also called simulation variables as their value results from a previously calculated water temperature.

A detailed overview for the code implementation of the Fluid Trajectory Model is shown in figure 3.4. Here, all the input parameters and simulation variables are presented and the principle of dividing the studied river into multiple elements, together with the time dependency of the simulation, is graphically clarified.

At the start of every temperature simulation with the Fluid Trajectory Model, all input parameters are set in accordance to the studied river and its current (estimated) meteorological parameters. Most of these input parameters remain constant throughout the entire simulation (green block in figure 3.4). The initial river temperature at the starting point of the studied river (T_{w,i_1}) is inserted and the number of elements or control volumes in which the user wants to divide the river is decided. The selected number of elements largely influences the remainder of the simulation as it determines the number of iterations within the model as well as the change in time per element. This time value is calculated by equation (3.3).

$$\Delta t_{element} = \frac{time_{sim}}{N} \tag{3.3}$$

where

$\Delta t_{element}$	:	time step within every element	$[s]$
$time_{sim}$	:	total time of the river simulation	$[s]$
N	:	number of elements or control volumes in the studied river	$[/]$

The total time of the river simulation and thus the time it takes the fluid to travel the entire length of the studied river can be determined by equation (3.4).

$$time_{sim} = \frac{L_{river}}{v_{stream}} \tag{3.4}$$

After assessing the different time-related characteristics of the specific simulation, the model will predetermine values for all time-dependent parameters in every element along the studied river. These parameters are shown in brown/orange in figure 3.4. A twenty-four hour average value for the ambient air temperature and the ground temperature is inputted in the model. Based on this information, sinusoidal varying values are predetermined relative to the average twenty-four hour input value of each parameter. Thus, the MATLAB program estimates values for ground and air temperature within every element along the river. This sinusoidal estimation depends on multiple factors. The total time and the time step of the specific simulation ($\Delta t_{element}$) are combined with the start time of the simulation ($time_{start}$) and time of sunrise ($time_{sunrise}$) for the specific period of the year. For a flow simulation running over the course of a couple of days, the air and ground temperature profile is sinusoidal with a vertical displacement along the temperature-axis due to their average twenty-four hour input value. This is however not a realistic approximation, since the number of hours with daylight (sun above the horizon) usually differs from the duration of nighttime dependent on the current season. Therefore, the number of hours with daylight ($hours_{daylight}$) is also included and the resulting temperature profile is now a combination of one sine wave for daylight and a second sine wave for nighttime. This results in a combination of two sine waves with different frequencies above and below their average value.

The implementation of these time-dependent parameters is best clarified by an example. Figure 3.2 illustrates this example, where both the ambient air temperature and the ground temperature are plotted. The conducted river simulation lasted several days, 83 hours to be exact. The combined sine curve approximation for both temperature plots and their periodic nature due to the multi-day simulation is clearly

visible. As this test simulates July conditions, daytime occupies a larger portion than nighttime over the course of 24 hours and the frequency of the lower half of each temperature plot is therefore lower. The dotted lines at $15°C$ and $19°C$ represent the original average inputs for respectively air and ground temperature in the MATLAB model.

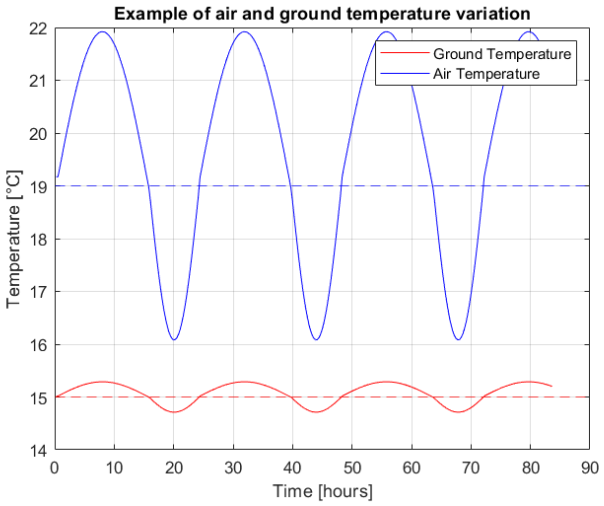

Figure 3.2: Illustration of air and ground temperature variation based on a random simulation in July

The simplified[1] formulas to further illustrate the concept of this sinusoidal variation are given by equation (3.5) and equation (3.6), whereby the former calculates the sine wave above the average input value and the latter modulates the lower half of this periodic signal. Note that the period of the double sine curve always equals 24 hours or a full day.

$$Y = A_{var} \cdot sin(X_{daytime} \cdot \frac{\Delta t_{element}}{hours_{daylight}} \cdot \pi) + Y_{avg} \qquad Y \geqslant Y_{avg} \tag{3.5}$$

$$Y = -A_{var} \cdot sin(X_{nighttime} \cdot \frac{\Delta t_{element}}{24 - hours_{daylight}} \cdot \pi) + Y_{avg} \qquad Y < Y_{avg} \tag{3.6}$$

where

Y	:	Y-value on variation graphs, corresponding to temperature	$[°C]$
A_{var}	:	amplitude of variation for T_{air} and T_{ground}	$[°C]$
$X_{daytime}$	:	counter running from 1 to $\Delta t_{element}/hours_{daylight}$	[/]
Y_{avg}	:	24-hour average Y-value, corresponding to the input value for T_{air} and T_{ground}	$[°C]$
$X_{nighttime}$	:	counter running from 1 to $\Delta t_{element}/(24 - hours_{daylight})$	[/]

The amplitude of variation determines the maximum deviation in both positive and negative direction with respect to the twenty-four hour average temperature. The variation in air temperature is estimated at approximately $2.5°C$ in this research, whilst the variation for the ground temperature is chosen at approximately $0.5°C$ based on air and ground temperature data provided by the Koninklijk Meteorologisch

[1] The full implementation that accounts for all different scenarios can be found in the MATLAB code in appendix A

Instituut[2] (KMI). Both counters are a mathematical method to calculate the varying values for both ground and air temperature following a sine wave. The range of the counters is chosen in such manner that both sine waves from equation (3.5) and (3.6) are completed during half a period. Each time a temperature curve crosses its twenty-four hour average value, the model switches in between equation (3.5) and (3.6) and the corresponding counter is set to 1 again.

Lastly, also the incoming solar radiative flux (q_{in}) is an important time-dependent parameter which is shown in brown/orange in figure 3.4. In this case, an average value for the incoming solar radiative flux during the hours of daylight ($hours_{daylight}$) is an input of the MATLAB code. This means that the Fluid Trajectory Model assumes incoming solar radiative flux to heat up the river during every hour of daylight. In online data sets, the average daily incoming solar radiative flux is usually in correlation with the specific hours of sunshine (no clouds) and thus its value might only correspond to a few hours of actual sunlight. This observation reveals a downside of the MATLAB model, since the real-time q_{in}-fluctuations due to clouds are neglected and the input of an average incoming solar radiative flux is distributed over all hours of daytime. However, a cloudy day can be modelled by lowering the average incoming radiative flux.

Compared to the ground and air temperature from equation (3.5) and (3.6), the incoming solar radiative flux is varied using just one sine curve with the average twenty-four hour input value corresponding the positive average amplitude value. A combined period of twenty-four hours is still respected and the negative values of the sine curve are set to zero. Therefore, q_{in} is positive during the hours of daylight and follows a sine curve. After sunset, q_{in} is simply set to zero until sunrise occurs again. The implementation of the incoming solar radiative flux can be visualised by another example. Figure 3.3 represents the incoming solar radiative flux (q_{in} on y-axis) for the same simulation as in figure 3.2. Note that the dotted line represents the model input of the average incoming solar radiative flux, which equalled $450\ W/m^2$ in this case. Lastly, the periodical character of the one-sided sine wave is illustrated since this simulation corresponds to a time period of 83 hours.

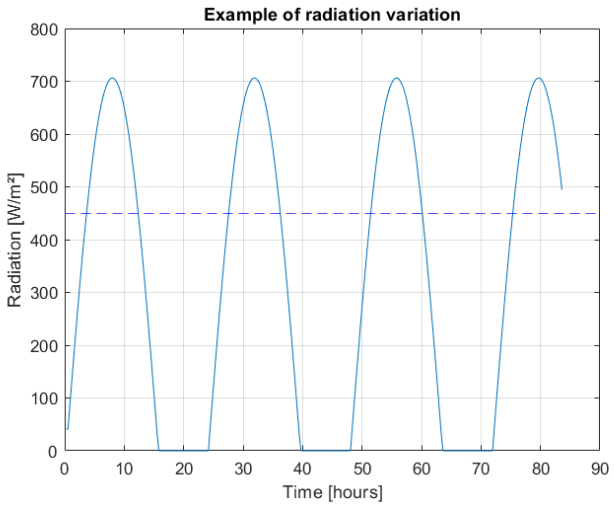

Figure 3.3: Illustration of incoming solar radiative flux variation based on a random simulation in July

[2] https://wow.meteo.be/nl/

The Fluid Trajectory Model opts to calculate all incoming solar radiative fluxes based on a single average input value. This approach is useful when very limited radiation data is available e.g. on a daily or monthly basis. Although, some regions or studied rivers provide data of incoming solar radiative fluxes on an hourly basis. In this case, more accurate simulations can be performed when a table with this detailed radiation data is directly inputted in the MATLAB model. Then, a different algorithm is implemented where the values for each element are no longer varied in a sinusoidal manner. A linear relationship is now computed between the subsequent values of the available data from the inputted table. The same conclusion is valid for both the implementation of the previously discussed air and ground temperatures. This method is applied in the third test of section 3.4.2. Concluding, arrays for each input parameter are constructed whereby the values correspond to the location of every element along the trajectory and the point in time when the fluid volume reaches this element. Accordingly, it is now possible to account for site-specific features such as shade from e.g. vegetation or buildings. This is done by setting the shade factor of the element(s) in the array that corresponds to the location of the observed shade equal to one.

Referring to figure 3.4, all necessary input parameters are now determined and the Fluid Trajectory Model is able to solve equation (2.2) to obtain the final temperature ($T_{w,e\,j}$) for every element along the studied river. In MATLAB, this is performed using a for-loop with the number of iterations equal to the predefined number of elements or control volumes. The index j in figure 3.4, varying between 1 and the number of elements, keeps track of the current position in the simulation and thus the element that is analyzed. A new initial temperature and updated values for every time- and temperature-dependent variable correspond to each j-value due to changes in water temperature and the time of the day. This time of the day is recalculated after every element. The different colors of the arrows for the flow chart in figure 3.4 are important to notice. The light blue arrows represent a step in the MATLAB code which is only run once, for the initial element in the simulation. The black arrows show calculations that are performed j-times and thus once for every element. Lastly, the red arrows are steps that need a calculated final temperature ($T_{w,e\,j}$) and they will therefore take place (j-1)-times, from the second until the final iteration.

Optionally, inflows or heat extractions are added to the simulation whenever they occur along the trajectory of the studied river. The available data on these inflows and heat extractions is also inserted as input parameters before starting the MATLAB code, in green in figure 3.4. The necessary inflow data to calculate their heat contribution are the location of the inflow(s) along the trajectory, the added mass flow of every inflow and the initial temperature of each inflow. The needed data on heat extractions comprises the location of implementation and the required rate of heat transfer. The individual heat transfer contribution of one or multiple inflows and/or heat extractions are included in the simulation when the fluid reaches the element at which a certain process was defined. That is, if the index j equals the element of inflow ($element_{inflow}$) or heat extraction ($element_{heat.extr.}$), the inflow or heat extraction is added to all other heat contributions at element j.

A major advantage to the Fluid Trajectory Model is the straightforward code implementation. The temperature equation for a moving control volume (2.2) is solved within every for-loop. A higher number of iterations is needed when the control volumes are reduced in order to travel the entire length of the predefined river. This corresponds to a higher number of calculated river temperatures along the trajectory of the fluid and therefore a larger amount of simulated data and river information, as further discussed in 3.4.1.

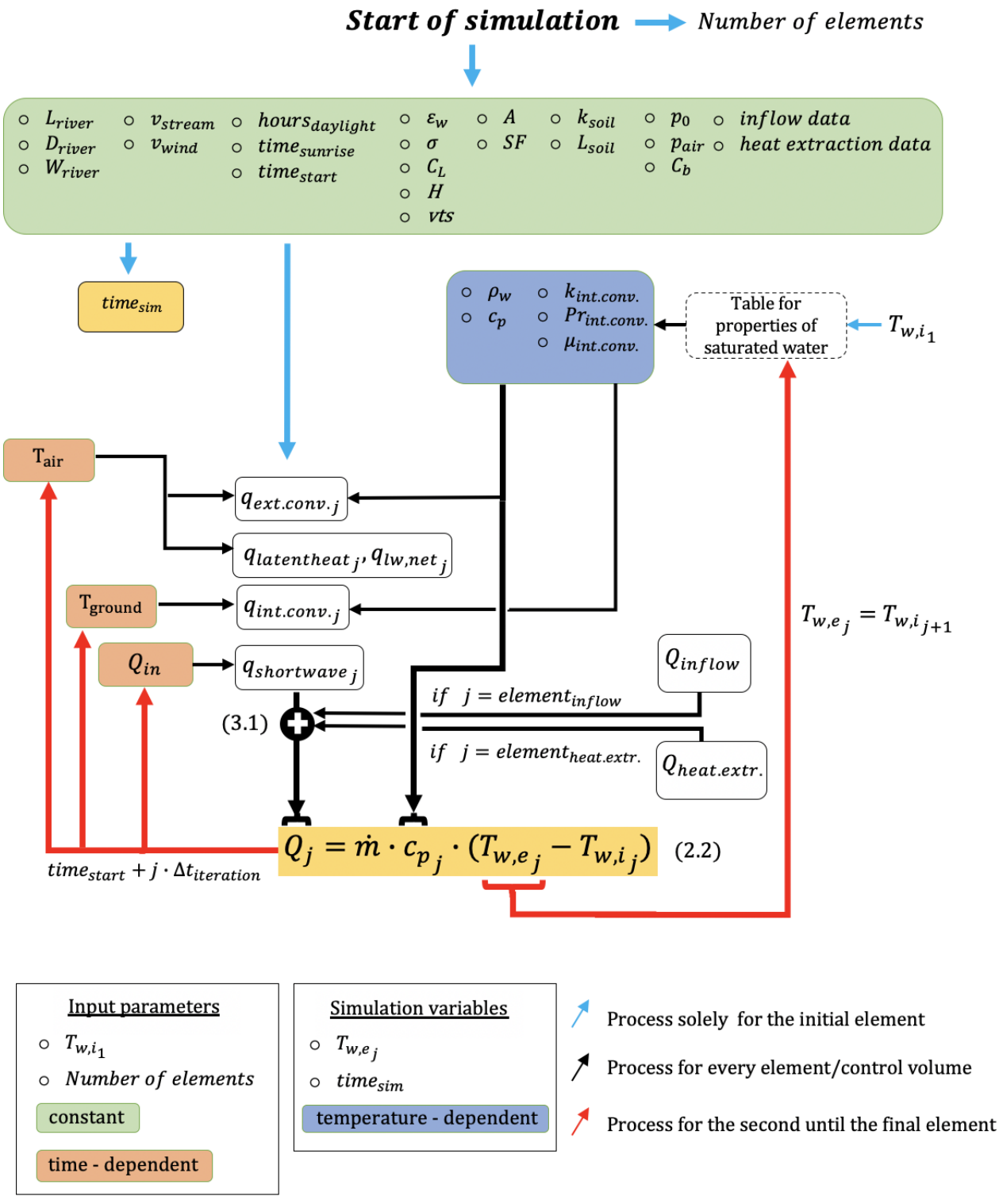

Figure 3.4: Flow chart of a multi-element river simulation by the Fluid Trajectory Model

3.2 Finite Element Model

The second mathematical river model is called the Finite Element Model. This model is based on the temperature equation for stationary control volumes (equation (2.3)), which is often used in literature. The Finite Element Model is also created in MATLAB and its solution strategy is based on the mathematical approach by Boyd and Kasper in 'Analytical methods for dynamic open channel heat and mass transfer: Methodology for heat source model version 7.0' [6]. The main purpose of this Finite Element Model is to validate the Fluid Trajectory Model, which is an original concept in this research. Since the mathematical approach of the Finite Element Model is based upon prior research [6], a correct implementation of this method should serve as a reference for the correctness of the Fluid Trajectory Model.

The Finite Element Model develops a finite element approximation to include the three modes of heat energy change and transport from equation (2.3): advection, dispersion, and heat transfer [6]. Relying on the theoretical background from section 2.2.1, the applied Eulerian approach enables the model to implement the phenomenon of dispersion. Furthermore, equation (2.3) is used to calculate the river temperatures at the edges or nodes of every finite element in the studied river for any point in time. The meshing of the river into finite elements is similar to the division into smaller control volumes or elements in the flow direction as performed in the Fluid Trajectory Model. Nevertheless, a finite element approach might be beneficial as it includes the interaction between neighbouring elements. Remark that the temperature dependency in time results from the term $(\frac{\partial T_w}{\partial t})$ in equation (2.3), whereas this time-dependent temperature is inherently present when using the Lagrangian method in section 3.1. This and other differences between both models are further elaborated in 3.3. Note that the assumptions of one-dimensional flow and steady-flow are still valid throughout the full implementation of this finite element method.

The implementation of the Finite Element Model uses the predictor-corrector approach suggested by MacCormick [21] to approximate the temperature difference over time $(\frac{\partial T_w}{\partial t})$ in equation (2.3) at a given location. A finite difference approximation is used along with two forward slope predictions based on Euler's method of numerically solving ordinary first-order differential equations. Afterwards, the average of both slope predictions is used backwards to perform a final corrector-calculation on the temperature difference over time [6]. The index t represents the time-value at which a certain variable is considered, whereas index i represents the location of this variable along the studied river. In fact, every i-value corresponds to the node in between two elements, with i_0 marking the start of the river and i_N representing the location of the endpoint. The complete code implementation for the Finite Element Model is summarized in figure 3.7.

The first forward slope approximation at node i is given by equation (3.7) [21].

$$s_{1,t} = -v_{stream} \cdot \frac{{T_{w_{i+1}}}^t - {T_{w_i}}^t}{dx} + D_L \cdot \frac{{T_{w_{i+1}}}^t - 2 \cdot {T_{w_i}}^t + {T_{w_{i-1}}}^t}{dx^2} + \frac{Q_i^t}{{c_p}^t \cdot {\rho_w}^t \cdot dx \cdot D_{river} \cdot W_{river}} \tag{3.7}$$

Next, the forward predictor-calculation using Euler's method is calculated using equation (3.8) [21].

$${T_{w_i}}^{t+1} = {T_{w_i}}^t + s_{1,t} \cdot dt \tag{3.8}$$

The second forward slope slope approximation at node i corresponds to equation (3.9) [21].

$$s_{2,t} = -v_{stream} \cdot \frac{{T_w}_i^{t+1} - {T_w}_{i-1}^{t+1}}{dx} + D_L \cdot \frac{{T_w}_{i+1}^{t+1} - 2 \cdot {T_w}_i^{t+1} + {T_w}_{i-1}^{t+1}}{dx^2} + \frac{Q_i^{t+1}}{{c_p}^{t+1} \cdot \rho_w{}^{t+1} \cdot dx \cdot D_{river} \cdot W_{river}} \quad (3.9)$$

Lastly, the backwards corrector-calculation is performed by equation (3.10) [21].

$${T_w}_i^{t+1} = {T_w}_i^{t} + (\frac{s_{1,t} + s_{2,t}}{2}) \cdot dt \quad (3.10)$$

where

$s_{1,t}$	:	first approximation of the slope	$[^\circ C/s]$
dx	:	longitudinal distance step (length of element or control volume)	$[m]$
dt	:	time step	$[s]$
$s_{2,t}$	:	second approximation of the slope	$[^\circ C/s]$

From equations (3.7), (3.8), (3.9), and (3.10), the temperature difference ($\frac{\partial T_w}{\partial t}$) over a certain time step (dt) is calculated at every fixed location i along the studied river. First, the predictor-temperature for a single time step is calculated from equation (3.7) and (3.8). Both equations are combined into a matrix equation so that all nodes along the river are calculated simultaneously, whereby index i ranges from 1 to the number of elements (N). Next, the computed temperatures at time $t+1$ are used to calculate the final corrector-temperatures for every node by combining equation (3.9) and (3.10) in a matrix form. A key element to this corrector-step is the evaluation of the heat exchange processes for every node at time $t+1$, resulting in a different total rate of heat transfer (Q_i^{t+1}). Thus, all temperatures at every time step and location are calculated twice. They are first predicted at time $t+1$, followed by a corrector-calculation for that same point in time using its initial predictor-values. This process is repeated for every time step and is further demonstrated in figure 3.5. The horizontal axis represents the nodes along the studied river, whereas the vertical axis indicates their corresponding temperatures after every time step. Recall that a predictor-calculation for every node along the river is needed before the corrector-calculations for that same time step can be initiated, corresponding to the gray and pink frame in figure 3.7 which represent the iterative sequence of the Finite Element Model.

In order to implement this predictor-corrector method in the MATLAB code of the Finite Element Model, two boundary conditions and one initial condition need to be defined which allow the simulation to numerically solve the equations. A visual representation of these boundary conditions and initial values is shown in figure 3.6. First, temperatures at the starting location i_0 need to be defined for every time-value (t_0, $t-1$, t, $t+1$, etc.) of the simulation. This is accomplished by e.g. inputting sensor-values of the temperature at location i_0 which are measured after every time step dt. Secondly, the temperature over the entire river at the start time, corresponding to time t_0, is assumed to be uniform and equals the initial temperature of the first element (i_0) at time t_0. Lastly, it is assumed that temperatures further downstream of the final element remain constant at each time step. To implement this boundary condition in the MATLAB code, one extra temperature at location t_{N+1} is added for every time step, which always equals the temperature at t_N.

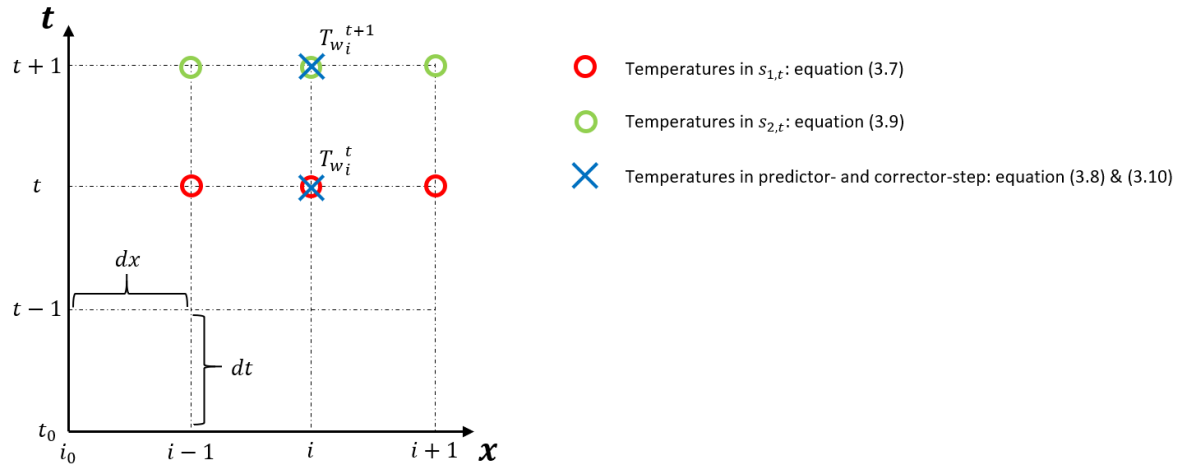

Figure 3.5: Schematic overview of the temperatures in the finite difference approximation by MacCormick

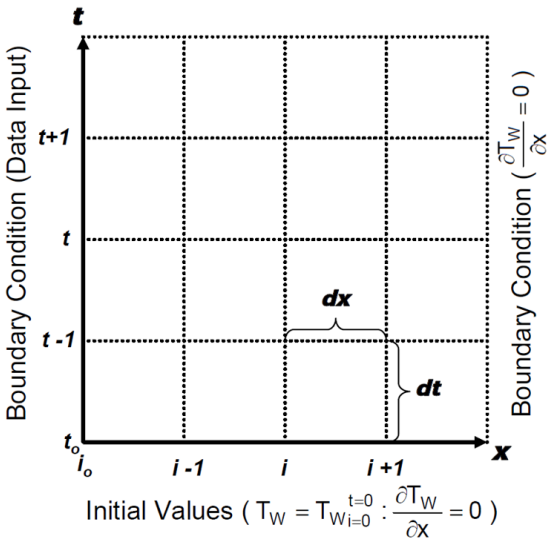

Figure 3.6: Initial and boundary conditions for the Finite Element Model adapted from Boyd and Kasper, 2003

An important asset to the Finite Element Model is the fact that time and location are now decoupled. In the Fluid Trajectory Model, the simulation of an element at a certain location along the studied river was correlated to the stream velocity. Therefore, every location of the moving fluid volume along the studied river corresponded to a unique point in time. In the Finite Element Model, the temperature at every node along the stream is calculated after every time step. The user is able to input the desired simulation time and is free to choose the number of time steps for that total duration, independent of the chosen number of elements along the stream. This is also indicated in figure 3.7. Much more data is generated as the studied river is always simulated in its totality for every time step. Doing so, a short river can easily be studied over the course of e.g. multiple days or the temperature at a fixed location along the stream can be simulated for a desired time duration. Decoupling time and location will also improve the ability of the Finite Element Method to solve various flow cases, as further detailed in section 3.3.

To further implement the Finite Element Model in the MATLAB code, the total rate of heat transfer into or out of the river (Q_i^t) is analyzed. This parameter is both time- and water temperature-dependent as determined from section 2.2.2 and equation (3.1). The total rate of heat transfer is thus recalculated for every node i at each point in time t (see figure 3.7). The time-dependent parameters are implemented similar to the Fluid Trajectory Model. One average twenty-four hour value is inputted for the incoming solar radiative flux, ground temperature, and air temperature, and their values are varied after every time step detailed in section 3.1. Parameters that depend on the water temperature are recalculated with every code iteration, as the water temperature will vary in both time and location. Furthermore, it is important that the total rate of heat transfer is implemented as a source term with a designated value. Otherwise, it is not possible to solve the temperature problem with the suggested predictor-corrector method.

Referring to section 2.2.2, the implementation of the internal forced convection (in the Fluid Trajectory Model) contradicts with the initial condition of a uniform initial river temperature. Its implementation is therefore altered as the internal forced convection heat flux for a constant surface temperature from equation (2.21) would initially remain equal to zero since $T_{w,i}$ and $T_{w,e}$ have identical values. Instead, the estimated rate of heat transfer between the river water and the ground ($Q_{estimate}$) from equation (2.23) will be used, which is an accurate substitute for the heat transfer between the river and the streambed. Possible inflows are also implemented differently compared to the method from equation (2.32) in the Fluid Trajectory Model. The Finite Element Model uses an estimated water temperature after occurrence of an inflow in order to input the rate of heat transfer from inflows as a source term. This estimated temperature is calculated by the following formula (3.11) [6].

$$T_{estimate}^t = \frac{\dot{m}_{inflow} \cdot T_{inflow} + \dot{m} \cdot T_{w\,i_{inflow-1}}^{\,t}}{\dot{m}_{inflow} + \dot{m}} \tag{3.11}$$

where

$T_{estimate}$: estimated water temperature after occurrence of inflow [K]

Note that the inflow is simulated in between the nodes $i_{inflow-1}$ and i_{inflow}. Once this estimated water temperature is calculated, the rate of heat transfer from the inflow can be expressed as a source term by equation (3.12).

$$Q_{inflow}^t = \dot{m}_{inflow} \cdot {c_p}^t \cdot (T_{inflow} - T_{estimate}^t) \tag{3.12}$$

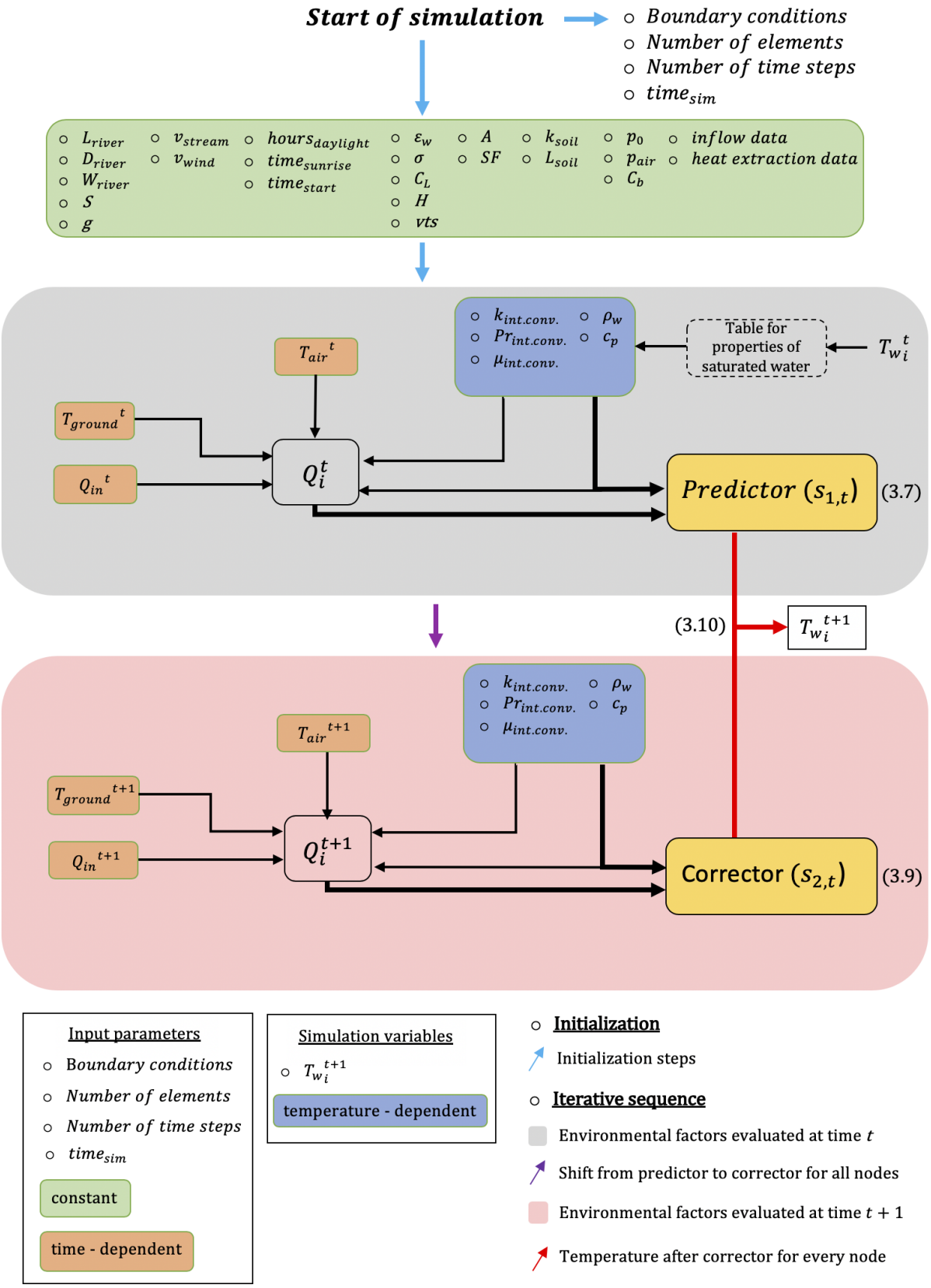

Figure 3.7: Flow chart of the Finite Element Model

3.3 Model Comparison

Two different mathematical river models are implemented in this research. The first model is the Fluid Trajectory Model, which is an original creation developed in this paper. The second model is the Finite Element Model, which is based on prior research as detailed in section 3.2. The main purpose of the Finite Element Model is to verify the solution strategy developed in the Fluid Trajectory Model. Both river models are created in MATLAB and aim to accurately simulate water temperatures along a studied river whilst each generating a distinct set of data.

Section 2.2.1 explained how the temperature equation for stationary control volumes (2.3) in the Finite Element Model can be reduced to the temperature equation for a moving control volume (2.2) from the Fluid Trajectory Model when dispersion and transient temperature factors are neglected. This highlights the two major differences between both equations. However, recall from section 3.1 that the temperature dependency in time is still introduced in the Fluid Trajectory Model by using equation (2.2) in combination with its Lagrangian solution strategy. In addition, both models have a nearly identical code implementation in terms of heat exchange processes and meteorological factors. Hence, identical river simulations and their resulting water temperatures can be compared at similar points in time and location, whereby possible temperature differences between both models are solely related to the effects of dispersion.

In order to compare both models in identical and realistic conditions, an arbitrary river simulation is developed for typical meteorological conditions of the region Leuven in the month of May. Average values for meteorological parameters[3], water temperature and river flow[4] are obtained from the KMI. The goal of this specific simulation is to detect possible differences in water temperature along the studied river due to dispersion. Therefore, the analyzed river or the applied geometrical and meteorological parameters are irrelevant as long as all input parameters for both models are identical. The resulting temperature curves from both models for a fluid volume along this arbitrary river are shown in figure 3.8.

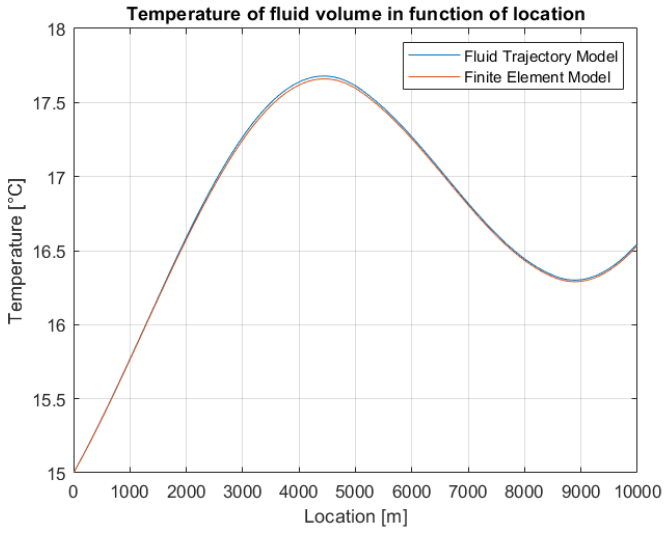

Figure 3.8: Temperature curves of both river models for an identical simulation in May

[3] https://wow.meteo.be/nl/

[4] https://www.waterinfo.be/default.aspx?path=NL/Thema/Overstroming_Actueel

The temperature plots of both the Fluid Trajectory Model and the Finite Element Model in figure 3.8 are almost identical, leading to the conclusion that the effects of dispersion are negligible when modeling the temperature of a fluid volume travelling through a studied river. The temperature equation for a moving control volume (2.2), in combination with the code implementation from section 3.1, is thus a valid approach that accurately simulates the water temperature along a studied stream.

Some important remarks on the conducted simulations from figure 3.8 should be mentioned. First, the temperatures of the Fluid Trajectory Method (blue in figure 3.8) represent all simulated data from this model. A fluid volume is followed as it travels the full length of the river (x-axis) whilst its corresponding temperature at every element (y-axis) is plotted. On the other hand, recall from section 3.2 that the Finite Element Model computes the water temperature at every node for every time step and only a fraction of this simulated data is thus shown in figure 3.8. Based on the chosen time step dt and the stream velocity, the computed temperatures from the Finite Element Model can be matched with the results from the Fluid Trajectory Model. In other words, the finite element plot in figure 3.8 is composed by selecting the temperatures on the diagonal ($T_{w_i}^{\ t}$, $T_{w_{i+1}}^{\ t+1}$, etc.) of figure 3.5 as the time step dt is matched with the time needed for the fluid to travel through a single element ($\Delta t_{element}$). The number of elements used in both models equalled 1,000 and thus the number of time steps in the Finite Element Method was also set at 1,000 for simplicity. The detailed results from both models for the conducted arbitrary simulation are given in table 3.1.

Table 3.1: Simulation results from both river models for an identical arbitrary test in May

Simulation results	**Fluid Trajectory Model**	**Finite Element Model**	**Deviation**
Initial temperature [$^\circ C$]	15	15	/
Final temperature [$^\circ C$]	16.5474	16.5293	0.0181
Distance [m]	10,000	10,000	/
Start time [h]	10 a.m.	10 a.m.	/
Total time [h]	23.1481	23.1481	/
Number of elements [/]	1,000	1,000	/
Number of time steps [/]	/	1,000	
Time step [s]	/	83.33	
Contributions [$\%$]			
-Shortwave radiation	51.0095	52.4333	1.4238
-Longwave radiation	(-) 13.688	(-) 13.4037	0.2843
-Latent heat	(-) 9.3903	(-) 8.2143	1.1760
-External convection	(-) 24.8213	(-) 24.4098	0.4115
-Internal convection	1.0909	1.539	0.4481
Computation time [s]	85	30	55

Table 3.1 confirms the similarities in simulation results for both models. The final temperature at a distance of $1,000\ m$ from the starting point only differs $0.0181^\circ C$. Note that this is the temperature after a simulation time ($time_{sim}$) of 23.1481 hours for both models, which equals the time the flow needed to travel from start to finish at the identical stream velocity. Furthermore, a time step is only defined for the Finite Element Model as a result of its decoupled time and location (see section 3.2). Lastly, also the contributions of every heat exchange process are similar as a result of the identical input data used in both tests. Small differences of approximately 1% can be related to the effects of dispersion included in the Finite Element Model. That is, dispersion induces temperatures differences along the studied river,

which will then alter the occurring heat exchange processes. This is however not the only source of error, since the internal convection in the Finite Element model is implemented in a slightly different manner as detailed in section 3.2. Thus, the influence of dispersion will be even less than previously stated. Note that a minus sign (-) refers to a heat exchange process having an overall cooling effect on the river.

The effect of modeling inflows and heat extractions in both models is still to be determined, since these heat exchange processes were not included in the simulation from figure 3.8. In essence, both processes will effect the water temperature of the studied river in a similar manner, either heating or cooling, and therefore only one of these heat exchange processes has to be examined. Thus, the influence of these extra inputs is determined by repeating the previous simulation for both models whereby e.g. an inflow is added halfway the studied river. As an illustrative example, an inflow with a mass flow ($\dot{m}_{inflow}$) equaling one-twentieth of the main river mass flow is added at a temperature of $35°C$. The resulting temperature curve for the Fluid Trajectory Model is shown in figure 3.9.

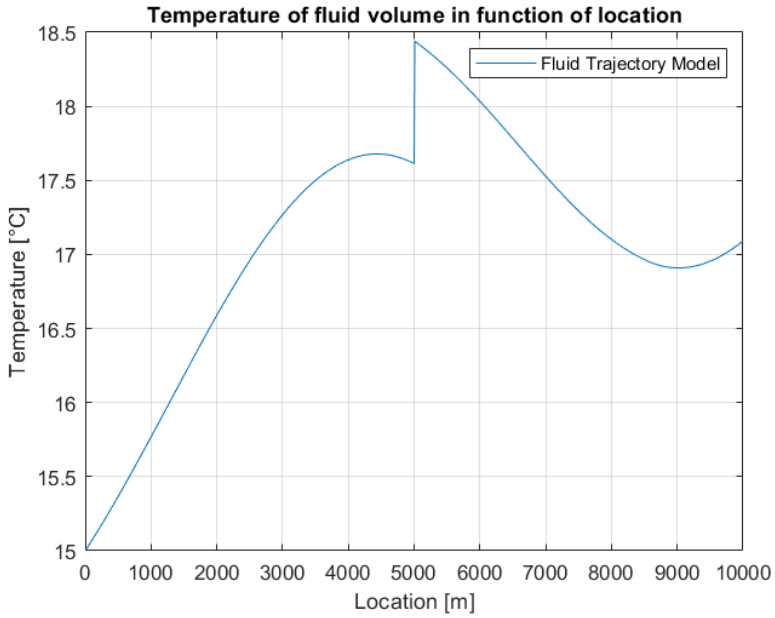

Figure 3.9: Temperature curve of Fluid Trajectory Model with inflow halfway through the simulation

The expected result is obtained since the river temperature suddenly increases at the location of the inflow as a result of its incoming temperature and mass flow. The temperature curve also follows the same pattern further downstream similar to figure 3.8, only at elevated temperatures. This temperature difference is again illustrated in figure 3.10. In this case, the conducted river simulation is performed with an identical river for which the length is extended three times. It is observed that the river temperatures will approximate the flow case without an inflow after a certain time or distance further downstream. The influence of the inflow decreases as the river travels further downstream. After a distance of approximately $22.5\ km$ in figure 3.10, the effect of an earlier occurring inflow further upstream becomes negligible as both temperature curves nearly realign. Recall that similar behavior would be obtained when modeling heat extractions. The phenomenon of regeneration after heat extraction is further detailed in section 4.4.1.

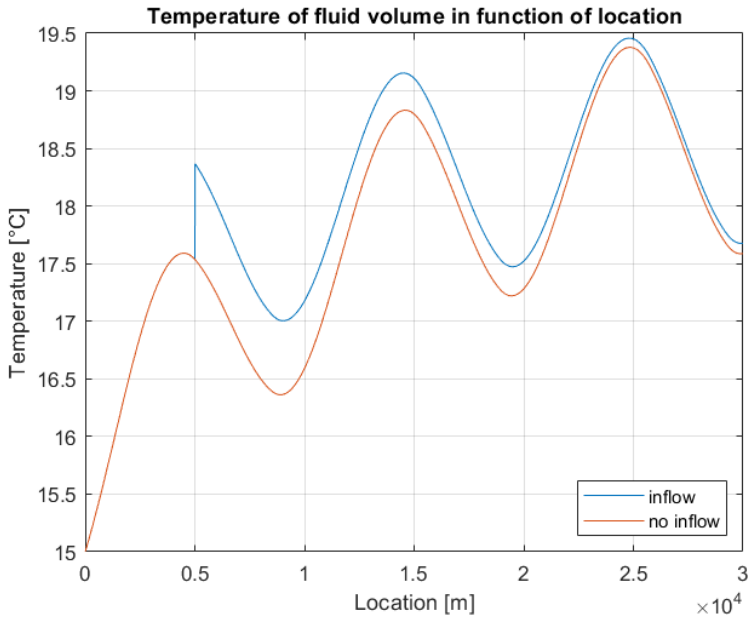

Figure 3.10: Visualization of temperature difference between curves of Fluid Trajectory Model with and without inflow halfway through the simulation

When an identical inflow is applied to the Finite Element Model, oscillations occur upstream of the inflow location in the simulated temperature plot as shown in figure 3.11. Thus, the Finite Element Model has difficulties to process the sudden inflow input in a stable manner. If the same number of elements (1,000) and number of time steps (1,000) as for the finite element plot in figure 3.8 are used, the flow case with the added inflow cannot be solved by the Finite Element Model. Divergence of the temperatures near the inflow occurs and MATLAB is no longer able to solve the simulation. An empirical explanation for this incident holds that larger time steps induce larger temperature variations in between subsequent time steps. Whenever these temperature changes exceed a certain threshold, the implemented algorithm of the Finite Element Model unintentionally causes temperature differences to further amplify and divergence will occur.

The Finite Element Model is able to increase the number of time steps for which the simulation of a studied river over a fixed period of time is analyzed. This is where the decoupling of time and location proves to be useful. Increasing the number of time steps enhances the stability and accuracy of the simulation [6]. This correlation to the stability criteria is a distinct feature of the number of time steps. To be able to solve the temperature plot in the case of an inflow with the Finite Element Model, the initial number of time steps (1,000) has to be increased. Figure 3.11 is obtained when the number of time steps is multiplied with a factor of 10 (10,000) as compared to the simulation in figure 3.8. Each time step thus equals 8.33 s. A longer duration per time step results in larger oscillations that start further upstream, whereby the simulation becomes unsolvable in extreme cases. Furthermore, the oscillations remain for every solved simulation, even if the number of time steps is increased to 100,000 and the computation time becomes an opposing factor. Contrarily, increasing the number of elements does not enhance a stable solution method. This parameter solely influences the accuracy of the simulation as further detailed in section 3.4.1. Again, note that the number of time steps can be chosen independently of the selected number of elements.

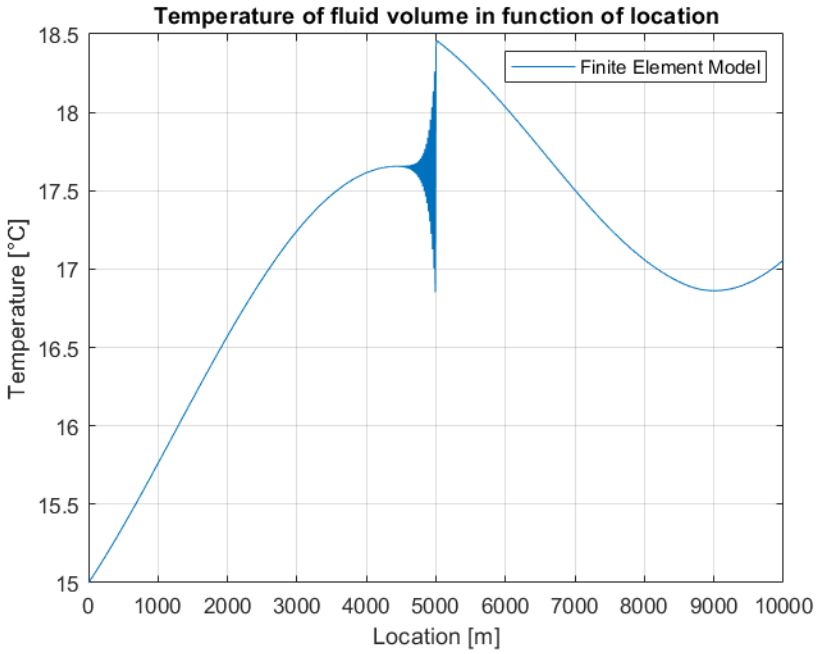

Figure 3.11: Influence downstream of inflow on temperature curves for an extended river

Both the Fluid Trajectory Model and the Finite Element Model have advantages and drawbacks, whereby either approach or implementation will be preferred for each distinct river simulation. The Fluid Trajectory Model applies a straightforward solution strategy with a concise and repetitive code implementation. However, this method yields limited data as solely the temperature of one fluid volume travelling through the studied river is simulated. The Finite Element Model uses a more elaborate solution strategy where a predictor-corrector method also models the effects of dispersion for neighbouring elements. However, the influence of these phenomena proved to be negligible in figure 3.8 which means both models are considered as equally accurate. The main advantage of the Finite Element Model is the large amount of generated data. Fluid volume simulations can be compared to the fluid trajectory method by diagonally plotting temperatures at corresponding points in time and location (node), as performed in figure 3.8. On the other hand, the Finite Element Model generates temperature data for one fixed point along the river for a desired duration. In addition, the temperature over the entire river at every time step is modeled. Examples of these applications are presented in section 3.4.2. Consequently, the Fluid Trajectory Model is more convenient to validate by a physical experiment as one would simply follow the studied river at the stream velocity and measure the temperature after every traveled element length (see section 3.4.3). Contrarily, experimental validation of the Finite Element Model requires a simultaneous temperature measurement after each time step at every node along the studied river and is therefore complicated to perform. Furthermore, the Fluid Trajectory is preferred whenever one or multiple inflows or heat extractions are present in the studied river. The code implementation of this model is suitable for sudden changes in parameters as every consecutive element is treated independently. In similar situations, the finite element method often encounters stability issues and its behavior becomes inconsistent. Therefore, river cases with inflows or heat extractions (see section 4.2) will be evaluated using the Fluid Trajectory Model. Lastly, the computation time of the Finite Element Model is less than half the time needed with the Fluid Trajectory Model for an equal number of elements, as presented in table 3.1. If the number of time steps in the Finite Element Model is doubled, the computation time increases with approximately 90%.

3.4 Model Validation

An essential phase after the creation of the models is their validation. That is, the accuracy of the created models is analyzed. In section 3.4.1, a grid study is conducted for both the Fluid Trajectory Model and the Finite Element Model. Section 3.4.2 comprises results from tests conducted on different rivers using meteorological and river data obtained from online data sets.

3.4.1 Grid study

A grid study yields results on the element precision that is needed for accurate results. The objective is to find a number of elements (N) which provide a final temperature that is approximately equal to the result obtained if N would be further increased, while keeping the computation time acceptable. In other words, an adequate trade-off must be found between the accuracy of the final temperature and the computation time. Note that the grid analysis conducted on each model is different from a convergence analysis, because both models use equations with only linear terms. That is, an exact solution will always result regardless of the chosen element length.

The conducted grid study on each model uses the same arbitrary river parameters as the simulation in section 3.3 with a river length of $10\ km$.

Fluid Trajectory Model

In equation 2.2, used in the Fluid Trajectory Model, the temperature difference is in nature integrated over the control volume. When the length of the control volume approaches zero, the solution will converge. The end temperature of the 10 kilometer long river is modelled five times, starting with 10 elements and increasing the number of elements each time with a multiplication factor of 10. The computation time is recorded for each test. Table 3.2 summarizes the obtained results.

Table 3.2: Outcome of grid study on Fluid Trajectory Model

Number of elements [/]	Element length [m]	Final temperature [$^\circ C$]	Computation time [s]
10	1,000	16.0096	2
100	100	16.5290	6.5
1,000	10	16.5474	60
10,000	1	16.5512	587
100,000	0.1	16.5517	5,849

Table 3.2 shows that convergence is found when the number of elements is increased. The computation time increases proportional with N. It is clear that using more than 1,000 elements is not recommended regarding the long computation time and only a slight difference in result ($0.0038^\circ C$ difference with 10,000 elements). A number of elements between 100 and 1,000 provides the best trade-off between computation time and result accuracy. This is further clarified in figure 3.12. Only the results from the first four number of elements are plotted (10 to 10,000) to enhance readability of the graph. From figure 3.12, it is clear that the temperature converges and the computation time increases linearly with the number of elements.

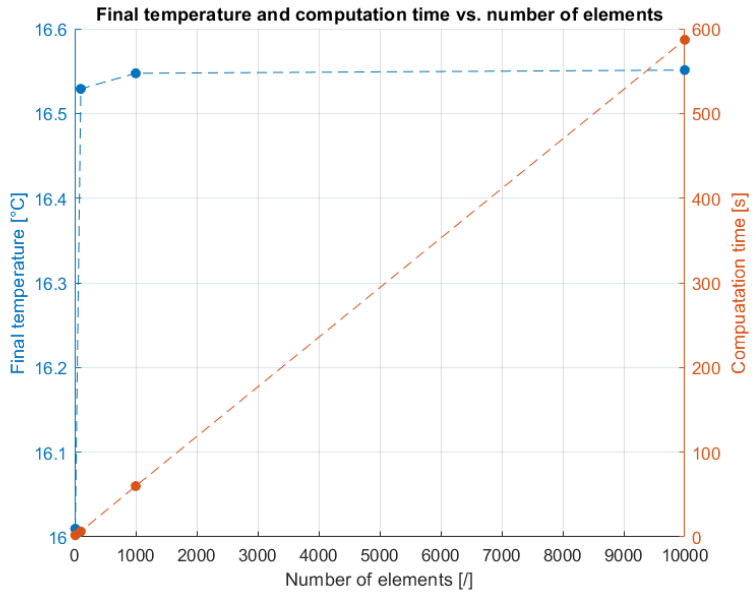

Figure 3.12: Temperature and computation time vs. number of elements for grid study on Fluid Trajectory Model

Figure 3.13 shows that using just 10 elements results in a rough temperature curve, while using 100 elements significantly smooths the curve. A smoother curve ensures that more accurate temperature values can be read along the trajectory.

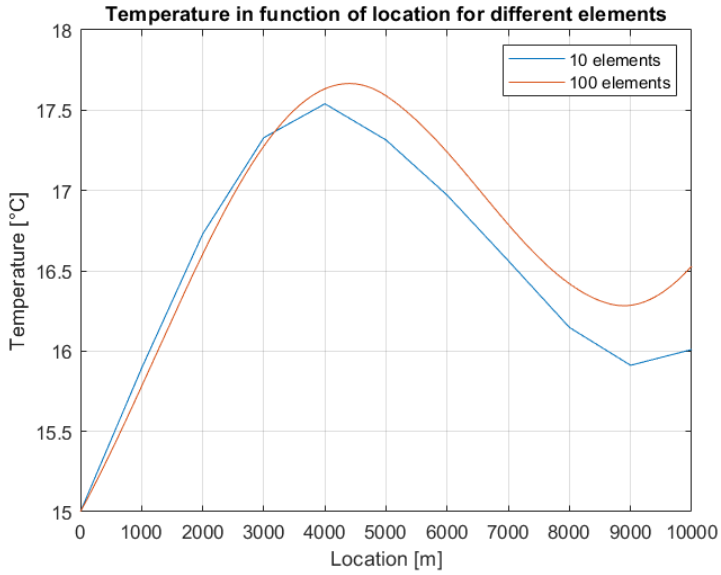

Figure 3.13: Temperature in function of location when different number of elements are used in the Fluid Trajectory Model

Finite Element Model

Equation (2.3), used in the Finite Element Model, contains partial derivatives. When the equation is solved, ∂x is approximated by using a finite difference (dx, element length). This finite difference is however only an approximation of the partial derivative (∂x). The approximation becomes more accurate with decreasing element length (grid size). Thus, the output temperature will convert when the grid size goes to zero or the number of elements (N) goes to infinity.

Different from the test on the Fluid Trajectory Model, the end temperature of the 10 kilometer long river is only modelled four times. This is a result of the additional time-step input parameter in the Finite Element Model. Running a fifth simulation, with e.g. 100,000 elements, would require the minimum amount of time steps for a comparable analysis to equal 100,000 as well. Doing so, the calculation time is significantly increased and accordingly the influence of the number of elements on the calculation time becomes less clear. Concluding, the temperature is solved four times with increasing number of elements, starting from 10 and a constant amount of time steps of 10,000 is used to correctly compare the solutions. Table 3.3 summarizes the obtained results.

Table 3.3: Outcome of grid study on Finite Element Model

Number of elements [/]	Element length [m]	Final temperature [$^{\circ}C$]	Computation time [s]
10	1,000	16.0434	195
100	100	16.4975	199.5
1,000	10	16.5348	308
10,000	1	16.5396	14,400

Similar to the conclusion drawn on the grid study of the Fluid Trajectory Model, the preferred amount of elements lies between 100 and 1,000. Figure 3.14 visualizes that using a value between 100 and 1,000 for N provides a result close to the converged final temperature while keeping the computation time short. The computation time during the tests attained high values due to a large amount of time steps (10,000).

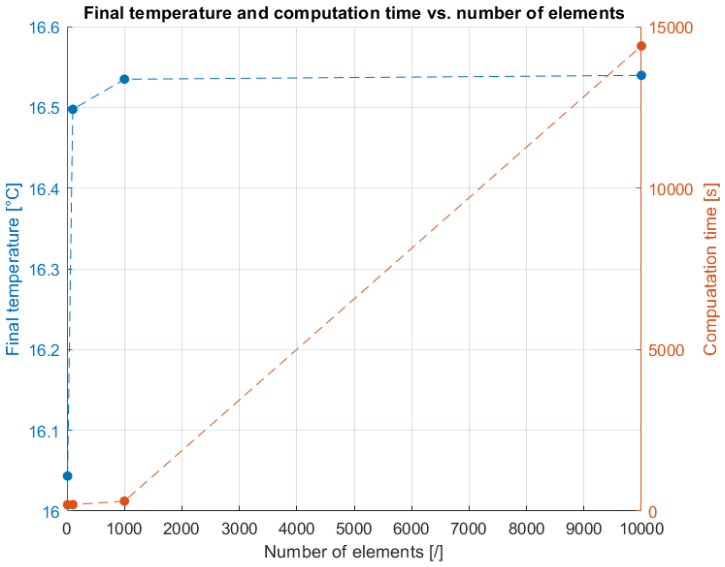

Figure 3.14: Temperature and computation time vs. number of elements for grid study on Finite Element Model

3.4.2 Test on online data sets

The accuracy of the Fluid Trajectory Model and the Finite Element model are tested across contrasting fields and seasons. Tests are conducted on the river Maas in the Netherlands during the winter and summer season and on the river Murg, located in Switzerland, during springtime. Different seasons were tested to evaluate the applicability of the models under different meteorological (air temperature, wind speed, solar radiation, humidity, etc.) circumstances with varying dominant exchange processes. The objective of these tests is to compare the temperature results from the created models with the corresponding temperatures retrieved from online data on the studied rivers.

Finding accurate and useful river and meteorological data on the internet is a real challenge and therefore, each selected study-site has its own shortcomings. Volume flow and temperature data from the river Maas, studied in the Netherlands, is obtained by the Rijkswaterstaat. Their website provides water data from different measuring stations throughout the Netherlands, measured with intervals of ten minutes. Data can be retrieved from archives, supplying values from approximately ten years ago up till now. Similarly, meteorological data of different stations in the Netherlands can be obtained from the KNMI with measurements going back twenty years in time. However, this meteorological data only contains daily averages compared to the ten-minute interval measurements of water data obtained by the Rijkswaterstaat. More updated meteorological data in time for different stations can be found on the website of MeteoSwiss. Here, data is updated every hour. MeteoSwiss/FOEN also provides river flow and temperature data at different stations which are updated every fifteen minutes. However, the meteorological and river data from MeteoSwiss can only be acquired from the last four days. Concluding, tests on the river Maas can be conducted at different seasons by using the archives of Rijkswaterstaat and KNMI, but only daily averages can be used for the meteorological data which means less accurate results. Meanwhile, more frequently updated values are available from MeteoSwiss for meteorological data, but only values from the past four days can be downloaded.

Fluid Trajectory Model test methodology

The Fluid Trajectory Model can be used to determine the temperature change between two measuring points from which data can be retrieved on the internet. The temperature of a certain upstream measuring point on the studied river is used as the input for the model. Using data found for the velocity or the fluid flow, the time it takes a fluid volume to reach the next (downstream) measuring station (at a certain distance from the upstream point) can be calculated. If the model is then solved as described in section 3.1, the temperature at the final location in the river is found. This value can then be compared to the online value found from the downstream measuring station at the moment in time corresponding to the starting time plus the time it took the fluid volume to reach that station.

Fluid Trajectory Model test 1 - river Maas in January

The first test conducted with the Fluid Trajectory Model consists of a test on the river Maas during wintertime. The water temperature measuring stations used in this test are located near the villages Grave (measuring point 1; 51.7589°N 5.7384°E) and Lith (measuring point 2; 51.8066°N 5.4400°E), located upstream and downstream respectively. The study site is presented in figure 3.15, which also depicts the distance between the two stations (24.5 kilometers). The simulated test starts on January 26th 2020 at noon (12 p.m.), with a temperature in Grave of $6.1^{\circ}C$. Using data from the Rijkswaterstaat [5] for the volume flow, river width, and river depth, the velocity of the water can be calculated. Based on this veloc-

[5] https://waterinfo.rws.nl/#!/kaart/waterafvoer/

ity and the distance between the two measuring stations, the time it takes the fluid volume to reach the station near Lith can be found. This value equals approximately 48 hours. Acknowledging this time span to travel the 24.5 kilometers and the start time of the simulation, the moment in time when the fluid volume reaches Lith occurs at 12 p.m. on January 28th. The temperature at that point in time for the measuring station in Lith was $6.1°C$ (value obtained from the Rijkswaterstaat[6]). Now, the Fluid Trajectory Model is run and its output value is compared with the measured $6.1°C$. The necessary model input parameters (see figure 3.4) are listed in table 3.4. The meteorological parameters are obtained from the weather station in Volkel[7] (51.6429°N 5.6546°E).

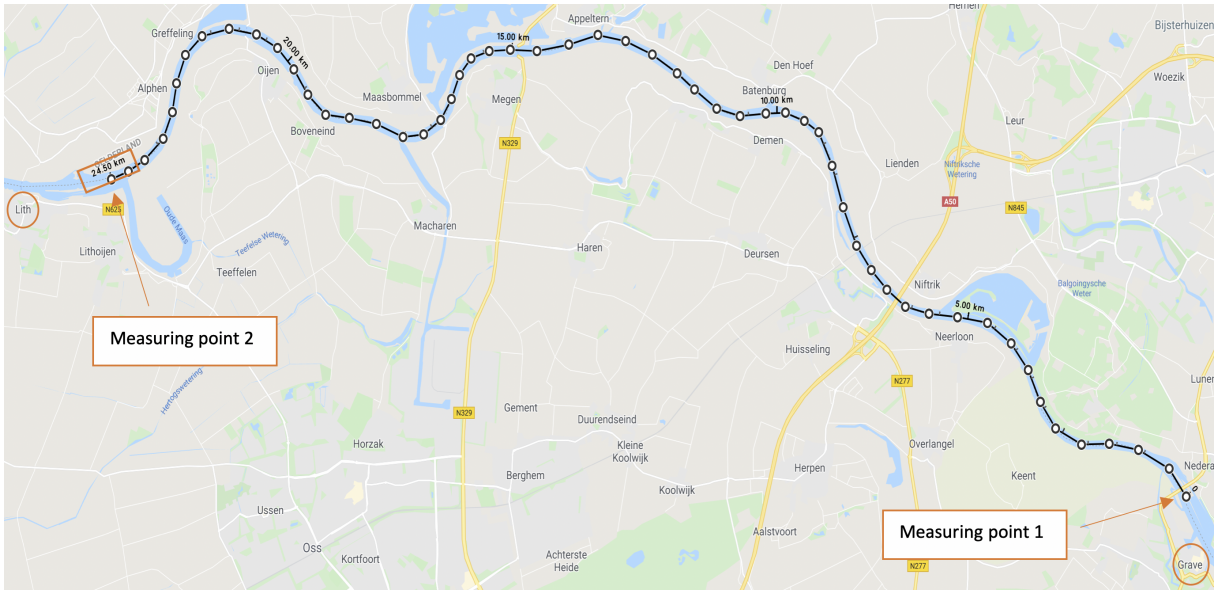

Figure 3.15: Study site river Maas on Google Maps, distance measured using Google Maps Tools

As previously stated, daily averages can be found for the meteorological data from the KNMI. Accordingly, every day will be solved separately using the Fluid Trajectory Model. Three days (January 26th, January 27th, and January 28th) are modelled, since it takes a fluid volume 48 hours to reach the measuring station of Lith when it started at 12 p.m. in Grave on January 26th. The first day, twelve hours are modelled, the second day twenty-four hours, and the last day again twelve hours. In other words, the Fluid Trajectory Model will be run three times where the daily average parameter values are varied using the algorithm discussed in section 3.1. The average meteorological and volume flow values for each day can be found in table 3.4. The input of the initial river temperature for the second day will be equal to the output of the first day and the same goes for the third day as its input is the output of second day. The temperature values obtained for every day/simulation are put chronologically into one array and the combined temperature results from the three simulations are then plotted (see figure 3.16). Note that each day corresponds to a certain traveled distance (L_{river}) obtained from the velocity of the stream and the actual length of the day that is modelled. Furthermore, the length of all elements must be the same during every modelled day. This element length is chosen to equal 10 meters, reasoned using section 3.4.1.

[6] https://waterinfo.rws.nl/#!/kaart/watertemperatuur/
[7] http://projects.knmi.nl/klimatologie/daggegevens/selectie.cgi

Table 3.4: Input parameters for test on river Maas in January

	Value		
Parameters	*January 26th*	*January 27th*	*January 28th*
L_{river} $[m]$	6,170	12,340	5,990
D_{river} $[m]$	10	10	10
W_{river} $[m]$	140	140	140
v_{stream} $[m/s]$	0.143	0.143	0.143
v_{wind} $[m/s]$	3.5	5.5	7.2
$Hours_{daylight}$ $[h]$	8.7	8.75	8.8
$Time_{sunrise}$ $[h]$	8.53	8.5	8.49
$Time_{start}$ $[h]$	12 p.m.	12 a.m.	12 a.m.
ε_w [/]	0.97	0.97	0.97
σ $[W/(m^2 \cdot K^4)]$	$5.67 \cdot 10^{-8}$	$5.67 \cdot 10^{-8}$	$5.67 \cdot 10^{-8}$
C_L $[\%]$	78	89	78
H $[\%]$	89	89	84
vts [/]	unknown	unknown	unknown
A [/]	unknown	unknown	unknown
SF $[\%]$	unknown	unknown	unknown
k_{soil} $[W/(m \cdot K)]$	0.8	0.8	0.8
L_{soil} $[m]$	0.5	0.5	0.5
p_0 $[hPa]$	1,013	1,013	1,013
p_{air} $[hPa]$	1,005	1,010	1,008
C_b $[hPa/K]$	0.62	0.62	0.62
$Inflow\ data$ [/]	unknown	unknown	unknown
$Heat\ extraction\ data$ [/]	unknown	unknown	unknown
T_{air} $[^\circ C]$	5.6	8.2	4.9
T_{ground} $[^\circ C]$	6.2	6.8	6.2
q_{in} $[W/m^2]$	131.55	57.14	93.43
$Input\ River\ Temperature; T_w, i_1$ $[^\circ C]$	6.1	result from day 1	result from day 2
$Number\ of\ elements$ [/]	617	1234	599

The temperature results of the test are depicted in figure 3.16. The final simulation temperature of the river Maas after modeling 24.5 kilometers or 48 hours is $5.965^\circ C$. This value corresponds to the river temperature in Lith. As previously stated, the temperature in Lith obtained from the Rijkwaterstaat was $6.1^\circ C$. Thus, the simulation error is only $0.135^\circ C$ which means that the Fluid Trajectory Model accurately models the real life outcome. The Fluid Trajectory Model also simulates the general behaviour in a closely related manner to the real life behaviour of the Maas. This was proven by assessing the online data of the temperature stations over the course of the three days. From this data it was found that during the three modelled days the temperatures of both stations stayed between $6.25^\circ C$ and $6.05^\circ C$, which is close to the range of the simulated temperatures in figure 3.16.

Although a small temperature difference is found, assessing the quality and accuracy of the result is not a straightforward task as it depends on many factors. First, values for various parameters could not be acquired from the online data sets, as can be seen in table 3.4. Therefore, estimations were made for these unknown values. The albedo factor typically ranges between 1% and 10% for water (see section 2.2.2). An average value of 0.05 is therefore used for A. The shading factor was estimated by observing the riparian vegetation with satellite images from Google Maps. Limited and not closely packed vegetation was observed. Besides, since the simulation takes place in January, the amount of foliage will be limited. Accordingly, a value of 10% is used for SF. The view to sky coefficient was chosen to be 1, meaning a clear view to sky. Lastly, inflows and heat extractions had to be considered. Since no information could

be obtained on any inflows or extractions, it was assumed they did not occur at all. All estimated values are summarized in table 3.5. Besides parameters that remain unknown, precision is also lost due to the lack of more frequently updated values for the meteorological parameters. While daily averages are more accurate than weekly averages, it would be beneficial to adopt e.g. hourly values. Concluding, the imprecision of the inputted data influences the accuracy of the obtained result.

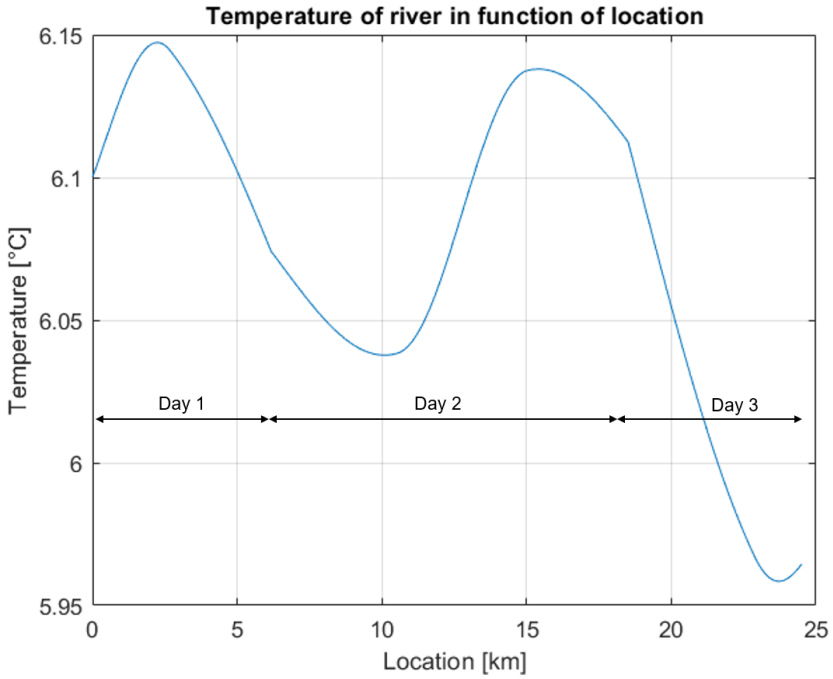

Figure 3.16: Temperature of the river Maas between Grave and Lith in January

Table 3.5: Estimated values for test on river Maas in January

	Value		
Parameters	*January 26th*	*January 27th*	*January 28th*
vts [/]	1	1	1
A [/]	0.05	0.05	0.05
SF [%]	10	10	10
$Inflow\ data$ [/]	none	none	none
$Heat\ extraction\ data$ [/]	none	none	none

The variety in simulated incoming solar radiation, over the three tested days, is created by the MATLAB algorithm from section 3.1 and is visualized in figure 3.17. Note that although the x-axis represents the distance traveled by the fluid volume, radiation values for every moment during the three days can be read. This is done by using the fluid velocity ($0.143\ m/s$) and the traveled distance to calculate the traveled time. For example, kilometer 10 is the equivalent of approximately hour 19 of the total 48 hours. From this figure, it is clear that the average radiation values on January 26th and January 28th are significantly higher than on January 27th. Figure 3.17 also clarifies the modeling time of each day. January 27th is completely modeled, while January 26th and January 28th are only modelled for half a day.

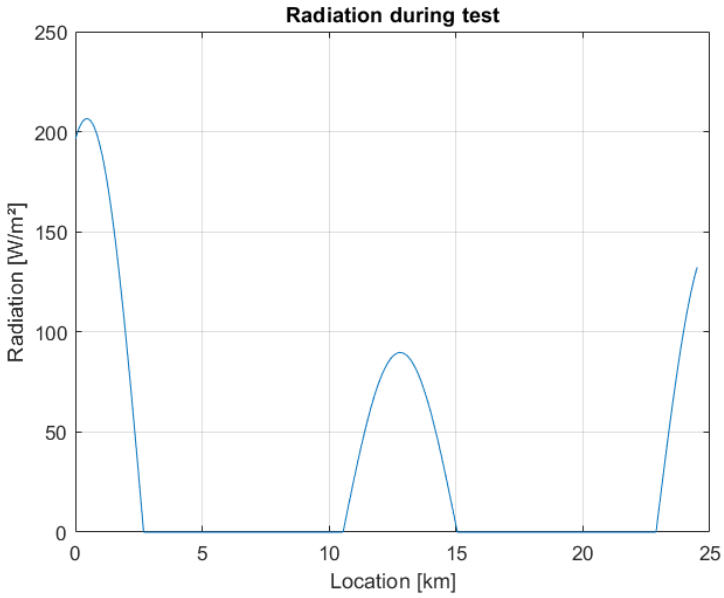

Figure 3.17: Incoming solar radiation values during test on river Maas in January

Furthermore, the ground temperature, air temperature, and streambed temperature are plotted in figure 3.18. From this figure, the drawback of using the MATLAB-algorithm from section 3.1 is visible when multiple consecutive days with distinct daily average values for the air and ground temperature are simulated. That is, if hourly values had been available for these parameters, the sudden increases and decreases in values at the beginning and end of each day would not occur. As described in section 2.2.2, the streambed temperature closely follows the river temperature.

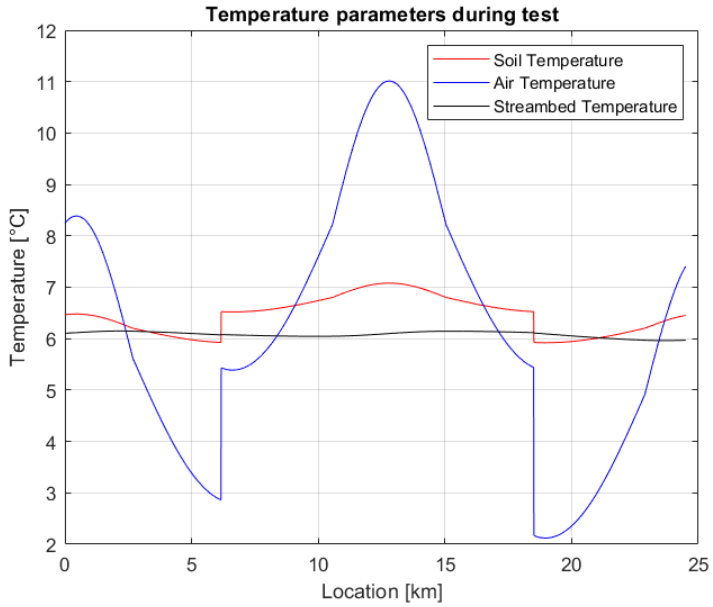

Figure 3.18: Ground, air, and streambed temperatures during test on river Maas in January

Lastly, the contributions of the different heat exchange processes are analyzed. Table 3.6 shows the contributions for each simulated day. Logically, the sum of the absolute values of the contributions is 100% on each day.

Table 3.6: Heat flow contributions on river Maas in January

	Contribution in %		
Heat exchange process	*January 26th*	*January 27th*	*January 28th*
Shortwave radiation	35.5	19.2	9.2
Longwave radiation	(-) 35.8	(-) 28.4	(-) 34.9
Latent heat	(-) 12.4	20.1	(-) 32.0
External convection	(-) 16.1	31.1	(-) 23.7
Internal convection	0.2	1.2	0.2
Inflows	0	0	0
Heat extraction	0	0	0

From table 3.6, it can be concluded that the contribution from internal convection is negligible. External forced convection has a positive value on day 2 and is negative on the first and last day. A positive value signifies that the air temperature is overall higher than the river temperature. On the second day, condense occurs since the latent heat has a negative sign, while on the first and third day water evaporates. The influence of solar radiation is largest on January 26th due to the high relative radiation value as depicted in figure 3.17. Longwave radiation is negative during every simulated day, which indicates that the amount of back radiative fluxes from the river to the atmosphere are higher than the amount of landcover and atmospheric radiation fluxes combined. January 27th heats up the river since every heat exchange process transfers heat to the river except for longwave radiation. This increase in temperature on the second day can be seen from figure 3.16 as well. On January 26th and 28th, all exchange processes are negative except for solar radiation, which indicates that the river is cooling down. The signs and magnitudes of all contributions are similar to other test results found in literature during winter months [13], which confirms that the general behaviour of the river temperature is accurately modelled.

Fluid Trajectory Model test 2 - river Maas in July

The second test conducted on the Fluid Trajectory Model also uses the river Maas between Grave and Lith as study site, this time during summer. The same strategy is used to solve for the final river temperature. The temperature of $24.1°C$ in Grave on July 2nd 2019 at 12 p.m. is used as the initial temperature. Since the volume flow (obtained from the Rijkswaterstaat) was considerably lower than the flow in wintertime, the stream velocity decreased and the test lasted longer. To be exact, it took a fluid volume 216.52 hours to travel the 24.5 kilometer distance between Grave and Lith. Accordingly, ten days are modeled or, in other words, ten simulations are run. The input data for each simulation is detailed in table 3.7.

Table 3.7 includes values for vts, A, and SF, while no data could be obtained for these parameters from online data sets. Thus, values are assumed similarly to the test in January. The view to sky coefficient is assumed to equal 1 throughout the entire test as done in the winter test. The average value from literature of 0.05 is again considered for the albedo factor. In summer, the trees along the streamline have thicker foliage which increases shade. However, the high position of the sun in summer reduces the shade of trees on the river. Therefore, a value of 10% is reused during each day for the shading factor. Lastly, no inflows or heat extractions are considered.

Table 3.7: Input parameters for test on river Maas in July

	Value									
Parameters	*July 2nd*	*July 3th*	*July 4th*	*July 5th*	*July 6th*	*July 7th*	*July 8th*	*July 9th*	*July 10th*	*July 11th*
L_{river} $[m]$	1,360	2,720	2,720	2,720	2,720	2,720	2,720	2,720	2,720	1,380
D_{river} $[m]$	10	10	10	10	10	10	10	10	10	10
W_{river} $[m]$	140	140	140	140	140	140	140	140	140	140
v_{stream} $[m/s]$	0.031	0.031	0.031	0.031	0.031	0.031	0.031	0.031	0.031	0.031
v_{wind} $[m/s]$	2.6	2.8	1.6	3.0	3.1	2.5	2.5	2.3	1.5	2.4
$Hours_{daylight}$ $[h]$	16.65	16.63	16.62	16.58	16.57	16.55	16.53	16.52	16.5	16.49
$Time_{sunrise}$ $[h]$	5.4	5.42	5.43	5.43	5.45	5.47	5.48	5.5	5.52	5.53
$Time_{start}$ $[h]$	12p.m.	12a.m.	12a.m.	12a.m.	12a.m.	12a.m.	12a.m.	12a.m.	12a.m.	12a.m.
ε_w $[/]$	0.97	0.97	0.97	0.97	0.97	0.97	0.97	0.97	0.97	0.97
σ $[W/(m^2 \cdot K^4)]$	5.67 $\cdot 10^{-8}$	5.67 $\cdot 10^{-8}$	5.67 $\cdot 10^{-8}$	5.67 $\cdot 10^{-8}$	5.67 $\cdot 10^{-8}$	5.67 $\cdot 10^{-8}$	5.67 $\cdot 10^{-8}$	5.67 $\cdot 10^{-8}$	5.67 $\cdot 10^{-8}$	5.67 $\cdot 10^{-8}$
C_L $[\%]$	22	22	67	67	67	56	78	67	89	78
H $[\%]$	61	62	59	60	75	68	70	61	75	73
vts $[/]$	1	1	1	1	1	1	1	1	1	1
A $[/]$	0.05	0.05	0.05	0.05	0.05	0.05	0.05	0.05	0.05	0.05
SF $[\%]$	10	10	10	10	10	10	10	10	10	10
k_{soil} $[W/(m \cdot K)]$	0.8	0.8	0.8	0.8	0.8	0.8	0.8	0.8	0.8	0.8
L_{soil} $[m]$	0.5	0.5	0.5	0.5	0.5	0.5	0.5	0.5	0.5	0.5
p_0 $[hPa]$	1,013	1,013	1,013	1,013	1,013	1,013	1,013	1,013	1,013	1,013
p_{air} $[hPa]$	1,020	1,018	1,016	1,013	1,015	1,012	1,017	1,019	1,016	1,017
C_b $[hPa/K]$	0.62	0.62	0.62	0.62	0.62	0.62	0.62	0.62	0.62	0.62
$Inflow\ data$ $[/]$	none	none	none	none	none	none	none	none	none	none
$Heat\ \ extraction\ data$ $[/]$	none	none	none	none	none	none	none	none	none	none
T_{air} $[^\circ C]$	17.2	16.1	17.2	19.6	17.8	14.7	14.1	15.4	15.0	19.5
T_{ground} $[^\circ C]$	19.8	20.1	20.5	19.5	20.5	20.5	19	20.2	20	20.4
Q_{in} $[W/m^2]$	418.25	394.04	481.35	420.69	288	332.33	210.73	396.15	216.11	311.49
T_w, i_1 $[^\circ C]$	24.1	result day 1	result day 2	result day 3	result day 4	result day 5	result day 6	result day 7	result day 8	result day 9
N $[/]$	136	272	272	272	272	272	272	272	272	138

The resulting temperature variation of a fluid volume when it travels from Grave to Lith is depicted in figure 3.19. The simulated end temperature after modeling 24.5 kilometers or approximately 216.5 hours is $22.29^\circ C$. Comparing with the data found online in Lith on July 11th at 12 p.m., it should have been $21.80^\circ C$. A difference of $0.49^\circ C$ between the real life value and the simulation is observed, which signifies that the output of the model again accurately models the real life situation.

The resulting error is larger than the $0.135^\circ C$ difference that resulted from the test in January. The reason for a bigger difference is a higher amount of days that needed to be modelled. That is, each extra modelled day contributes to more imprecision because of unknown parameters as previously described. Due to this uncertainty in parameters, it makes more sense to draw conclusions on the general behaviour of the temperature curve instead of assessing the specific final result. Figure 3.19 shows an approximate repetitive behaviour on the third and fourth modelled day. Afterwards, from day five till day seven, a significant drop in temperature occurs. When analyzing the average values for the air temperature and the solar radiation in table 3.7, it is found that colder days occurred with less solar radiation from the 6th (day 5) till the 8th (day 7) of July. When the air temperature is low compared to the river temperature, the river will be cooled down greatly due to external convection. Since less solar radiation persisted, the cooling from external convection was not offset by the suns radiation and a significant temperature drop

resulted. On the 8th day, the incoming solar radiation was high which can be seen in the peak on day 8 in figure 3.19 as well. Concluding, the trend seen in figure 3.19 could have been expected when analyzing the meteorological data.

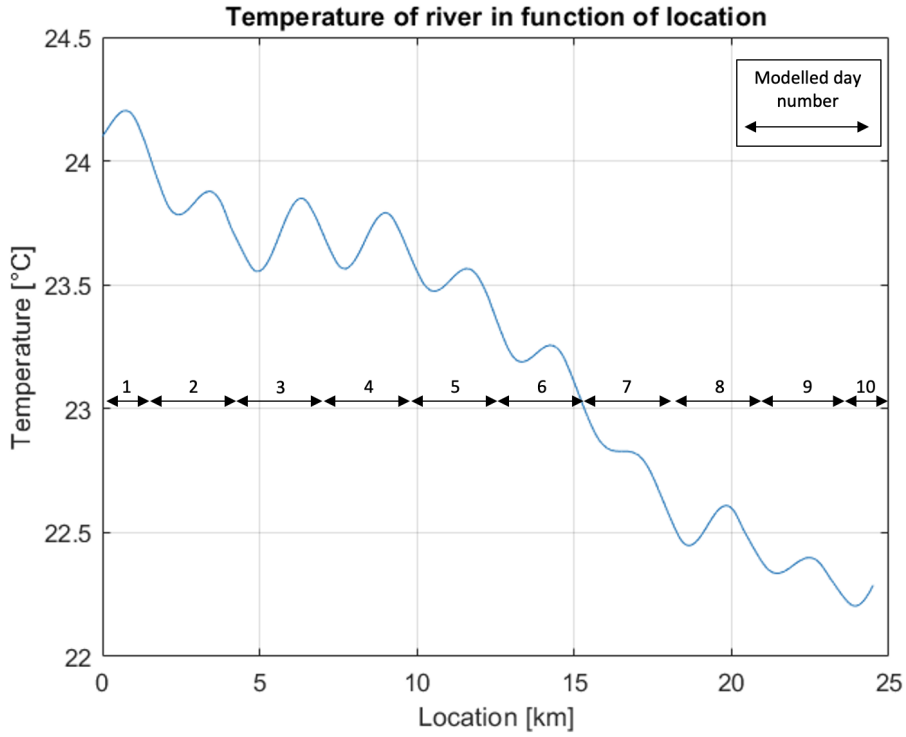

Figure 3.19: Temperature of the river Maas between Grave and Lith in July

The simulated temperature curve in figure 3.19 can be evaluated in greater detail if the temperature trend that occurred at the measuring station of Lith is studied, based on the online available data. When doing so, note that analyzing the temperatures at one measuring point is different from analyzing the output of the Fluid Trajectory Model. That is, the model simulates different measuring points between the two stations instead of examining the temperature at one fixed station. However, online data showed that the temperatures measured at the same time in Grave and Lith only differed with $0.1°C$ on average. Thus, measurements at any location between the two villages will yield approximately the same results over time as the measurements at either station. To conclude, it is justified to compare the temperature at a certain point in time from the model to one of the measuring stations temperature at the same point in time. In figure 3.20, temperature data obtained from the Rijkswaterstaat of the measuring station in Lith is shown. The data is plotted from July 2nd at 12 p.m. (hour 0) till July 11th at 12 p.m. (hour 216). In other words, the x-axis in figure 3.20 represents the duration that measurements were taken in Lith starting at noon on July 2nd. It is important to understand that this measuring time corresponds to a traveled distance of the Fluid Trajectory model in figure 3.19. For example, hour 48 in figure 3.20 corresponds to a traveled distance of approximately 5,400 meters at the velocity of the fluid ($0.031\ m/s$). This means that figure 3.19 and figure 3.20 can be compared to one another. Moreover, it is clear that each day corresponds to one period of temperature rise ('hills' in the figures) on both figures which makes it easy to compare each day between both figures.

Comparing figure 3.19 and figure 3.20 yields results on the accuracy of the created Fluid Trajectory Model. During the second and the third day, significant peaks in temperature are found in figure 3.20. However, the modelled second and third day depicted in figure 3.19 do not experience these high temperature values. Presumably, these peaks originate from inflows, which are not simulated using the Fluid Trajectory Model since no data could be obtained on any possible occurring inflow. When days five, six, and seven are compared between both figures, a similar trend is perceived. During the time span of these days, the temperature on both figures drops with approximately $1.2°C$. The temperature drop is a consequence of lower air temperatures and lower incoming solar radiation fluxes (see table 3.7). On the eight day, the river was heated in real life, due to relatively high solar radiation fluxes, as can be seen from the temperature increase in figure 3.20. The same conclusion can be drawn for the simulated day in figure 3.19. On both graphs, the temperature drops between day eight and ten. In summary, the general behaviour of the Fluid Trajectory Model closely relates to the river behaviour that can be found in real life. As a result, the Fluid Trajectory Model can be identified as an accurate model to simulate the temperature variation of a river.

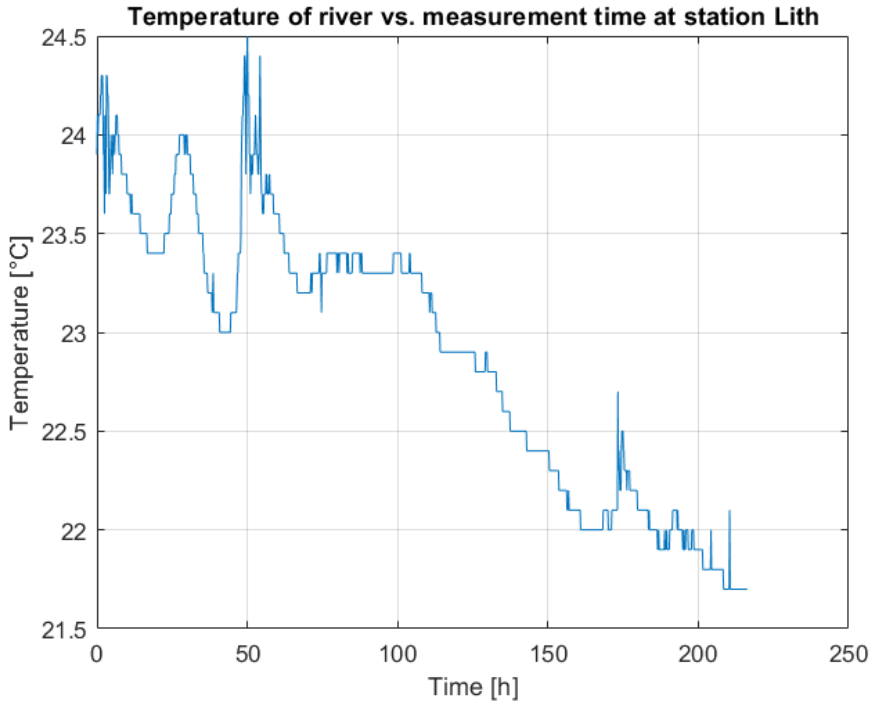

Figure 3.20: Temperature data from the Rijkswaterstaat at station in Lith during modelling period

The moments of increase and decrease of the river temperature can be further clarified using figure 3.21 and figure 3.22. Figure 3.21 represents the incoming solar radiation values during each day, simulated by the algorithm integrated in the MATLAB code of the Fluid Trajectory Model. High radiation values are perceived on the third, fourth, and eight day which clarifies the increase in temperature on these days in figures 3.19 and 3.20. Moreover, the decrease in temperature on day five, six, and seven are also proved based on the low radiation values during these days. This decrease in temperature is not solely due to low radiation values, but also due to low air temperatures (see figure 3.22) which influences different heat exchange processes (longwave radiation, latent heat and external convection). The variation in soil temperature in figure 3.22 is rather small, approximately a variation of only $2°C$. As a consequence, the soil temperature has a low contribution to the change in river temperature.

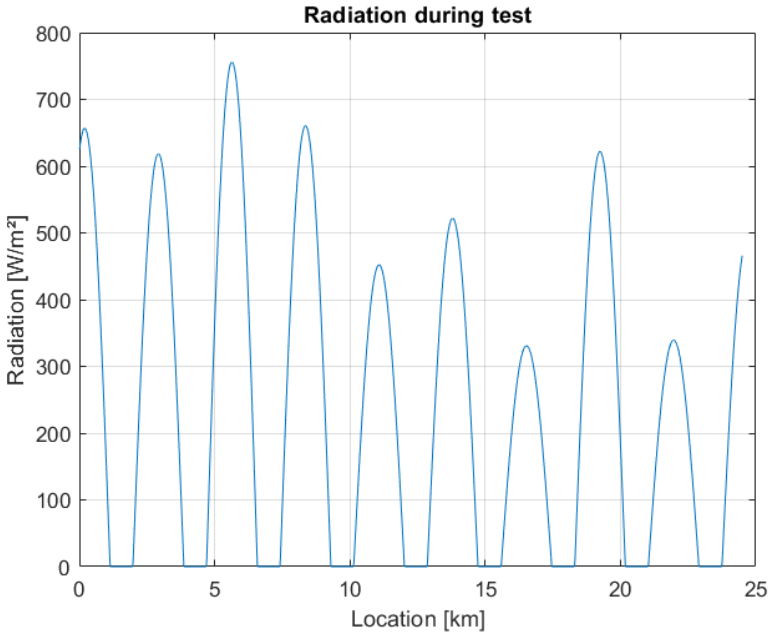

Figure 3.21: Incoming solar radiation values during test on river Maas in July

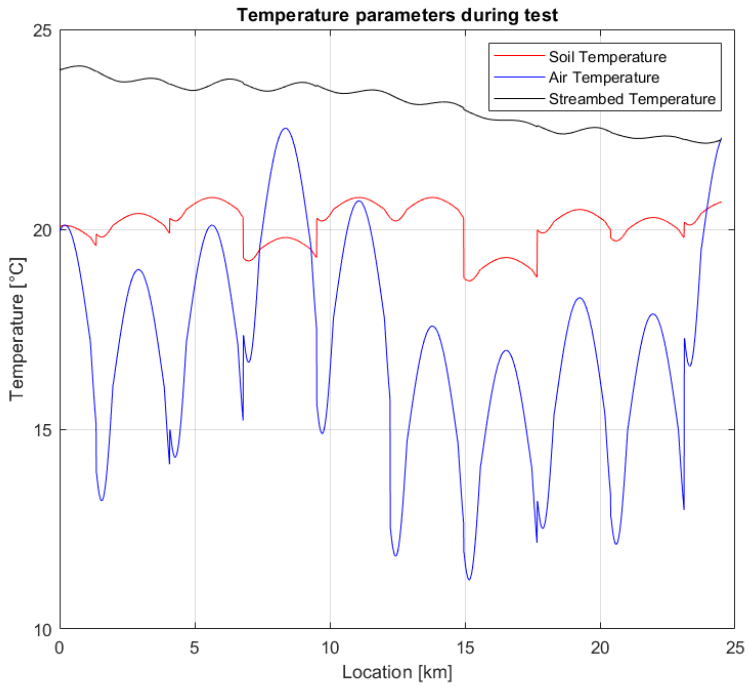

Figure 3.22: Ground, air, and streambed temperatures during test on river Maas in July

Lastly, the contributions of the heat exchange processes are analyzed. Table 3.8 summarizes the daily contributions. Since all contributions, except for shortwave radiation, have negative values on each day, it results that the river temperature dropped significantly whenever the solar radiation values were below average. Which means day five, six, and seven resulted in the most significant cooling of the river, a conclusion that was drawn based on different perspectives earlier on.

Comparing the contributions during summertime (table 3.8) to the contributions in wintertime from the previous test (table 3.6), differences can be distinguished. The influence of shortwave radiation was considerably lower during the test in January than its influence during the summer test. This results from a smaller solar zenith angle during summer months compared to winter months [22]. When the contribution of shortwave radiation decreases, the contributions of the other heat exchange processes increase which is also perceived when comparing both tables. The contribution of internal convection is negative during every day of the test in January while the opposite is perceived for the test in July. Thus, the ground will have a cooling effect on the temperature of the river Maas during summer months while the river will be heated by the ground during wintertime.

Table 3.8: Heat flow contributions on river Maas in July

	Contribution in %									
Heat exchange process	*July 2nd*	*July 3th*	*July 4th*	*July 5th*	*July 6th*	*July 7th*	*July 8th*	*July 9th*	*July 10th*	*July 11th*
Shortwave radiation	39.4	30.2	42.6	44.2	32.9	31.1	23.3	40.1	31.4	46.9
Longwave radiation	(-) 13.1	(-) 15.3	(-) 12.4	(-) 11.1	(-) 12.4	(-) 14.1	(-) 13.4	(-) 13.0	(-) 11.7	(-) 6.5
Latent heat	(-) 20.7	(-) 23.7	(-) 17.5	(-) 27.4	(-) 25.9	(-) 21.1	(-) 23.5	(-) 20.1	(-) 17.6	(-) 22.3
External convection	(-) 25.9	(-) 30.0	(-) 26.8	(-) 16.2	(-) 28.1	(-) 33.3	(-) 39.0	(-) 26.6	(-) 39.0	(-) 24.1
Internal convection	(-) 0.9	(-) 0.8	(-) 0.7	(-) 1.1	(-) 0.7	(-) 0.4	(-) 0.8	(-) 0.2	(-) 0.3	(-) 0.2
Inflows	0	0	0	0	0	0	0	0	0	0
Heat extraction	0	0	0	0	0	0	0	0	0	0

Fluid Trajectory Model test 3 - river Murg

For the third and final test on the Fluid Trajectory Model, the river Murg in Switzerland is studied. The main reason for shifting to this river lays in the frequently updated meteorological data provided by MeteoSwiss[8]. Their website provides hourly averaged data instead of the daily average values of the KNMI used in the previous tests. Using more frequently updated data should signify that the model will generate more accurate results.

The specified study site is located between the water measuring stations of FOEN[9] near the villages of Wängi (47.5007°N 8.9548°E) and Frauenfeld (47.5536°N 8.8988°E) (see figure 3.23). The measuring station Murg-Wängi is located upstream, thus water flows from Wängi to Frauenfeld. The distance between the two measuring station equals 11.8 kilometers (see figure 3.23).

The methodology to solve for an output temperature will be different than the method used for the river Maas, which means that the model is slightly adapted. The hourly average meteorological data will be inputted directly into the model using an array for each parameter (air temperature, ground temperature, incoming radiation, wind velocity, and humidity) (see table 3.10). The amount of array cells equals the amount of hours that needs to be modelled. During every modelled hour, the values for the different meteorological parameters will not be held constant. A linear relationship is created between the average values of the next and previous hour to smooth the hourly variation of each parameter. This methodology

[8] https://www.meteoswiss.admin.ch/home/measurement-values.html?param=messnetz-automatisch
[9] https://www.hydrodaten.admin.ch/en/2126.html

is illustrated for the first three hours in figure 3.24. The average input values are located at every half hour of the corresponding hour.

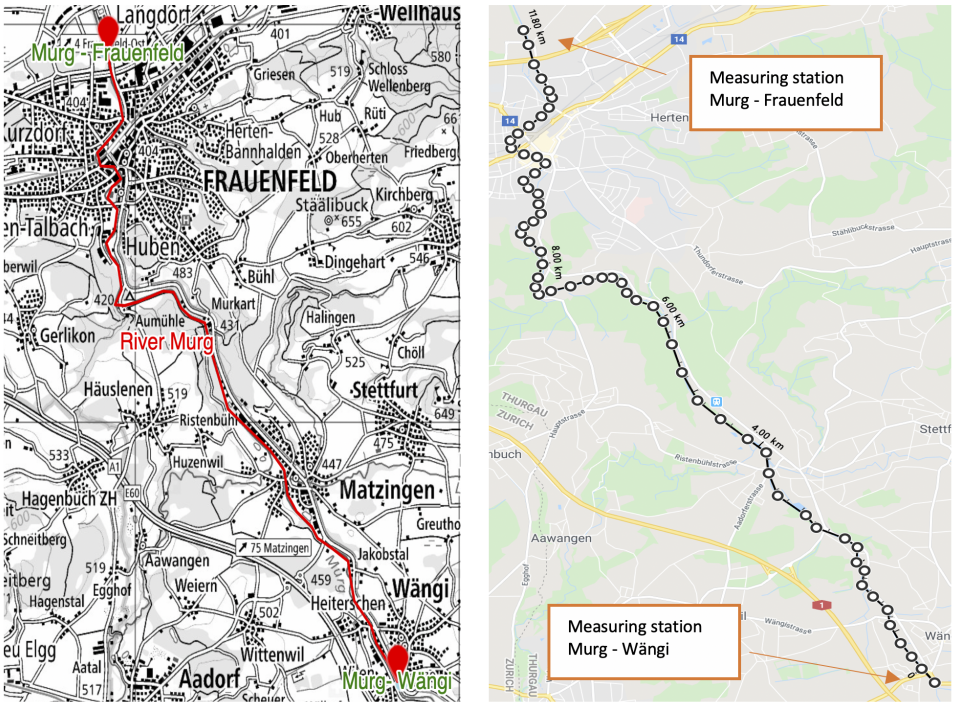

Figure 3.23: Study site of river Murg, distance measured using Google Maps Tools

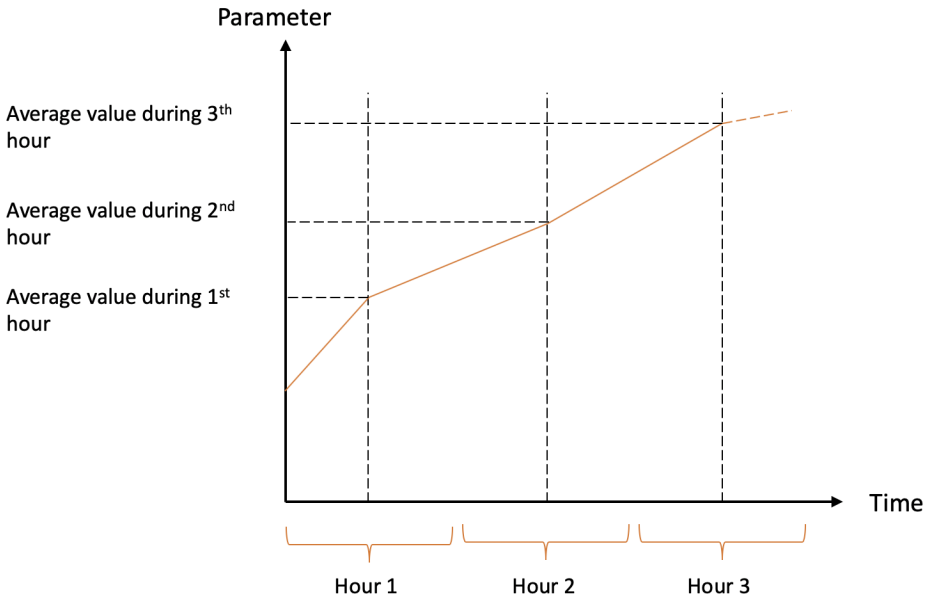

Figure 3.24: Variation over time of transient parameters for test on river Murg

The temperature of $8.7°C$ on April 8th 2020 at 7 a.m. in Wängi is used as the initial water temperature (value acquired from FOEN). The volume flow on the same point in time equalled $1.2\ m^3/s$ at the measuring station in Wängi (value obtained from FOEN). The average river width and depth for the river Murg are 12 meters and 30 centimeters respectively. Resulting from these dimensions and the volume flow, the river velocity was $0.33\ m/s$ on April 8th at 7 a.m. in Wängi. This value for the stream velocity will be held constant for the entire simulation. Based on this flow velocity and the distance between the two measuring points, it took a fluid volume nine hours and fifty minutes to reach Frauenfeld starting from Wängi. Thus, the fluid volume reached Frauenfeld at 4:50 p.m. on April 8th. The value obtained from FOEN for that point in time in Frauenfeld is $13°C$. The necessary inputs for the Fluid Trajectory are detailed in table 3.9 and table 3.10. The former table includes all the constant inputs for the simulation and the latter consists of parameters that change during the simulation. The values in table 3.10 are obtained from MeteoSwiss at the weather station in Aadorf (47.4884°N 8.9035°E).

Table 3.9: Constant input parameters for test on river Murg

Parameters	Value
L_{river} $[m]$	11,800
D_{river} $[m]$	0.30
W_{river} $[m]$	12
S $[/]$	0.02
g $[m/s^2]$	9.81
v_{stream} $[m/s]$	0.33
$Hours_{daylight}$ $[h]$	13.25
$Time_{sunrise}$ $[h]$	6.80
$Time_{start}$ $[h]$	7 am
ε_w $[/]$	0.97
σ $[W/(m^2 \cdot K^4)]$	$5.67 \cdot 10^{-8}$
C_L $[\%]$	0
vts $[/]$	1
A $[/]$	0.05
SF $[\%]$	60
k_{soil} $[W/(m \cdot K)]$	0.8
L_{soil} $[m]$	0.5
p_0 $[hPa]$	1,013
p_{air} $[hPa]$	1,018
C_b $[hPa/K]$	0.62
$Inflow\ data$ $[/]$	none
$Heat\ extraction\ data$ $[/]$	none
T_w, i_1 $[°C]$	8.7
$Number\ of\ elements$ $[/]$	118

Table 3.10: Transient meteorological input parameters for test on river Murg

	Time									
Parameters	*Hour 1*	*Hour 2*	*Hour 3*	*Hour 4*	*Hour 5*	*Hour 6*	*Hour 7*	*Hour 8*	*Hour 9*	*Hour 10*
v_{wind} $[m/s]$	0.70	0.61	0.31	0.81	3.11	2.61	2.31	1.81	1.89	2.50
H $[\%]$	83.7	80.2	71.4	55.9	37.6	37.1	35	32.4	30.6	29.3
T_{air} $[°C]$	3	4	7.8	12.2	16.7	18	18.9	19.6	20.3	20.7
T_{ground} $[°C]$	8	9	10	10	11	11	12	14	15	15
q_{in} $[W/m^2]$	76	231	431	585	705	773	793	756	671	537

The values for the view to sky coefficient, the albedo factor and the shading factor in table 3.9 are assumptions. The view to sky coefficient and albedo follow the same assumptions as reasoned in the previous tests. The shading factor is determined by satellite images of the studied site using Google Maps. A part of the studied site is shown in figure 3.25. From figure 3.25, it is clear that a high amount of riparian vegetation exists at the studied area. Therefore, an estimated shade factor of 60% is used.

Figure 3.25: Image of the studied site of the river Murg that visualizes the riparian vegetation

The simulated temperature along the modelled distance is depicted in figure 3.26. The resulting simulated temperature in Frauenfeld at 4:50 p.m. is $12.945°C$. This value only differs $0.055°C$ from the real life value in Frauenfeld at that point in time. Thus, the use of hourly average values on meteorological data, compared to the daily averages in the previous tests, increased the model accuracy as expected.

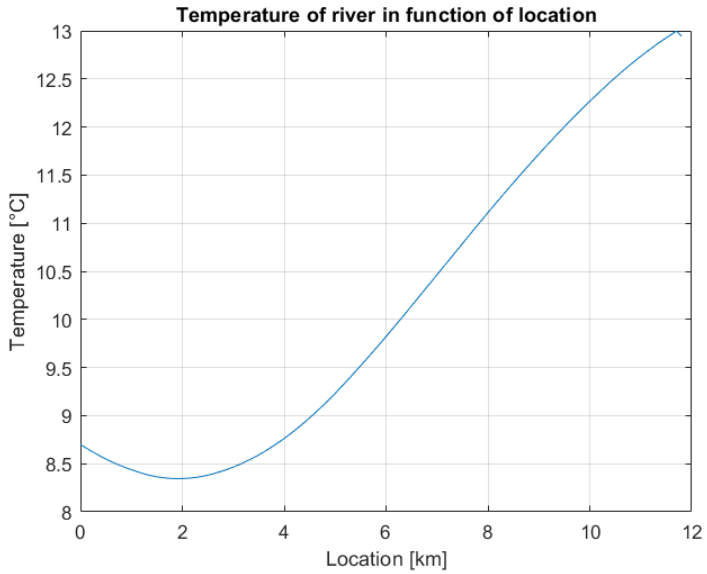

Figure 3.26: Temperature of the river Murg between Wängi and Frauenfeld

The hourly average values of the solar radiation, the air temperature, and the ground temperature, which are connected trough a linear relationship, are displayed in figure 3.27 and figure 3.28. These figures explain the fluctuations in the water temperature between Wängi and Frauenfeld. In the morning, cold air temperatures cool the river while in the afternoon a significant increase in the air temperature causes the river to warm up. Radiation values also intensify during the course of the day, increasing the temperature of the river.

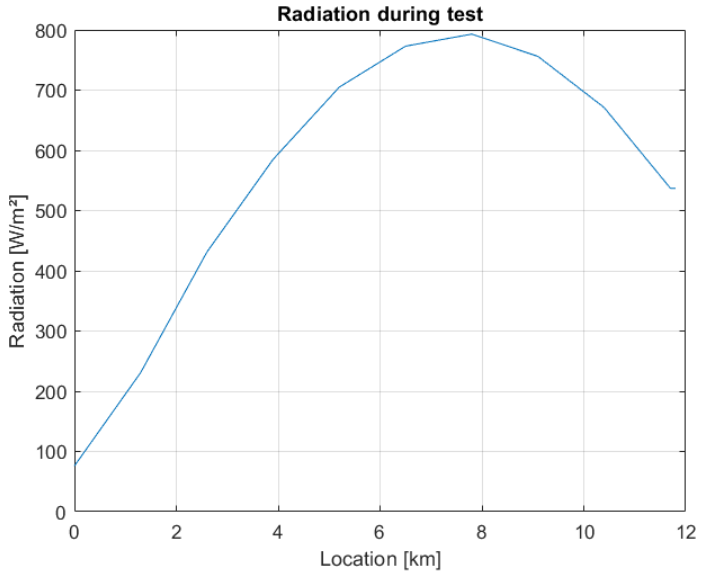

Figure 3.27: Incoming solar radiation values during test on river Murg

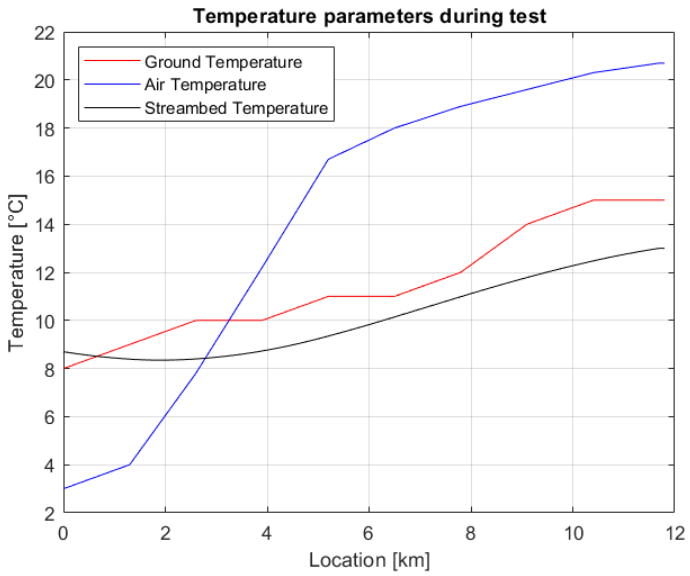

Figure 3.28: Ground, air, and streambed temperatures during test on river Murg

The contributions of the different heat exchange processes during the test are listed in table 3.11. Although a high shading factor is used, shortwave radiation is the largest contributor to the heat budget. This is due to the high values of incoming solar radiation (see table 3.10). Since the air temperature is greater than the temperature of the water for the majority of the test, external convection has a positive value. The same conclusion holds for the ground temperature and thus internal convection. Water evaporates from the river since a negative value for the latent heat is observed. Lastly, longwave radiation is negative which signifies more longwave radiative fluxes are emitted by the river than received.

Table 3.11: Heat flow contributions on river Murg

Heat exchange process	Contribution in %
Shortwave radiation	55.3
Longwave radiation	(-) 19.9
Latent heat	(-) 10.3
External convection	14.4
Internal convection	0.1
Inflows	0
Heat extraction	0

From the three conducted tests on the Fluid Trajectory Model, it can be concluded that the output of the model approximates real life river temperatures. Moreover, the general behavior of a fluid volume in a studied river is accurately simulated in various test scenarios. Furthermore, the accuracy can be enhanced by using more frequently updated online meteorological data as inputs for the model.

Finite Element Model test methodology

One of the advantages of the Finite Element Model is the ability to analyze the water temperature over time at a desired fixed location (see section 3.3). When a river is studied based on two measuring stations at a certain distance from one another, this ability can be tested. That is, the real life temperature values from the upstream temperature station will serve as the sensor-value inputs at location i_0 in the finite element model. After running the model, the simulated temperature values over time at the location of the downstream station can be assessed. These values should correspond to the values that can be found online for that measurement station.

Finite Element Model test - River Maas

The river Maas between Grave and Lith (see figure 3.15) will be used as the study site to test the Finite Element Model. The real life temperatures found in Grave serve as the sensor-value inputs for the Finite Element Model and simulated output temperatures at the location of Lith will be plotted. These values should correspond to the real life values found at the temperature station in Lith. The time period of the conducted test comprises the entire month of March in 2020. It is for this reason that the study site of the river Maas is used, since data going thirty days back in time is not available for the river Murg.

The water temperature values in Grave from the Rijkswaterstaat, recorded with an interval of 10 minutes, are used as the sensor values for the model and they are detailed in appendix A. The daily average values for the meteorological parameters at each day in March are also found in appendix A. The ground temperature, air temperature, and incoming solar radiation are varied based on their daily averages using the MATLAB algorithm discussed in section 3.1. Additionally, appendix A includes the temperatures found in Lith from the online archives of the Rijkswaterstaat. These real life values will be compared to simulated

results of the Finite Element Model at the location of Lith. Values for necessary inputs that were held constant during the entire month or were needed to initialise the Finite Element Model are listed in table 3.12.

Table 3.12: Necessary input parameters for Finite Element Model test not listed in appendix A

Parameter	Value
L_{river} $[m]$	24,500
D_{river} $[m]$	10
W_{river} $[m]$	140
v_{stream} $[m/s]$	0.7
ε_w [/]	0.1
σ $[W/(m^2 \cdot K^4)]$	$5.67 \cdot 10^{-8}$
vts [/]	1
A [/]	0.05
k_{soil} $[W/(m \cdot K)]$	0.8
L_{soil} $[m]$	0.5
P_0 $[hPa]$	1,013
C_b $[hPa/K]$	0.62
$Inflowdata$ [/]	0
$Number\ of\ elements$ [/]	1,000
$Number\ of\ timesteps$ [/]	446,400

A graphical overview of the incoming solar radiation, air temperature, and ground temperature are given in figure 3.29 and figure 3.30.

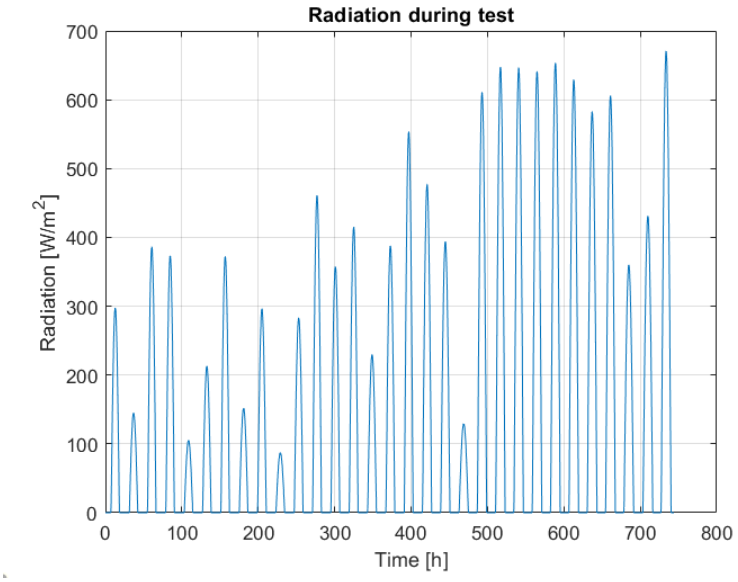

Figure 3.29: Incoming solar radiation values during Finite Element Model test

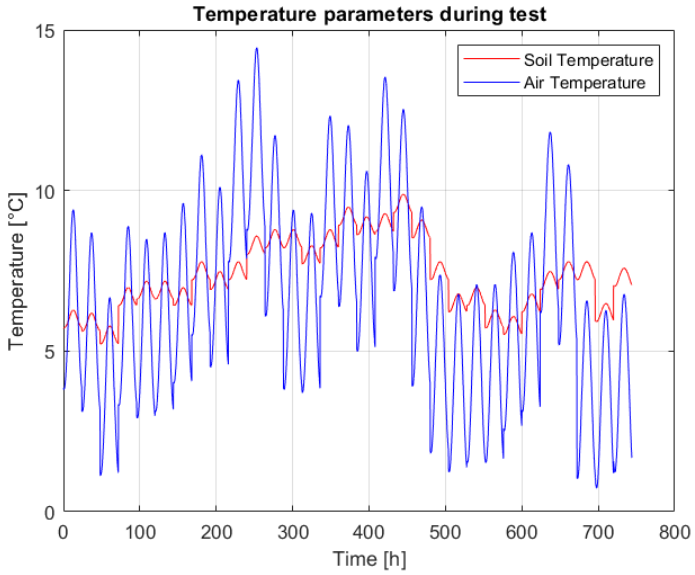

Figure 3.30: Ground and air temperature during Finite Element Model test

When the temperature values of Grave are inputted and the other necessary inputs, listed in table 3.12 and appendix A, are implemented in the model, the simulation can be run. The result of the conducted test is depicted with the blue graph in figure 3.31. The orange graph in figure 3.31 represents the measured values in Lith, obtained from the Rijkswaterstaat. From figure 3.31, it is clear that the simulated result closely approximates the real life situation.

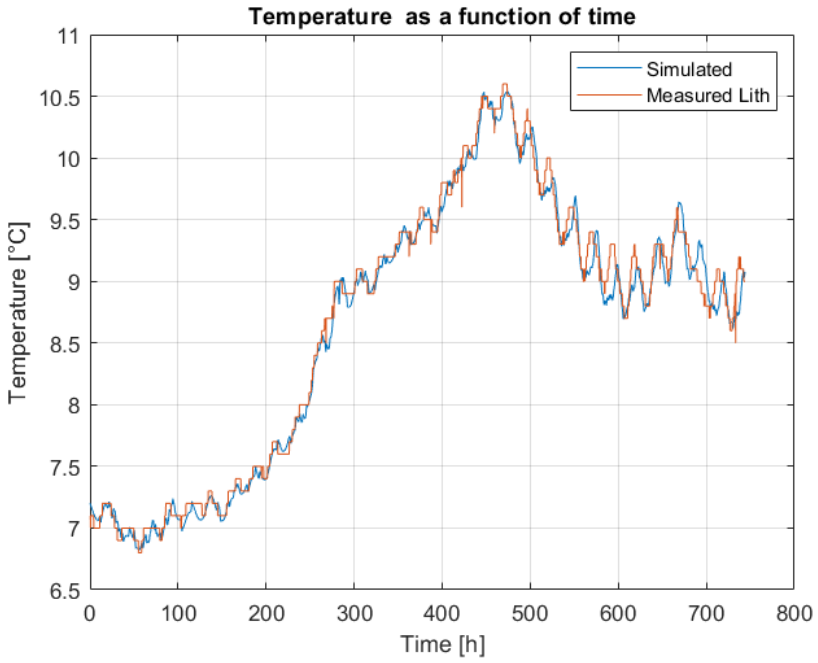

Figure 3.31: Simulated and real life temperature values at the measurement station in Lith

The feature of the Finite Element Model to accurately analyze the water temperature over time at a specific location was demonstrated using this test on the river Maas. The model could have been used to follow a fluid volume travelling the stream as well (see section 3.2). However, these tests were already conducted using the Fluid Trajectory Model and from section 3.3, it follows that similar results would be obtained when using the Finite Element Model. From this chapter, it is found that both the Finite Element Model and the Fluid Trajectory Model attain results which approximate reality to a close extent. Thus, the models have proven to reach a degree of accuracy which enables their further use in this research for the assessment of heat potential.

3.4.3 Physical test

The tests conducted in section 3.4.2 use inputs found from online archives of river and meteorological data. While the outcomes of these online based tests assure an overall accurate behaviour of the models, a physical test enables more precise results and a more comprehensive validation. As explained in section 1.4, this research will only propose a methodology for conducting a physical test without results on the actual completion of the proposed test. Note that the suggested test methodology is solely applicable on the Fluid Trajectory Model. The reason to only evaluate the Fluid Trajectory Model with a physical test is a consequence of the convenience in validating this model compared to the Finite Element Model as described in section 3.3.

Test methodology

The Fluid Trajectory Model can be evaluated by following a fluid volume along the trajectory of a river. One way to physically imitate this model is by following a certain part of a river by using a kayak or canoe. During the navigation downstream the river, water temperature measurements must be recorded at a certain time interval or traveled distance interval. While water temperature measurements are recorded by someone in the kayak, meteorological measurements must be made which will serve as inputs for the model. Note that the first recorded water temperature will also serve as an input for the Fluid Trajectory Model. After completion of the measurements, the recorded river temperatures can be compared to the temperatures generated by the model along the trajectory. The same time or distance interval must be used in the model as was practiced in real life to correctly compare each water temperature measurement. Note that navigating the kayak should be done at the same speed of the flowing water. That is, the person navigating the kayak can only steer to maintain the right direction in the river but cannot accelerate or decelerate by paddling.

Study site

A section of the river Dyle near the city of Leuven is proposed as the study site. Note that the study can be repeated at different locations along the river.

The physical setting of the suggested test is the part of the Dyle between the village Korbeek-Dijle (50.838374°N 4.643668°E) and the castle of Arenberg in Leuven (50.863290°N 4.684079°E). The route from Korbeek-Dijle to the castle of Arenberg, depicted in figure 3.32, is a frequently traveled route for kayaking.

Figure 3.32: Google Maps image of river Dyle studied between Korbeek-Dijle and Arenberg castle

Input data

The required inputs needed for operating the Fluid Trajectory Model consist of four main parts, listed below. Accurate data must be used within each category in order to assess the correctness of the model and its outputs.

- Geometric data
- Meteorological data
- River flow data
- River temperature data

Geometric study site data consists of the river length, river width, and river depth. The length of the studied part is calculated using Google Maps (white dots in figure 3.32) and equals 6.02 kilometers. The river width is also assessed with Google Maps and equals 9.38 meters on average. The average river depth can not be measured using Google Maps and must be measured in real life when the test is conducted. This can be done by using a meter ruler and performing depth measurements at different intervals along the studied path. The mean depth is found by adding the measurements together and dividing the total sum by the number of recordings.

Meteorological data includes air temperature, ground temperature, incoming solar radiation, shading, humidity, wind velocity, cloud cover, sunrise time, and hours of daylight. Data on the air temperature, solar radiation, humidity, wind velocity, and cloud cover can be found on the website of the KMI. However, the nearest weather station is located in Zaventem at approximately 15 kilometers from Leuven. This difference in location causes inaccuracies in the weather data used for the model. Thus, measurements should be recorded at the site using appropriate tools for each parameter. Air temperature and ground temperature can be measured with a classic thermometer and soil probe thermometer respectively. Incoming shortwave radiation from the sun is most accurately measured using a pyranometer. Using a second pyranometer, facing the river surface, the reflected part of the incoming solar radiation can be measured. From

these measurements, the reflected portion or the albedo factor can be calculated needed in equation 2.7. The shading factor needed in equation 2.7 has to be determined from observation. An estimation on the percentage of shading on the river surface should be made over the entire studied river part. Humidity is best measured using a hygrometer. An anemometer should be used to determine the wind velocity. The cloud cover is hard to assess at the site. Instead, an infrared satellite view of Belgium from the KMI should be used to determine the cloud cover at the studied site. Sunrise time and hours of daylight are to be determined using KMI data as well.

Throughout this research a steady-flow has been assumed, which indicates that flows, velocities, and river dimensions are held constant. In other words, average values are assumed for these properties. When one conducts the proposed test, the flow velocity of the main stream should be measured multiple times and at different locations. The average velocity can be computed using these recordings. The flow velocity can be measured by recording the time it takes a floating object to travel a specified distance. From the velocity and cross section (determined from the geometric parameters), the volume flow can be calculated. Note that this method does not consider the varying river velocity with river depth since only the velocity at the river surface is measured. Therefore, a more detailed approach consists of using a water flow probe which accurately measures the average volume flow over the cross section of the river. The same principles should be used for determining the volume flows of incoming side streams, which are required to estimate the influence of inflows on the heat budget when no data on these inflows is available.

River temperature data of the main stream and incoming side streams are best recorded using a thermocouple. Two persons should operate the kayak when traveling the river. One person measures the temperature at specific time intervals while the other person maintains the correct orientation and speed. The temperature of the inflows must be measured at the same time intervals as the main river temperature is measured.

Chapter 4

Model Application

This chapter provides an answer on the heat potential of the river Dyle in Leuven. Both summer and winter conditions will be analyzed and the results are computed with the Fluid Trajectory Model. From section 3.3, it results that this model is best suited to model test cases with inflows and heat extractions. Furthermore, no increase in accuracy is obtained when using the Finite Element Model.

Section 4.1 describes the segment of the river Dyle that is simulated using the Fluid Trajectory Model. Section 4.2.2 details the demand of heat extraction from surface water for residential buildings in Leuven. In section 4.2.2, an assessment is made on the heat potential of the Dyle by using the Fluid Trajectory Model. The acquired potential is afterwards compared to the heat demand in Leuven. A sensitivity analysis is conducted to indicate the influence of varying factors on the heat potential. Section 4.4.1 analyzes the influence on the applicability of heat extraction from the Dyle in Mechelen (more downstream than Leuven) when regulations on river cooling are considered. Lastly, this chapter will generally assess the influence of river cooling through heat extraction on the physical and ecological processes in a river.

4.1 Study Site and Input Data

Since the heat potential of the river Dyle for Leuven is analyzed as well as the influence on the heat potential in Mechelen (see section 4.4.1), the study site comprises the part of the Dyle between Leuven and Mechelen. More specifically, the model will simulate the Dyle from the point it enters the city of Leuven until it arrives in the city center of Mechelen. Figure 4.1 depicts the modelled site. The distance between the start and end point of the modelled part of the Dyle (see figure 4.1) measures approximately 34 kilometers.

The necessary meteorological data for the model are obtained from two different websites provided by the KMI. Air temperature, wind speed, humidity, and air pressure data is collected from a meteostation in Haacht[1]. Incoming solar radiation is obtained from monthly average archive values of Leuven[2]. Volume flow data is collected from the VMM[3] at the measuring station of Wilsele/Dijle. River temperature data is collected from a different website[4] provided by the VMM at the measuring station Heverlee/Arenberg Castle, which is in close proximity to the start point of the test.

[1] https://wow.meteo.be/nl/

[2] http://www.meteo.be/resources/climatology/climateCity/pdf/climate_INS24062_nl.pdf

[3] http://geoloket.vmm.be/Geoviews/index.php?resetsession=Y

[4] https://www.waterinfo.be/default.aspx?path=NL/Thema/Overstroming_Actueel

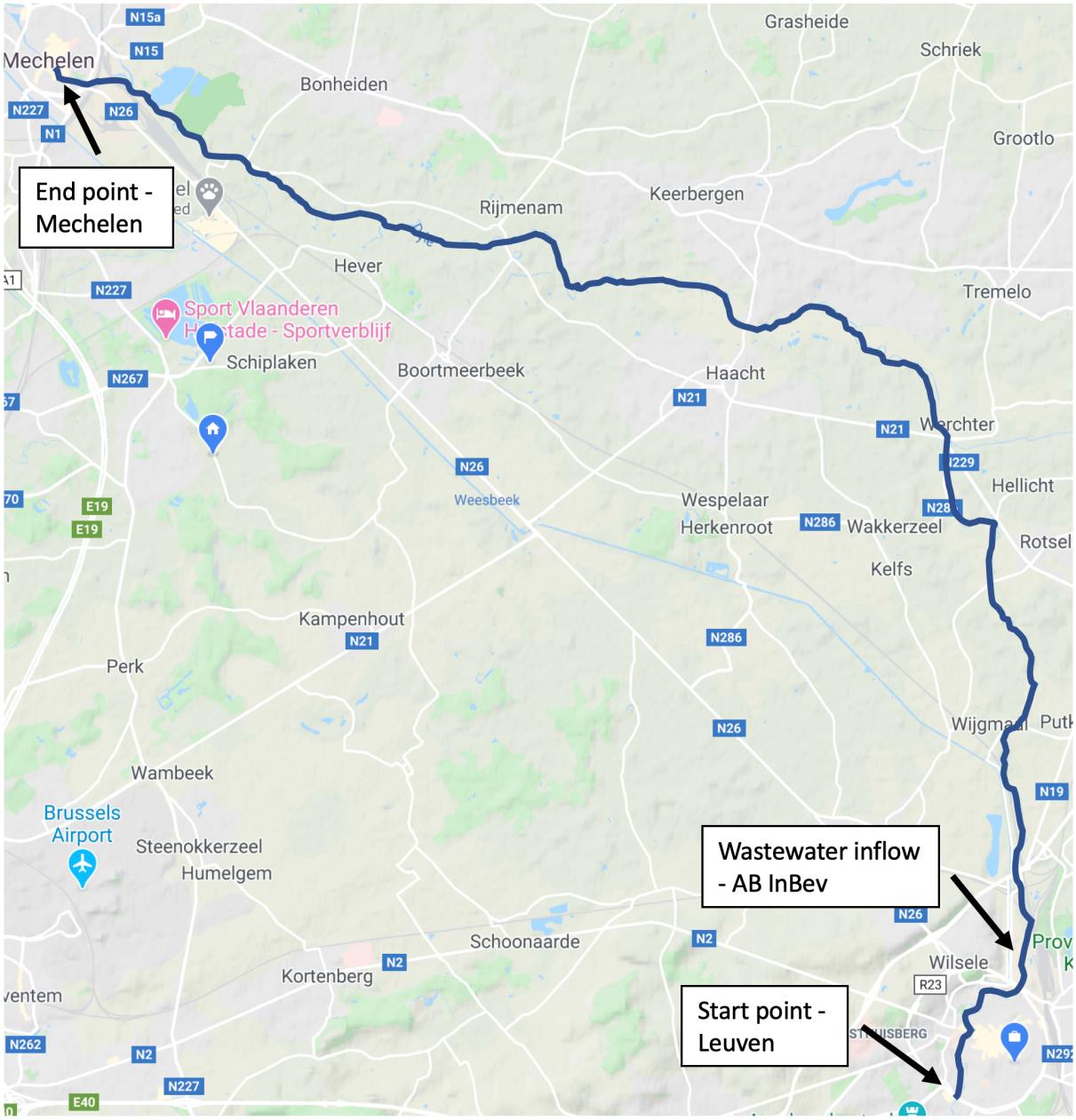

Figure 4.1: Google Maps image of river Dyle (blue line) studied between Leuven and Mechelen

The data provided by the KMI and the VMM, through the previously stated websites, all have discontinuities in measurement frequency (some years have no measurements at all). However, in July 2016 and February 2016, data was found for all the necessary input parameters. Accordingly, tests during these months will be used to asses the heat potential during summer and winter respectively. The necessary input data for both tests can be found in appendix B . Also, data was found on the temperature and discharge rate of wastewater at the brewery of AB InBev from the VMM. This data is included as inflow data in Apppendix B. The inflow is located 3.5 kilometers after the starting point, illustrated in 4.1.

The same methodology for solving the Fluid Trajectory Model is used as described in 3.4.2. The results in temperature variation of the river Dyle between Leuven and Mechelen, when including the modelling of heat extraction, are detailed in 4.2.2.

4.2 Heat Extraction Potential

4.2.1 Heat demand

The heat demand for Belgian cities and villages near rivers has been studied in other research [23]. This research estimates the heat demand by analyzing the monthly gas consumption for heating in kWh. The amount of energy needed for heating through gas is assumed to be fully replaced by the heat extracted from surface water by a heat pump. The research also enables to analyze different areas of applicability (size of heat network) surrounding a river. Table 4.1 summarizes the heat demand for Leuven and Mechelen during the year of 2017. A heat network of $500\ m$ and $1,000\ m$ are considered. A network of $1,000\ m$ signifies that the network stretches to a distance of $1,000\ m$ on both sides of the river. In other words, the total width of the network is $2,000\ m$. An example of a $500\ m$ and $1,000\ m$ heat network is given for Leuven in figure 4.2. The pink area represents the part of the city center (fulfilling a minimal population density) located between 0 and $500\ m$ from the river, the green area between 0 and $1,000\ m$. The gaps between the colored parts in figure 4.2 represent locations at which a certain population density is not met. Consequently, these areas are not included in the research of heat demand.

Table 4.1: Heat demand in Leuven and Mechelen

	Heat consumption during 1 hour [kWh]			
	Leuven heat network size [m]		***Mechelen heat network size [m]***	
Month	*500*	*1,000*	*500*	*1,000*
January	27,165	69,156	40,038	77,289
February	24,730	62,958	36,450	70,363
March	19,358	49,282	28,532	55,078
April	11,066	28,172	16,310	31,486
May	4,922	12,531	7,255	14,005
June	2,385	6,071	3,515	6,785
July	2,004	5,101	2,953	5,700
August	2,253	5,737	3,321	6,412
September	4,007	10,201	5,906	11,401
October	10,132	25,795	14,934	28,829
November	18,935	48,204	27,908	53,873
December	25,937	66,030	38,228	73,796

The data for February and July, listed in table 4.1, will be used in section 4.2.2 to analyze whether these demands can be fulfilled by the heat potential of the river Dyle.

From table 4.1, it is concluded that the maximum amount of heat which a heat pump would need to extract in Leuven is approximately $70\ MW$. This value exceeds the maximum capacity of $35\ MW$ for industrial heat pumps [24]. Therefore, multiple heat pumps are needed to fulfill the demand. Extraction is chosen to occur at only one location. Thus, a cascading system of heat pumps will be implemented at the extraction location. The location of extraction is chosen in the center of Leuven (1.5 kilometers downstream of starting point) since this eases the distribution of heat to the surrounding residential buildings.

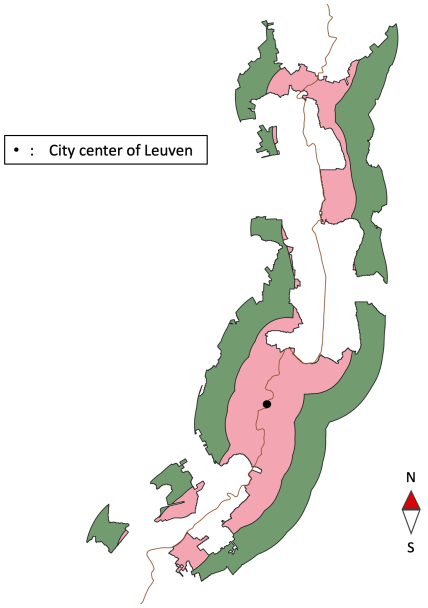

Figure 4.2: Heat network of Leuven around river Dyle. Pink: $500\ m$ network. Green: $1,000\ m$ network. River Dyle depicted in orange

4.2.2 Heat potential

The heat potential of a river is defined as the maximum heat that can be extracted without the water temperature dropping below a critical value. In Belgium, the VMM currently only defined a limit on the temperature change when heat is discharged into the river. Thus, a limitation on the temperature drop due to heat extraction has not been determined yet. However, the same value for the maximum temperature decrease (heat extraction) will presumably be adopted by the VMM as currently practiced for the maximum temperature increase (heat discharge). The latter is imposed at $3°C$ for all rivers in Belgium [25]. Accordingly, the research will use a maximum permitted temperature drop of $3°C$ along the entire course of the river Dyle to asses its heat potential. This section analyzes the river water temperature drop when the heat defined in section 4.2.1 would be extracted from the Dyle in Leuven.

The first test on the Dyle is performed with the input parameters from February 2016 in appendix B. As detailed in section 4.1, the Dyle is modelled between Leuven and Mechelen, where an inflow is implemented at the brewery of AB InBev (see figure 4.1). A heat extraction for both the $500\ m$ and $1,000\ m$ heat network is performed in the center of Leuven corresponding to the city's heat demand from the month of February in table 4.1. The test is performed by the Fluid Trajectory Model and thus a fluid volume is followed as it travels from Leuven to Mechelen whereby its water temperature is plotted along the trajectory. Based on the stream velocity of $0.343\ m/s$, the distance Leuven-Mechelen of $34\ km$ takes approximately 27 hours to complete. Accordingly, similar to both tests on the Maas in chapter 3, the duration to complete the trajectory takes multiple days. This implies that parameters for two consecutive days are needed in this winter test and thus data in appendix B is stated for both February 15th and 16th. The solution strategy from test 1 and 2 in chapter 3 is repeated and the Fluid Trajectory Model is run twice, again varying the daily average input parameters for both days as described in section 3.1. The simulated temperatures along the trajectory after heat extraction in Leuven are shown in figure 4.3, together with the behavior of the river if no heat extraction would have occurred.

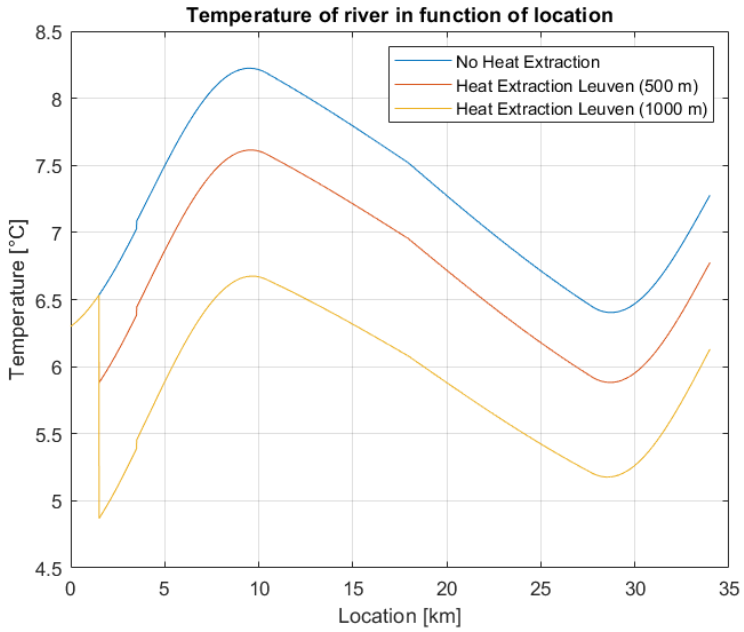

Figure 4.3: Temperature of the river Dyle between Leuven en Mechelen in February. Heat extraction in Leuven at 1.5 kilometers. Wastewater inflow from AB InBev at 3.5 kilometers

Figure 4.3 visualizes the influence of heat extraction from both heat networks on the river Dyle. When the $500\ m$ network extracts its heat demand of approximately $24.7\ MW$, the temperature of the Dyle drops with $0.65°C$. The heat network of $1{,}000\ m$ has a heat demand of approximatly $63\ MW$, resulting in a larger temperature drop of $1.66°C$. Both heat demands are fulfilled without violating the $\pm 3°C$ temperature regulation, signifying that Leuven is able to fully replace heating through gas by extracting heat from surface water using a heat pump. However, this statement is only valid for the specific test conditions. The heat potential should constantly be re-evaluated due to varying input parameters (see section 4.3) and meteorological conditions. Furthermore, the inflow of waste water from AB InBev $3.5\ km$ downstream of the starting point can be observed on each plot as the water temperature slightly increases at this location.

The concept of regeneration is crucial when studying these heat extractions from the Dyle. Regeneration signifies the effect of the heat extraction on the downstream temperatures of the river. Dependent on the magnitude of the performed heat extraction, the water temperature is altered for a certain amount of time further downstream compared to the scenario where no heat extraction occurs. The magnitude of regeneration depends on the actual difference between the water temperature and both the air and ground temperature, comprising all heat exchange processes expect shortwave radiation. A larger temperature drop due to heat extraction will hereby induce faster initial regeneration. The possible regeneration of the Dyle is visualized in figure 4.3 by a third plot which simulates the temperature of the fluid along the trajectory without heat extraction. Comparing both heat network plots to the expected flow scenario along this studied trajectory indicates the impact of their heat extraction. Consequently, heat extractions further downstream are limited to a temperature drop less than $3°C$ as long as the temperature curve has not rejoined the originally expected flow scenario. In this case, heat extraction in the center of Leuven can undermine the heat potential in Mechelen, dependent on the temperature regeneration in between both cities. Numeric values of this regeneration are presented in table 4.2.

Table 4.2: Actual and available temperature drops in the center of Leuven and Mechelen in February for both heat network sizes of Leuven

	Actual temperature drop [$^\circ C$]		**Remaining heat potential [$\%$]**	
	Leuven heat network size [m]			
Location	*500*	*1,000*	*500*	*1,000*
$Center\ of\ Leuven$	0.65	1.66	78.33	44.67
$Mechelen$	0.50	1.14	83.27	62.12

The actual temperature drop in table 4.2 represents the difference between the actual river temperature and the expected river temperature if no heat extraction had occurred. The temperature drops for each plot (or per network size of Leuven) are listed for both the center of Leuven ($1.5\ km$) and Mechelen ($34\ km$). The remaining heat potential is a measure of the additional amount of heat that can be extracted without exceeding the $\pm 3^\circ C$ regulation and at identical test conditions. These values are also presented for the center of Leuven and Mechelen based on the applied heat network size of Leuven. Table 4.2 confirms that the actual temperature drop in the center of Leuven is larger when a larger heat demand or network is applied. Consequently, the temperature in Mechelen follows that same trend as regeneration has not been fully completed over the traveled trajectory. The opposite conclusions can be drawn for the remaining heat potentials, since they will increase up to a maximum of 100% after full regeneration. The remaining heat potential percentages increase as the fluid travels further downstream, which also proves that regeneration is occurring between Leuven and Mechelen. Consider e.g. the $1000\ m$ network where to heat potential increases from 44.67% in Leuven (location of heat pumps) to 62.12% in Mechelen as a result of temperature regeneration along the trajectory. A detailed discussion on the downstream heat potential of Mechelen, resulting from the extracted heat in the center of Leuven, is presented in section 4.4.1.

Recalling that the Dyle is able to fulfill the heat demand for both network sizes in Leuven during the month of February and at the specific test conditions, a second simulation is performed to evaluate the heat potential during the month of July. The heat demand of the city is much lower during the summer and multiple input parameters of the model are altered. Therefore, the behavior of the Dyle is again investigated after extraction of the corresponding heat demand for Leuven in July. This summer test is performed on the same study site with heat pumps in the center of Leuven and an inflow at AB InBev. The heat demand is given in table 4.1 and all input parameters are listed in appendix B. The Dyle's water temperature along the trajectory in July and the influence of the heat extraction from both heat networks in Leuven is presented in figure 4.4.

Figure 4.4 shows a temperature drop at a location of $1.5\ km$ for both heat network sizes, as this is the location of heat extraction in the center of Leuven. Compared to the winter test, both network heat demands have decreased. The heat demand from table 4.1 for the $500\ m$ network is approximately $2\ MW$, while the $1,000\ m$ network demands approximately $5\ MW$. The corresponding temperature drops are $0.08^\circ C$ and $0.22^\circ C$. Both temperature drops are situated within the $\pm 3^\circ C$ temperature regulation and thus the Dyle is able to meet the heat demand of the suggested heat networks during summer conditions. Note that this conclusion is again only valid for the specific test conditions as the heat potential will vary with changing input parameters. Comparing the results of figure 4.3 to figure 4.4, it is concluded that the larger heat demand during the winter induces a larger temperature drop. Further conclusions on the influencing parameters of the heat potential are discussed in section 4.3. In figure 4.4, the temperature increase due to the inflow at AB Inbev is again visible for the three plots at $3.5\ km$ and the test simulated the Dyle over the course of three different days due to a stream velocity of just $0.21\ m/s$. Therefore, data for July 12th, 13th, and 14th is provided in appendix B.

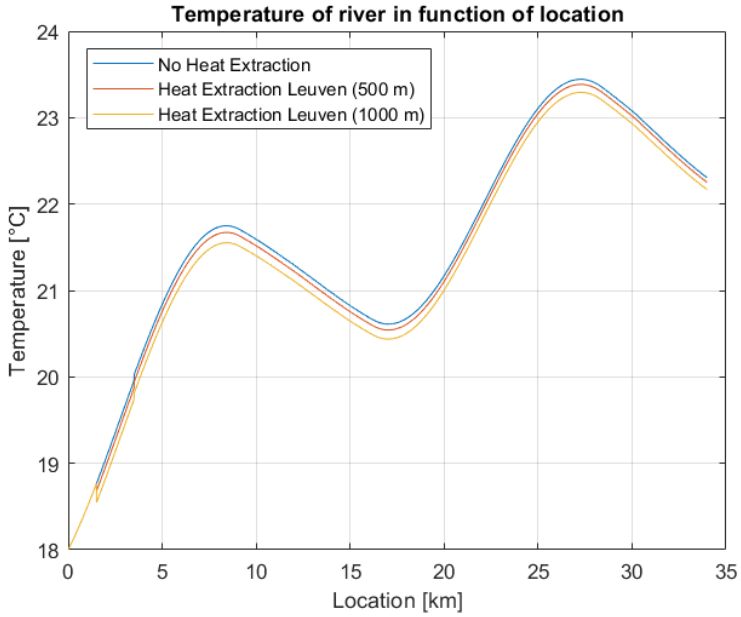

Figure 4.4: Temperature of the river Dyle between Leuven en Mechelen in July. Heat extraction in Leuven at 1.5 kilometers. Wastewater inflow from AB InBev at 3.5 kilometers

Numeric values of the actual temperature drop and remaining heat potential in both the center of Leuven and Mechelen is given in table 4.3. In comparison to table 4.2, the actual temperature drops are smaller and they lead to much higher remaining heat potentials. Again, the regeneration phenomenon is present since temperature drops decrease and heat potentials increase as the water flows from the center of Leuven to Mechelen.

Table 4.3: Actual and available temperature drops in the center of Leuven and Mechelen in July for both heat network sizes of Leuven

	Actual temperature drop [$^{\circ}C$]		**Remaining heat potential [$\%$]**	
	Leuven heat network size [m]			
Location	*500*	*1,000*	*500*	*1,000*
$Center\ of\ Leuven$	0.08	0.22	97.33	92.66
$Mechelen$	0.05	0.14	98.33	95.33

In conclusion, the Fluid Trajectory Model proves that the Dyle is able to provide the demanded heat by a $1,000\ m$ heat network in Leuven without exceeding the $\pm 3^{\circ}C$ temperature regulation. The occurrence of regeneration is also visualized in each test, where a larger heat extraction initially speeds up this process. After travelling a certain distance downstream, the influence of any earlier upstream heat extraction becomes negligible at a remaining heat potential of e.g. 99%. (see also figure 3.10). Furthermore, the two conducted river simulations show a major difference in temperature drop as the city's heat demand greatly varies throughout the year. Since both winter and summer conditions are analyzed, it might be concluded that the Dyle is able to fulfill Leuven's heat demand throughout the entire year. However, recall that the heat potential does not solely depend on the actual heat demand as multiple input parameters will influence the observed temperature drop.

4.3 Sensitivity Analysis

In this section the influence of different input parameters on the heat potential of the river Dyle is evaluated using the results obtained in the previous section 4.2.2. Recall that the Fluid Trajectory Model uses equation (2.2) in combination with equation (3.1) to compute the river temperatures along the studied trajectory. Heat extraction occurs at a single element and thus solely the behavior of an induced temperature difference within one element is evaluated. At this specific location or element, the rate of heat transfer from heat extraction ($Q_{heat.extr.}$) is typically two or three orders of magnitude larger than the heat contribution of all other heat fluxes in equation (3.1) combined. Thus, the actual heat extraction is the only heat exchange process that is considered when evaluating the magnitude of the induced temperature drop. Furthermore, equation (2.2) indicates that the temperature drop will also depend on the mass flow rate of the stream and the specific heat of the river water. In order to draw meaningful conclusions for each parameter, the two remaining variables are consecutively kept constant in this sensitivity analysis.

First, the influence of the heat demand is analyzed. In this research, the heat demand equals the total rate of heat transfer that is extracted from the fluid volume ($Q_{heat.extr.}$) at the location of the heat pump(s). Referring to the winter and summer simulations from section 4.2.2, the heat demand varies according to the size of the surrounding heat network and the time of the year. The simulation of the Dyle in February yielded temperature drops of $0.65°C$ and $1.66°C$, corresponding to a heat demand of approximately 24.7 MW and 63 MW for the different heat networks. The ratio between both the temperature drops and the heat demands equals approximately 2.5, with a deviation of only 0.08 due to neglecting all other heat exchange processes acting on this element. Therefore, it is concluded that the magnitude of the heat demand is directly proportional to the observed temperature drop. Similar results are obtained when the conducted test in July is analyzed.

Secondly, the effect of the mass flow is evaluated. From equation (2.2), it results that the mass flow is inversely proportional to the observed temperature drop when the heat extraction rate of heat transfer and specific heat remain constant. To illustrate the relation between mass flow and temperature drop, the heat extraction from the February test on the $1,000$ m heat network in section 4.2.2 is repeated with varying mass flow values. The heat demand is kept constant at 63 MW and also the specific heat remains unchanged. The corresponding temperature drops for the Dyle in February are shown in figure 4.5. Recall that the actual temperature drop was computed at $1.66°C$, with a mass flow of approximately $9,000$ kg/s.

Figure 4.5 confirms that an increased mass flow decreases the temperature drop at a specific constant heat demand. In order to satisfy the $\pm 3°C$ temperature regulation during these specific February conditions, the mass flow of the Dyle cannot decrease below $5,000$ kg/s. Possible decreases in mass flow might result from warm and dry weather for an extended period of time, as the mass flow of the Dyle used in e.g. the July test from section 4.2.2 dropped to $5,500$ kg/s. Any inflows will slightly increase the mass flow of the river. In all other cases, the mass flow of a river can be assumed constant over limited periods of time. That is, regular monitoring at the location of interest is required in order to evaluate changes in mass flow. In this research, the mass flow of a river is determined based on an average river cross section and velocity (see equation (2.1)) and it is kept constant over its entire trajectory during simulations (disregarding inflows).

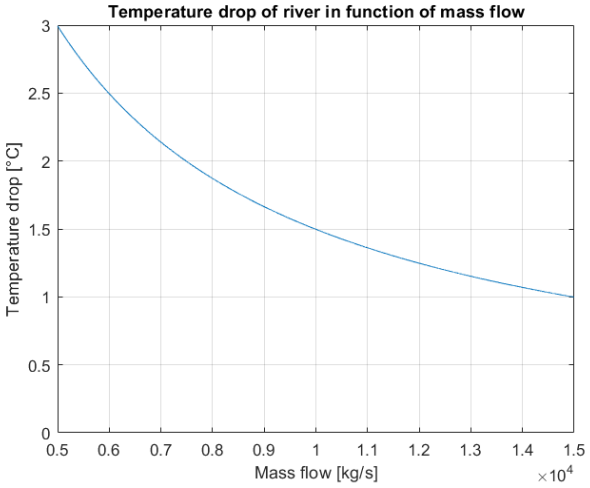

Figure 4.5: Temperature drop of the Dyle for varying mass flows after extraction of $63\ MW$ in Leuven in February

The specific heat of the river water is the final parameter that directly influences the temperature drop due to heat extraction. Similar to the mass flow, the specific heat in equation (2.2) is inversely proportional to the temperature drop at constant heat demand and mass flow. The value for the specific heat depends on the current water temperature and is determined from the table of saturated water properties. In other words, the influence of the specific heat is based on the value obtained from the water temperature right before heat extraction. However, this specific heat value only ranges between $4,217\ J/(kg \cdot K)$ and $4,179$ $J/(kg \cdot K)$ when the river water is heated from $0°C$ to $40°C$. In most cases, the temperature of a river only varies within a limited section of this temperature interval throughout an entire year e.g. from $5°C$ to $20°C$. Thus, the effect of the specific heat on the temperature drop due to heat extraction is negligible.

In conclusion, the sensitivity of the observed temperature drop in a river due to heat extraction is influenced by both the heat demand of the surrounding heat network and the actual mass flow of the river. Increasing the rate of heat transfer by a heat pump proportionally enlarges the induced temperature drop, while a larger mass flow of the stream will reduce the temperature drop it experiences. As mentioned in section 4.2.2, the heat potential of a river during the computed simulations is only valid for the specific test inputs and the temperature drop should be re-evaluated with updated input parameters at each point in time. From the sensitivity analysis in this section, it is proven that solely the mass flow of the river has to be monitored at a constant heat demand. Reusing the February test from section 4.2.2 as an example, new conclusions can be illustrated on the heat potential of Leuven. Remark from table 4.1 that the heat demand in February from the $1,000\ m$ heat network is the third largest demand of the entire year, approximately $6\ MW$ less than the maximum demand in January. A temperature drop of $1.66°C$ was computed at a mass flow of approximately $9,000\ kg/s$. Assuming a similar mass flow in January, the temperature regulations are met since only a slightly larger temperature drop will be induced. Knowing that the heat demand is smaller for the remaining nine months of the year, the $3°C$ temperature regulation is always met if the mass flow is larger than $5,000\ kg/s$ (see figure 4.5). Moreover, the mass flow is even allowed to drop below this threshold as the heat demand is lower during these nine other months of the year. Thus, the heat potential of a river can be accurately estimated over a longer period of time based on the desired heat network and a prediction of the mass flow using yearly data or regular monitoring. Lastly, the water temperature right before extraction will not effect the observed temperature as the influence of the specific heat of the stream is negligible.

4.4 Impact Analysis

4.4.1 Impact on application possibilities downstream

As previously stated, the Dyle is allowed to experience a maximum temperature drop of $3°C$ along its entire course. Thus, every city on the trajectory of the Dyle that extracts heat using heat pumps will contribute to reaching this limit. Consequently, if a particular city would extract a certain amount of heat that results in a temperature drop of $3°C$, the cities further downstream are no longer permitted to extract heat. Note that this conclusion is only valid when no regeneration occurs, as mentioned in section 4.2.2. The most important cities along the Dyle are Waver, Leuven, and Mechelen. In this research, it is assumed that only Leuven and Mechelen will extract heat from surface water in the Dyle. Accordingly, the remaining heat potential in Mechelen (downstream) will be assessed based on the extraction in Leuven (upstream) during both a winter and summer month. This discussion will be based on the numerical values obtained in section 4.2.2.

Table 4.2 provides information on the remaining heat potential in Mechelen after heat has been extracted in Leuven during February when regeneration is taken into account. From this table, it follows that an implementation of a $500\ m$ heat network in Leuven results in a maximal possible available temperature drop of $2.50°C$ (83.27% of $3°C$) in Mechelen. With an implemented heat network of $1,000\ m$ in Leuven, the maximal allowed temperature drop in Mechelen is only $1.86°C$. Acknowledging these values, the heat potential in Mechelen for February is analyzed. This analysis will assess a heat demand according to a $1,000\ m$ heat network in Mechelen, equaling approximately $70.4\ MW$. If this heat demand can be provided by the potential of the Dyle, it follows that heat can also be delivered to a $500\ m$ heat network in Mechelen. The results are summarized in table 4.4 and figure 4.6.

Table 4.4: Temperature drop due to heat extraction in Mechelen and Leuven in February

Leuven heat network size	Remaining temperature drop right before extraction in Mechelen [$°C$]	Temperature drop after extraction in Mechelen [$°C$]
$500\ m$	0.50	2.36
$1,000\ m$	1.14	3.00

The temperature drop in Mechelen, according to a heat network of $1,000\ m$, equals $1.86°C$. As a result, the temperature drop after heat extraction in Mechelen is exactly equal to the critical $3°C$ when the heat network size in Leuven also equals $1,000\ m$. When a $500\ m$ network is considered in Leuven, the temperature drop remains below the critical value of $3°C$ as it equals $2.36°C$. From table 4.1, it follows that the heat demand for both Leuven and Mechelen is higher in January and December than during February. Accordingly, the temperature drop in January and December will exceed the maximum allowed $3°C$ at a similar mass flow (see section 4.3) since the temperature drop in February is already on the verge of violating the critical value. However, the temperature drop will stay below $3°C$ for all other months since the heat demands during these months are much lower than in February. Therefore, it is concluded that the heat demand can be attained by the heat potential for a heat network of $1,000\ m$ in both Leuven and Mechelen during all months except for January and December. Note that the threshold of $3°C$ would be violated in February if no regeneration between Leuven and Mechelen occurred, which signifies the importance of modelling the river temperature over the entire trajectory. If Mechelen would implement a heat network of only $500\ m$, the resulting temperature drop will always be lower than the critical $3°C$ since the heat demand is significantly lowered when the heat network size is halved. For example, if Meche-

len implemented a heat network of $500\ m$ in February, the resulting temperature drop would be $0.95°C$. Consequently, the maximum temperature drop (after extraction for a heat network of $1,000\ m$ in Leuven) is only $2.09°C$.

Figure 4.6 visualizes the effect of regeneration on the temperature drop in function of the location between Leuven and Mechelen. From figure 4.6 it is clear that after heat has been extracted in Leuven, the resulting temperature drop decreases over distance and time (regeneration). The blue graph in figure 4.6 serves as a visual representation of the difference in temperature between the yellow graph (heat extraction in Leuven for $1000\ m$ network) and the blue graph (no heat extraction) in figure 4.3 at every location between Leuven and Mechelen. Similarly, the orange graph in figure 4.6 shows the difference in temperature between the orange graph (heat extraction in Leuven for $500\ m$ network) and the blue graph (no heat extraction) in figure 4.3. Figure 4.6 also illustrates the temperature drops right before and right after heat extraction in Mechelen (at a location of $34\ km$), which are quantified in table 4.4.

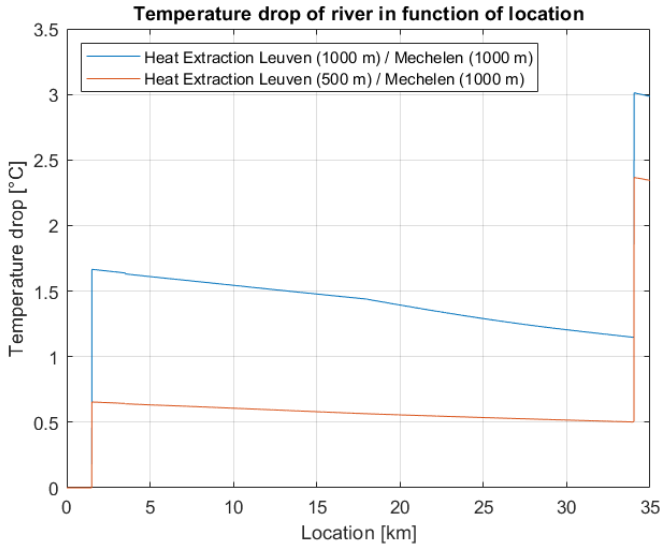

Figure 4.6: Temperature drop between Leuven and Mechelen representing the effect of regeneration in February. Heat extraction in Leuven at 1.5 kilometers and heat extraction in Mechelen at 34 kilometers. Wastewater inflow from AB InBev at 3.5 kilometers

As previously stated, the temperature drop will only exceed the critical threshold of $3°C$ during January and December when a heat network size of $1,000\ m$ is implemented for both Leuven and Mechelen. This is further clarified by analyzing the temperature drop in July. During this month the heat demand for a $1,000\ m$ network in Mechelen equals $5.7\ MW$. This heat demand corresponds to a temperature drop of $0.25°C$ at the given mass flow in July. Table 4.5 summarizes the total temperature drop when regeneration between Leuven and Mechelen is taken into account. Table 4.5 indicates that both Mechelen and Leuven can implement a $1,000\ m$ heat network without the river Dyle experiencing a critical temperature drop during summertime. Moreover, approximately only 10% of the critical value is reached, which signifies that larger heat networks could be implemented in both Leuven and Mechelen during summer months.

Figure 4.7 illustrates the temperature drops in table 4.5. The regeneration effect is visible as the temperature drop decreases with increasing travel distance of the followed fluid volume between Leuven and

Mechelen. Again, the graphs in this figure can be used as a visual representation of the difference in temperature between the graphs of heat extraction and no heat extraction in figure 4.4.

Table 4.5: Temperature drop due to heat extraction in Mechelen and Leuven in July

Leuven heat network size	Remaining temperature drop right before extraction in Mechelen [$^{\circ}C$]	Temperature drop after extraction in Mechelen [$^{\circ}C$]
$500\ m$	0.05	0.30
$1,000\ m$	0.14	0.39

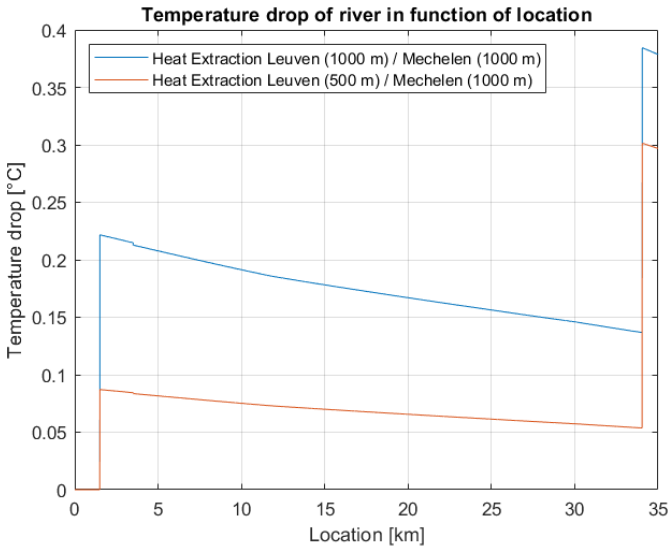

Figure 4.7: Temperature drop between Leuven and Mechelen representing the effect of regeneration in July. Heat extraction in Leuven at 1.5 kilometers and heat extraction in Mechelen at 34 kilometers. Wastewater inflow from AB InBev at 3.5 kilometers

Concluding, it is found that heat extraction from the river Dyle can provide energy to large scale heat networks of $1,000\ m$ in Leuven and Mechelen during every month of the year except for January and December. These $1,000\ m$ heat networks can provide energy to all the residential buildings in the city of Leuven and the city of Mechelen. Note however that this conclusion is only valid for the specific experiments that are conducted within this research. That is, regeneration between the cities of Leuven and Mechelen is highly dependent on the air and ground temperature as previously discussed and these parameters vary throughout every day of a month. For example, it is concluded from the tests that the temperature drop in February was maximally $3^{\circ}C$. If a different day were modeled in the same month, the critical value of $3^{\circ}C$ might have been exceeded due to different values for the air and ground temperatures. Furthermore, not only the regeneration after heat extraction but also the initial temperature drop due to heat extraction depends on different parameters e.g. mass flow (see section 4.3). Nonetheless, the Fluid Trajectory Model is able to quickly assess the different heat potentials when these inputs are varied. As a result, the model can be used to accurately analyze the heat potential for Leuven and Mechelen based on current conditions at every point of the year. This enables the cities to estimate their heat network size which can be provided by energy from the river Dyle at any time. Thus, if heat network sizes within cities are adaptable on demand, the model can aid to estimate the maximum size of the heat network that can be implemented.

4.4.2 Impact on physical and ecological processes

Thermal river pollution is defined as the direct and indirect effects on the temperature of a river due to its exploited use by humans. Heat extraction from surface water for the heating of buildings is one form of thermal pollution in a river [26]. In this research no attempt was made in conducting tests to asses the impact of heat extraction since this is beyond the scope of the work. Besides, a test on the river Dyle in Leuven could not be conducted since a system for heat extraction is not yet applied. Moreover, acknowledging the complex interactions of ecosystem processes a qualitative synthesis is recommended over a quantitative research [26]. Thus, this section focuses on the general physical and ecological impacts of the thermal use of rivers and describes considerations that must be made when applying this method.

Water temperature is a key abiotic property that governs practically all physical and chemical characteristics of the waterbody. By doing so, it influences the behaviour of fish (digestion, reproduction, growth, and dispersal), the rate of photosynthesis by aquatic plants, and the breakdown process of grass/plant substances in the water by fungi and invertebrates [27] [28]. The behaviour of fish and invertebrates alters as the river temperature changes since their body temperature closely follows the ambient water temperature [26]. When the river temperature is lowered due to heat extraction, most of their physiological processes will decelerate. Metabolic processes, such as digestion, will slow down and the aquatic organisms will have a lower reaction speed to stimuli and they will feed less [29]. Moreover, every organism has a certain thermal tolerance, a range in which they optimally grow and reproduce [29]. Optimal reproduction occurs in narrow range that is different for each organism [30]. Defining thresholds is a difficult task because of the complex nature of an organisms thermal tolerance [26]. Apart from a thermal tolerance, organisms experience thermal limits. When the river temperature falls below the lower bound, death will occur [29]. The thermal tolerance and limit can change throughout the lifetime of an organism. That is, organisms can acclimatize to a gradual change in temperature of their living environment [31]. From literature it is found that certain fish can acclimatize to a temperature change of $1^{\circ}C$ in twenty-four hours [32]. Sensitiveness to a changing temperature is a function of the ecosystem where the aquatic organisms are living in. When the ecosystem already experiences a significant variability in temperature under normal circumstances it yields that impacts due to thermal pollution are less severe [33].

Extracting heat from surface water creates a thermally heterogeneous waterbody that extends until the temperature change is fully incorporated in the ambient water. Local effects, close to the location of heat extraction, are considerably larger and easier to detect than consequences at the scale of the whole waterbody [29]. Although no large scale change may be perceived, local effects can cause attraction or avoidance of aquatic organisms resulting in the replacement of native by invasive species [34]. Several factors influence the spatial effect of thermal pollution and can be adopted to mitigate the consequences. Exchanging heat as close as possible to the surface of the water enhances a faster thermal mixing with the atmosphere which results in a reduced thermal load on the waterbody [29]. Obviously, a large amount of heat exchange results in a waterbody that is significantly thermally altered. In addition, heat exchange at river locations of high flow velocity enhances the rate of thermal mixing due to turbulence [35]. The same conclusion can be drawn on locations where the rivers cross section is minimal.

In the future, climate change will cause waterbodies such as rivers to warm up [36]. From that point of view, extracting heat from surface water can counteract the thermal stress opposed by a changing climate.

Chapter 5

Conclusions

In this research, two MATLAB models are created to simulate the temperature behaviour of rivers. Both models enable the analysis of the heat potential in the river Dyle. The Fluid Trajectory Model allows a straightforward implementation to model heat extraction from surface water in the studied river together with possible inflows and all other present heat exchange processes. The Finite Element Model incorporates a more elaborate approach based on prior research to simulate river temperatures whereby the effects of dispersion are implemented. Besides generating a distinct set of data, the Finite Element Model served to validate the approach of the Fluid Trajectory Model. It was demonstrated that no notable improvement in accuracy resulted from using a finite element approximation and multiple independent test scenarios proved the correctness of the temperature results from both models. Nonetheless, the Fluid Trajectory Model practices a more consistent solution strategy to model sudden changes introduced by inflows and heat extractions. Additionally, the computation time of the Fluid Trajectory Model equals approximately half the time needed to solve the Finite Element Model. In conclusion, the concise approach of the Fluid Trajectory Model is best suited to accurately simulate heat extraction(s) from the Dyle.

The heat potential in Leuven is studied during the months of February and July, whereby the heat demand for a $1,000\ m$ heat network equals $63\ MW$ and $5\ MW$ respectively. Simulation results showed that a temperature drop of $1.66°C$ was induced in February, whereas the river temperature lowered with $0.22°C$ in July. Based on regulations from the VMM, a maximum temperature drop of $3°C$ is adopted in this research. Consequently, a remaining heat potential of 44.67% in February and 92.66% in July resulted in Leuven. Since all computed temperatures are only valid at the specific test conditions, a sensitivity analysis on the observed temperature drop in a river due to heat extraction is needed to accurately estimate the heat potential over a longer period of time. It was shown that the heat demand of the studied heat network is directly proportional to the induced temperature drop, whilst the mass flow of the stream has an inversely proportional influence on the observed temperature decrease. Therefore, a substantiated estimation on the heat potential of the Dyle throughout the entire year is possible based on the desired heat demand in Leuven and predictions on the mass flow using yearly data or regular monitoring. It is hereby concluded that heat extraction from the river Dyle can provide the demanded heat to a $1,000\ m$ heat network in Leuven during every month of the year without exceeding the imposed temperature regulations. A cascading system of heat pumps is thus able to supply heat from surface water in the Dyle to residential buildings in Leuven as a substitute for gas. Furthermore, the impact on the application possibility in Mechelen is investigated. Regeneration of the river temperature occurs after heat extraction in Leuven as the Dyle travels $34\ km$ further downstream before arriving in Mechelen. The rate of regeneration is dependent on the air and ground temperature of the specific test and this phenomenon increases

the remaining heat potential in Mechelen. Heat extractions from the Dyle that aimed to supply a $1,000$ m heat network in both Leuven and Mechelen resulted in a total temperature drop of $3°C$ in February and $0.39°C$ in July. The effects of regeneration caused the temperature drop in February to decrease with $0.52°C$ between Leuven and Mechelen, corresponding to an increased heat potential of 17.45% in Mechelen. In July, the heat potential in Mechelen increased with 2.67%, resulting from a gradual decrease in temperature drop of $0.08°C$. Based on the result in February, it is found that also Mechelen can provide the demanded heat to its residential buildings during every month of the year except for January and December. However, the total temperature drop in February of exactly $3°C$ resulted at the specific test conditions of the simulation. This drop in river temperature causes uncertainty whether the entire month of February will effectively meet the critical temperature regulation, taking into account fluctuations in meteorological conditions. Lastly, an impact analysis of heat extraction on physical and ecological processes showed that the behaviour of fish and invertebrates alters when the river temperature is changed. Optimal reproduction and metabolic processes are disturbed when sudden temperature drops exceed the thermal tolerances of these aquatic organisms, whereas death will occur beyond their thermal limits. In addition, heat extraction from surface water creates thermally heterogeneous waterbodies causing local avoidance of native species. This thermal load on the river can be reduced by extracting heat closely to the surface of the water to enhance faster thermal mixing with the atmosphere.

The Fluid Trajectory Model, developed in this research, is able to estimate the heat potential of multiple cities along the same river. The maximum allowed heat network size for each city at a given point in time can be computed in order to meet the imposed temperature drop regulations. The created model is adaptable and flexible, enabling the user to accurately investigate different sites of interest. Thus, the model serves as a tool to asses the applicability of heat pump systems to extract heat from surface water in any city. Through this ability, the model can act as a fundamental framework in developing a rational and efficient method for the heating of buildings and accordingly mark a positive impact on our climate and ecosystems.

Chapter 6

Recommendations

This master's thesis can be used as fundamental research for the following topics:

- The influence of heat extraction on the river Dyle can be extended by using the models to simulate other cities besides Leuven and Mechelen with a similar heat extraction system.
- A test can be carried out on the river Dyle to analyze the influence of heat extraction on the existing physical and ecological processes. A study on e.g. algae can be used to evaluate the possible effects of heat extraction.
- The models from this research can be used to create a heat potential map of all rivers in Belgium. This map can serve as a tool to aid the implementation of heat extraction systems along these rivers.
- Within this research, the heat extraction potential for the heating of residential buildings is analyzed. However, the created models can also be used to estimate the potential of rivers for the cooling of buildings.

Bibliography

[1] E. Worrell, L. Bernstein, J. Roy, L. Price, and J. Harnisch. Industrial energy efficiency and climate change mitigation. *Energy Efficiency*, 2:109–123, 2008.

[2] A. Allouhi, Y. El Fouih, T. Kousksou, A. Jamil, Y. Zeraouli, and Y. Mourad. Energy consumption and efficiency in buildings: Current status and future trends. *Journal of Cleaner Production*, 109, 2015.

[3] H. Averfalk, P. Ingvarsson, U. Persson, M. Gong, and S. Werner. Large heat pumps in swedish district heating systems. *Renewable and Sustainable Energy Reviews*, 79:1275–1284, 2017.

[4] J. Gao, Y.and Wu and Y. Cheng. Study on the heating modes in the hot summer and cold winter region in china. *Procedia Engineering*, 121:262–267, 2015.

[5] X. Chen, G. Zhang, J. Peng, X. Lin, and T. Liu. The performance of an open-loop lake water heat pump system in south china. *Applied Thermal Engineering*, 26:2255–2261, 2006.

[6] M. Boyd and B. Kasper. Analytical methods for dynamic open channel heat and mass transfer: Methodology for heat source model version 7.0. *Watershed Sciences Inc.*, 2003.

[7] Y. A. Çengel and A. J. Ghajar. *Heat and Mass Transfer: Fundamentals and Applications, Fifth Edition in SI Units*. McGraw-Hill Education, 2015.

[8] J. D. Stephen, M. H. David, and A. M. Iain. River temperature modelling: A review of process-based approaches and future directions. *Earth-Science Reviews*, 175:97–113, 2017.

[9] B. F. Hugo, E. L. John, C. Y. K. Robert, I. Jörg, and H. B. Norman. *Mixing in Inland and Coastal Waters*. Academic Press, San Diego, 1979.

[10] J. Martin and S. Mccutcheon. *Hydrodynamics and Transport for Water Quality Modeling*. Taylor & Francis, 1998.

[11] A. Glose, L. K. Lautz, and E. A. Baker. Stream heat budget modeling with hflux: Model development, evaluation, and applications across contrasting sites and seasons. *Environmental Modelling & Software*, 92:213–228, 2017.

[12] B. W. Webb and Y. Zhang. Intra-annual variability in the non-advective heat energy budget of devon streams and rivers. *Hydrological Processes*, 18(11):2117–2146, 2004.

[13] M.B. Kalinowska. Effect of water-air heat transfer on the spread of thermal pollution in rivers. *Acta Geophys*, 67:597–619, 2019.

[14] M. Bessafi, V. Oree, A. Khoodaruth, G. Jumaux, F. Bonnardot, P. Jeanty, M. Delsaut, J. Chabriat, and M. Z. Dauhoo. Downscaling solar irradiance using dem-based model in young volcanic islands with rugged topography. *Renewable Energy*, 126:584–593, 2018.

[15] W.P. Kustas, A. Rango, and R. Uijlenhoet. A simple energy budget algorithm for the snowmelt runoff model. *Water Resources Research*, 30:1515–1527, 1994.

[16] S.L. Dingman. *Physical Hydrology*. Macmillan Publishing Company, 1994.

[17] D.R. Maidment. *Handbook of hydrology*. Civil engineering. McGraw-Hill, 1993.

[18] T. Dunne and L. B. Leopold. *Water in environmental planning*. San Francisco : W. H. Freeman, 1978.

[19] W. Trabert. Neue beobachtungenûber verdampfungsgeschwindigkeiten. *Meteorol Z*, 13:261–263, 1896.

[20] N. Abu-Hamdeh and R. Reeder. Soil thermal conductivity: Effects of density, moisture, salt concentration, and organic matter. *Soil Science Society of America Journal*, 64:1285–1290, 2000.

[21] R. W. MacCormick. *The effect of viscosity in hypervelocity impact cratering.* Am. Inst. Aeronaut. Astronaut., 1969.

[22] T. He, J. Masek, Y. Shuai, C. Schaaf, and Z. Wang. Angular effects and correction for medium resolution sensors to support crop monitoring. *IEEE Journal of Selected Topics in Applied Earth Observations and Remote Sensing*, 7:4480–4489, 2014.

[23] W. Meynendonckx. *Heatmap van koude/warmte-voorziening via oppervlaktewater*. KU Leuven, 2020.

[24] EHPA. Large scale heat pumps in europe. `https://www.ehpa.org/fileadmin/red/03._Media/03.02_Studies_and_reports/Large_heat_pumps_in_Europe_MDN_II_final4_small.pdf`, 2020.

[25] VMM. Leefmilieu, wetgeving, milieuhinder, hinder, verontreiniging, veiligheidsrisico, vergunning. `https://www.vmm.be/wetgeving/vlarem-i`, 2018.

[26] A. Gaudard, C. Weber, T. Alexander, S. Hunziker, and M. Schmid. Impacts of using lakes and rivers for extraction and disposal of heat. *Wiley Interdisciplinary Reviews: Water*, 5(5):e1295, 2018.

[27] B. Sinokrot and H. Stefan. Stream temperature dynamics: Measurements and modeling. *Water Resour. Res.*, 29:2299–2312, 1993.

[28] S. Broadmeadow, J.G. Jones, T. Langford, P. Shaw, and T. Nisbet. The influence of riparian shade on lowland stream water temperatures in southern england and their viability for brown trout. *River Research and Applications*, 27:226–237, 2011.

[29] T. Langford. *Ecological Effects of Thermal Discharges*. Pollution Monitoring Series. Springer Netherlands, 1990.

[30] J. Matousek, V. Stejskal, M. Prokešová, and J. Kouril. The effect of water temperature on growth parameters of intensively reared juvenile peled coregonus peled. *Aquaculture Research*, 48, 2016.

[31] Y. Souchon and L. Tissot. Synthesis of thermal tolerances of the common freshwater fish species in large western europe rivers. *Knowledge and Management of Aquatic Ecosystems*, 405, 2012.

[32] F. E. J. Fry. *Thermal effects on fish ecology*. Thermobiology. 1967.

[33] J. Mulhollem, R. Colombo, and D. Wahl. Effects of heated effluent on midwestern us lakes: implications for future climate change. *Aquatic Sciences*, 78:743–753, 2016.

[34] S. Emde, J. Kochmann, T. Kuhn, D. Dörge, M. Plath, F.h Miesen, and S. Klimpel. Cooling water of power plant creates ”hot spots” for tropical fishes and parasites. *Parasitology research*, 115, 2015.

[35] Matt H. Effects of the discharge of thermal effluent from a power station on lake wabamun, alberta, canada - the epipelic and epipsamic algal communities. *Hydrobiologia*, 45:199–215, 1974.

[36] N. Poff, M. Brinson, and J. Day. Aquatic ecosystems global climate change - potential impacts on inland freshwater and coastal wetland ecosystems in the united states. *Pew Center for Global Change*, 2002.

Appendix A

Electronic Appendices

The appendices listed below are electronically available upon request and will therefore not be provided in this paper.

- MATLAB file of the Fluid Trajectory Model
- MATLAB file of the Finite Element Model
- Excel file of input data for the Finite Element Model test on the river Maas

Appendix B

Input Data Heat Potential Analysis

Input Data Dyle February 2016

	Value	
Parameters	*February 15th*	*February 16th*
L_{river} $[m]$	17,900	16,100
D_{river} $[m]$	1.5	1.5
W_{river} $[m]$	17.5	17.5
v_{stream} $[m/s]$	0.343	0.343
v_{wind} $[m/s]$	1.20	0.72
$Hours_{daylight}$ $[h]$	9.98	10.02
$Time_{sunrise}$ $[h]$	7.95	7.92
$Time_{start}$ $[h]$	9:30 a.m.	12 a.m.
ε_w $[/]$	0.97	0.97
σ $[W/(m^2 \cdot K^4)]$	$5.67 \cdot 10^{-8}$	$5.67 \cdot 10^{-8}$
C_L $[\%]$	50 (assumption)	50 (assumption)
H $[\%]$	84.25	82.31
vts $[/]$	1 (assumption)	1 (assumption)
A $[/]$	0.05 (assumption)	0.05 (assumption)
SF $[\%]$	5 (assumption)	5 (assumption)
k_{soil} $[W/(mK)]$	0.8	0.8
L_{soil} $[m]$	0.5	0.5
p_0 $[hPa]$	1,013	1,013
p_{air} $[hPa]$	1,017.34	1,034.58
C_b $[hPa/K]$	0.62	0.62
$Inflow\ temperature$ $[^\circ C]$	20	/
$Inflow\ discharge$ $[m^3/day]$	3,357	/
$Inflow\ location$ $[m]$	3,500	/
$Heat\ extraction$ $[MW]$	62.958 ($1{,}000$ m heat network); 24.730 (500 m heat network)	/
$Heat\ extraction\ location$ $[m]$	1,500	/
T_{air} $[^\circ C]$	3.3	-0.25
T_{ground} $[^\circ C]$	4	3
q_{in} $[W/m^2]$	502	502
$Input\ River\ Temperature;\ T_w, i_1$ $[^\circ C]$	6.3	result from day 1
$Number\ of\ elements$ $[/]$	1,790	1,610

Input Data Dyle July 2016

	Value		
Parameters	*July 12th*	*July 13th*	*July 14th*
L_{river} $[m]$	11,850	18,140	4,010
D_{river} $[m]$	1.5	1.5	1.5
W_{river} $[m]$	17.5	17.5	17.5
v_{stream} $[m/s]$	0.21	0.21	0.21
v_{wind} $[m/s]$	0.84	0.34	0.72
$Hours_{daylight}$ $[h]$	16.17	16.13	16.10
$Time_{sunrise}$ $[h]$	5.7	5.72	5.73
$Time_{start}$ $[h]$	9:50 a.m.	12 a.m.	12 a.m.
ε_w [/]	0.97	0.97	0.97
σ $[W/(m^2 \cdot K^4)]$	$5.67 \cdot 10^{-8}$	$5.67 \cdot 10^{-8}$	$5.67 \cdot 10^{-8}$
C_L $[\%]$	50 (assumption)	50 (assumption)	50 (assumption)
H $[\%]$	76.81	82.29	78.84
vts [/]	1 (assumption)	1 (assumption)	1 (assumption)
A [/]	0.05 (assumption)	0.05 (assumption)	0.05 (assumption)
SF $[\%]$	5 (assumption)	5 (assumption)	5 (assumption)
k_{soil} $[W/(mK)]$	0.8	0.8	0.8
L_{soil} $[m]$	0.5	0.5	0.5
p_0 $[hPa]$	1,013	1,013	1,013
p_{air} $[hPa]$	1,012.54	1,014.77	1,020.87
C_b $[hPa/K]$	0.62	0.62	0.62
$Inflow\ temperature$ $[^\circ C]$	27	/	/
$Inflow\ discharge$ $[m^3/day]$	4,471	/	/
$Inflow\ location$ $[m]$	3,500	/	/
$Heat\ extraction$ $[MW]$	5.101 ($1,000\ m$ network); 2.004 ($500\ m$ network)	/	/
$Heat\ extraction\ location$ $[m]$	1,500	/	/
T_{air} $[^\circ C]$	17.81	14.21	15.39
T_{ground} $[^\circ C]$	19.5	19.0	18.5
q_{in} $[W/m^2]$	874	874	874
$Input\ River\ Temperature$; T_w, i_1 $[^\circ C]$	18	result from day 1	result from day 2
$Number\ of\ elements$ [/]	1,185	1,814	401

FACULTY OF ENGINEERING TECHNOLOGY
GROUP T LEUVEN CAMPUS
Andreas Vesaliusstraat 13
3000 LEUVEN, België
tel. + 32 16 30 10 30
fet.groupt@kuleuven.be
www.fet.kuleuven.be